2540 Dole St., Holmes 302
Dept. of Mechanical Engineering
University of Hawaii
Honolulu, Hawaii 96822, USA
www.eng.hawaii.edu/~asl

Autonomous Systems Laboratory

Annual Report

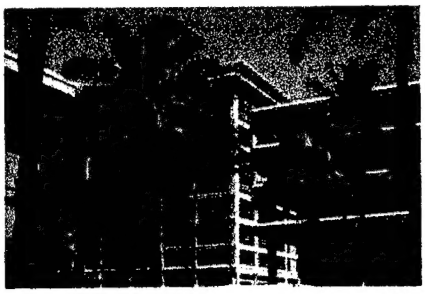

Development of a Semi-Autonomous Underwater Vehicle for Intervention Missions (SAUVIM)

Submitted to the Office of Naval Research

July 31, 1999

Summary

Technical Progress Report: Year 2 (August 1, 1998 – July 31, 1999)

The SAUVIM proposal was submitted under the ONR Annual Announcement of the July 11, 1996 Commerce Business Daily, and the project officially began on August 1, 1997 with an 18-month, $2.237 million research fund from the Office of Naval Research's Undersea Weapons Technology Program directed by Mr. James Fein. The first progress report was submitted to ONR during Mr. Fein's site visit of October 28, 1997. The second progress report was submitted to ONR during the Advisory Committee's (AdCom) site visit of February 24, 1998. The First Annual Progress Report was submitted to ONR in August 1998 and presented during the site visit of September 15-16, 1998. With the departure of Mr. James from ONR, Mr. Chris Hillenbrand became the new ONR Program Director for the SAUVIM project. The fourth progress report was submitted during Mr. Hillenbrand's site visit of April 8, 1999. During all site visits, each SAUVIM research group gave a presentation of their current progress. This is the Second Annual Progress Report and describes the overall technical progress of the project during the 1998-1999 year.

Objective

The primary research objective is to develop a Semi-Autonomous Underwater Vehicle for Intervention Missions (SAUVIM). Unlike the fly-by autonomous underwater vehicles (AUV), SAUVIM will have a manipulator work package. It will require an advanced control system and a precise sensory system to maintain high accuracy in stationkeeping and navigation.

Background

Most intervention missions - including underwater plug/unplug, construction & repair, cable streaming, mine hunting, and munitions retrieval - require physical contact with the surroundings in the unstructured, underwater environment. Such operations always increase the level of risk and present more difficult engineering problems than fly-by and non-contact type operations. For these intervention operations, the vehicle requires a dexterous robotic manipulator; thus the overall system becomes a high degree-of-freedom (dof), multi-bodied system from the coupling effects of the vehicle and the manipulator motions. These operations require precise force/torque feedback with high degree of accuracy even in the presence of unknown, external disturbances, i.e. undersea currents. All these issues present very complex engineering problems that have hindered the development of AUVs for intervention missions. Currently, the state-of-the-art in machine intelligence is insufficient to create a vehicle of full autonomy and reliability, especially for intervention missions.

The development of '*undersea robots that can intelligently work with arms than just swim*' will have a great impact on worldwide underwater robotic vehicle technology and provide a cost-effective engineering solution to many new underwater tasks and applications that fly-by type submersibles have not been able to handle. The proposed vehicle – SAUVIM - is in response to the current local and national needs for the development of this technology and will ultimately be useful in many intervention missions. One such application field is the Pacific Missile Ranging Facility (PMRF) in Hawaii.

Progress

The SAUVIM project was proposed as a two-phase research and development program. Phase I has three parts: (1) to study the major research components, (2) to develop and integrate the basic software and hardware of SAUVIM, and (3) to test the vehicle in a shallow water environment. Phase II is a continuation and completion of the research and development of Phase I with deep water environment testing.

As stated in the original proposal, the project consists of five major components:

- Adaptive, Intelligent Motion Planning;
- Automatic Object Ranging and Dimensioning;
- Intelligent Coordinated Motion/Force Control;
- Predictive Virtual Environment; and
- SAUVIM Design.

Thirty-three people are currently working for the SAUVIM project. There are 8 faculty members, 4 full-time staff members, 12 graduate students, and 9 undergraduate students supported by this grant. The Advisory Committee was formed to provide technical advice and direction by reviewing research directions and progress, and to provide advice and assistance in exploring potential applications and users. The four-member Advisory Committee consisted of Mr. Fred Cancilliere of the Naval Undersea Warfare Center, Dr. Alexander Malahoff of the University of Hawaii, Dr. Homayoun Seraji of the Jet Propulsion Laboratory, and Mr. Dick Turlington of the Pacific Missile Range Facility. Two additional members - Dr. Paul Yuen of the University of Hawaii and Mr. James Fein, the original ONR Program Director - have been included in the Advisory Committee. The SAUVIM organizational chart is shown in Figure A, and the updated research schedule is shown as a Gantt chart in Figure B.

Achievements

The second–year achievements in each topic are summarized below.

- Adaptive, Intelligent Motion Planning (AIMP) – The AIMP aims at developing SAUVIM's motion planning, which is intelligent and adaptive in that the system is capable of decision-making at a task or mission level and can deal with unknown or time-varying environment. Motion planning for an AUV can be decomposed into path planning and trajectory generation, although they are not completely independent of each other. Path planning is a computation and optimization of a collision-free path in an environment with obstacles. Trajectory generation is the scheduling of movements for an AUV along the planned path over time. To simultaneously compensate for these objectives, a genetic algorithm (GA) based 3D-motion planner is implemented for both an off-line and on-line cases. An off-line case is when an environment is a known and static, while an on-line case must be capable of modifications in response to dynamic,

environmental changes. The utilization of GA-based approach has two advantages: 1) it is adaptive and 2) the dimension of space has less effect on performance than other methods.

The AIMP software has gone through three version upgrades. The first was *Version 1.alpha*, which integrates the off-line and on-line algorithms in C with a graphic user interface using OpenGL. This software version was tested on the Autonomous Systems Laboratory's autonomous underwater vehicle - ODIN. The second was *Version 1.0*, which integrates the path planning and trajectory generation algorithms. The third was *Version 1.1*, which optimizes the original software organization and data structures, and includes a database of mapping data on the main memory. Also, a Software Development Process (SDP) has been developed and implemented to oversee the various developments in software version changes. Several papers have been published in these subjects.

- Automatic Object Ranging and Dimensioning (AORD) – The main objective of the AORD is to develop a multiple sensor configuration to be utilized during SAUVIM's intervention missions. This three-sensor system consists of (1) a laser ranging sensor (LRS), (2) a passive arm sensor (PA) and (3) a manipulator homing sensor (MHS). The laser ranger, the homing sensor, and the passive arm have all been designed and prototyped. According to initial feasibility and prototype tests, all three sensors showed good performance.

  The underwater version of the PA has been fabricated and is being assembled. The PA is made of 6061-Aluminum, and it has two three-axis gimbaled joints and a single-axis hinge joint. The entire PA structure is compensated with mineral oil. It utilizes the original software developed for the prototype.

  The underwater versions of the LRS and the MHS are in the process of fabrication and assembly. The camera housings for both systems have been manufactured using 6061 aluminum with vacuum-sealed lens and underwater connectors have been ordered. The software for both systems has been developed using the prototypes.

- Intelligent Coordinated Motion/Force Control (ICM/FC) – The major objective of the ICM/FC is simple yet complex. The control of an AUV and its manipulator is a multi-bodied, dynamic problem of vast unknowns; therefore, this task is subdivided into four sub-tasks, which are Theoretical Modeling (TM), Low-Level Control (LLC), High-Level Control (HLC), and Dry Test Design and Set-up (DTDS).

  The objective of TM is to determine the theoretical dynamics and control of an underwater vehicle-manipulator system (UVMS). Using a Quasi-Lagrange approach, the dynamic equations of motion for a general UVMS were derived. With these equations of motion, a new drag force optimization or Drag Minimization (DM) algorithm utilizing resolution of kinematic redundancy and gradient projection method has been formulated. A direct force control scheme and an impedance control scheme have been derived. Computer simulations were performed for a 6 dof underwater vehicle and an on-board 3 dof robotic manipulator for trajectory following tasks using non-regressor based adaptive controller and computed torque control techniques. Several papers have been published in these techniques.

  The LLC has two objectives: 1) to design and develop an advanced vehicle control system for navigation and hovering, and 2) to design and develop an advanced coordinate motion/force control system of the vehicle and manipulator during the intervention mode. During this portion of Phase I, the focus has been on continuing efforts in obtaining high performance in navigation and hovering, and the development of a localization technique. The navigation and hovering uses

the on-board sonar, inertial navigation, and pressure sensors. The localization technique being developed is an evidence grid approach. The grid method accumulates occupancy evidence from an array of spatial locations and slowly resolves the ambiguities as the AUV travels. Both the navigation and hovering, and localization techniques are being tested on ODIN.

HLC's objective is to develop a supervisory control module that will minimize human involvement in the control of the underwater vehicle and its manipulation tasks. This module involves the development of high-level task planning where a mission is always composed of two parts: the goal and the method of accomplishment. In other words, "what do I need to do" and "how do I do it." Following this strategy, a new high-level architecture of vehicle control, named the Intelligent Task-Oriented Control Architecture (ITOCA), is being developed for SAUVIM. ITOCA is an effective and efficient operation running on the VxWorks real-time operating system (RTOS) environment. ITOCA is four layers: a planning layer, a control layer, an execution layer and an evaluation layer. Every mission is broken into many smaller missions and the simplest mission is considered a task. The combination of different tasks in different sequences accomplishes various missions. Presently, a preliminary, pilot algorithm is being considered and developed. The HLC is one of the major research tasks for Phase II.

The objective of DTDS is to design and fabricate a manipulator-vehicle dry test-bed which will allow high-level, manipulator force/position control algorithm developments. The test-bed will have a fully functional manipulator mounted on a free-moving base, thus allowing translational (x-axis and y-axis) and rotational (roll and pitch) motions. A simple and inexpensive, free moving platform of springs and dampers have been designed to support the PUMA arm to facilitate the initial force/torque algorithm development. The initial DTDS has been completed; however, with the acquirement of the Ansaldo 7-dof manipulator and constraints in time, the focus of the DTDS has been changed to the development of the Ansaldo software in conjunction with the TM group. Currently the Ansaldo manipulator runs off a VME bus system using VxWorks and Matlab with Simulink.

- Predictive Virtual Environment (PVE) – The PVE is aimed at developing a supervisory monitoring system for SAUVIM to smoothly and realistically integrate mapping data with on-line sensory information even in the midst of delayed and limited information. This virtual reality (VR) based system must also be able to accurately predict the current status and location of the vehicle under these conditions. The development for the PVE has been modular. The various modules are: the SAUVIM Simulation Software (SSS); the SAUVIM Video Overlay Software (SVOS); the Communication Software (CS); and the artificial neural network (ANN) Video Prediction Software (VPS). The SSS has been upgraded from its *Version 1* to *Version 1.1*, which includes the incorporation of a Magellan spaceball mouse, an accurate 3D graphical model of SAUVIM and the Ansaldo manipulator, scene-smoothing methods using interpolation techniques, and an easy-to-use user interface. The SVOS was developed to overlay video images of the seafloor (texture and color) to the graphic images to provide more accurate monitoring of the vehicle, manipulator and environment. The CS for SAUVIM is an extension of the NSF's MVS project. Currently the MVS system uses a cellular phone to communicate the vehicle data from the test-site to the monitoring computer located on campus for data fusion. Experiments are being conducted with the ODIN AUV. Finally, the VPS is in its infancy; however, several ANN methods have been tested for optimal computation time and position accuracy. Experiments have been performed in the laboratory and have generated positive results.

- SAUVIM Design (SD) – This task is the main objective of the SAUVIM project. It is an effort to design and develop efficient, reliable hardware/software architectures of SAUVIM. Due to the immense demand of this task, it is divided into five sub-tasks, which are Reliable, Distributed

Control (RDC), Mission Sensor Package (MSP), Hydrodynamic Drag Coefficient Analysis (HDCA), Mechanical Analysis and Fabrication (MAF), and Mechanical-Electrical Design (MED).

The goal of RDC is to develop a reliable and efficient computing architecture for signal and algorithmic processing of the entire SAUVIM system. The proposed system is a multi-processor system based on a 6U VMEbus and the VxWorks real-time operating system. This system is capable of high processing throughput and fault tolerance. Currently the system consists of two VMEbuses, which are the navigation control system and the manipulator control system. The main VMEbus, or the navigation control system, has two Motorola M68060 CPU boards, a multi-port RS232 interface board, and an I/O board with a Pentium MMX processor based PC104+ board, which is connected via a RS232 port. The navigation control system handles the communication, supervision, planning, low-level control, self-diagnostics, video imaging, etc. The data exchange between the two CPUs is conducted via shared memory. The second VMEbus, or the manipulator control system, has one Motorola M68040 CPU and an I/O board. Two PC104 boards are connected serially to this CPU. The manipulator control system is independent and dedicated to the manipulator control. Many of the hardware components have been tested and are being interface with its respective software systems. Various optimization changes have been implemented to minimize communication and computation. This development will continue throughout the vehicle's development process.

The objective of the MSP is to provide semi-continuous records of SAUVIM water depth, temperature, conductivity, computed salinity, dissolved oxygen, magnetic signature of the seafloor, pH and turbidity during the survey mode. In the intervention mode, the MSP also provides compositional parameters at a selected seafloor target, including pumped samples from submarine seeps or vents. The MSP is an independent system with its own PC 104 CPU and its own power supply residing in a separate pressure vessel. All of the sensors have been purchased, and an initial field test at the Loihi Seamount has been conducted. Continual tests are being conducted to optimize the scientific sensor data-gathering capabilities.

The HDCA is used to determine the hydrodynamic coefficients via a numerical solution of full Navier-Stokes equations using PHOENICS, a commercial computational fluid dynamics (CFD) code. Initial results from the PHOENICS software have produced mixed results. The current vehicle fairing has produced a drag coefficient of 0.40; however, it has not yet been verified. Other CFD software and model testing is being conducted to verify the drag coefficient results before the implementation of the vehicle fairing on SAUVIM.

The MAF has three objectives. Its primary goal is to design and fabricate composite pressure vessels with end caps and connector openings for full ocean depths taking stress, buckling, hygrothermal effects, and fatigue analysis into account; and its two secondary goals are to design and fabricate the SAUVIM fairing and to analyze the SAUVIM frame. A thorough analysis and comparison of the Ti-6Al-4V, AS4/Epoxy, and AS4/PEEK pressure vessels manifest the advantage of composite materials in reduction of weight, size and strength. Using these results, a scaled model prototype using AS4/PEEK has been fabricated and tested. A 1/3 sized prototype is being fabricated and will also be tested. For the shallow water vehicle test, a full-sized, fiberglass pressure vessel with aluminum end caps have been manufactured and tested. These vessels are being used to determine the final hardware layout. The aluminum frame has been designed and fabricated. The initial fairing analysis has been made, and fairing optimizations are being considered.

The MED is the integration of the mechanical and electrical components for SAUVIM. First, the design specifications were established for the fairing, frame, instrument pressure vessels, buoyancy systems, mission sensor, passive arm and robotic manipulator tasks. Second, after scrutinizing review of SAUVIM's major components - i.e. sensors, actuators and infrastructure - in terms of power consumption, compatibility, weight distribution, buoyancy distribution, hydrodynamic effects and task effectiveness, all major components have been purchased. Technical drawings of the vehicle frame, fairing, and related sub-structures have been completed. Many of the mechanical and electrical components have been fabricated and are being integrated with the overall electrical layouts.

The main body of this report is devoted to the detailed descriptions about the major technical progress and achievements during the 1998-1999 year.

Table of Contents

SAUVIM Organizational Chart

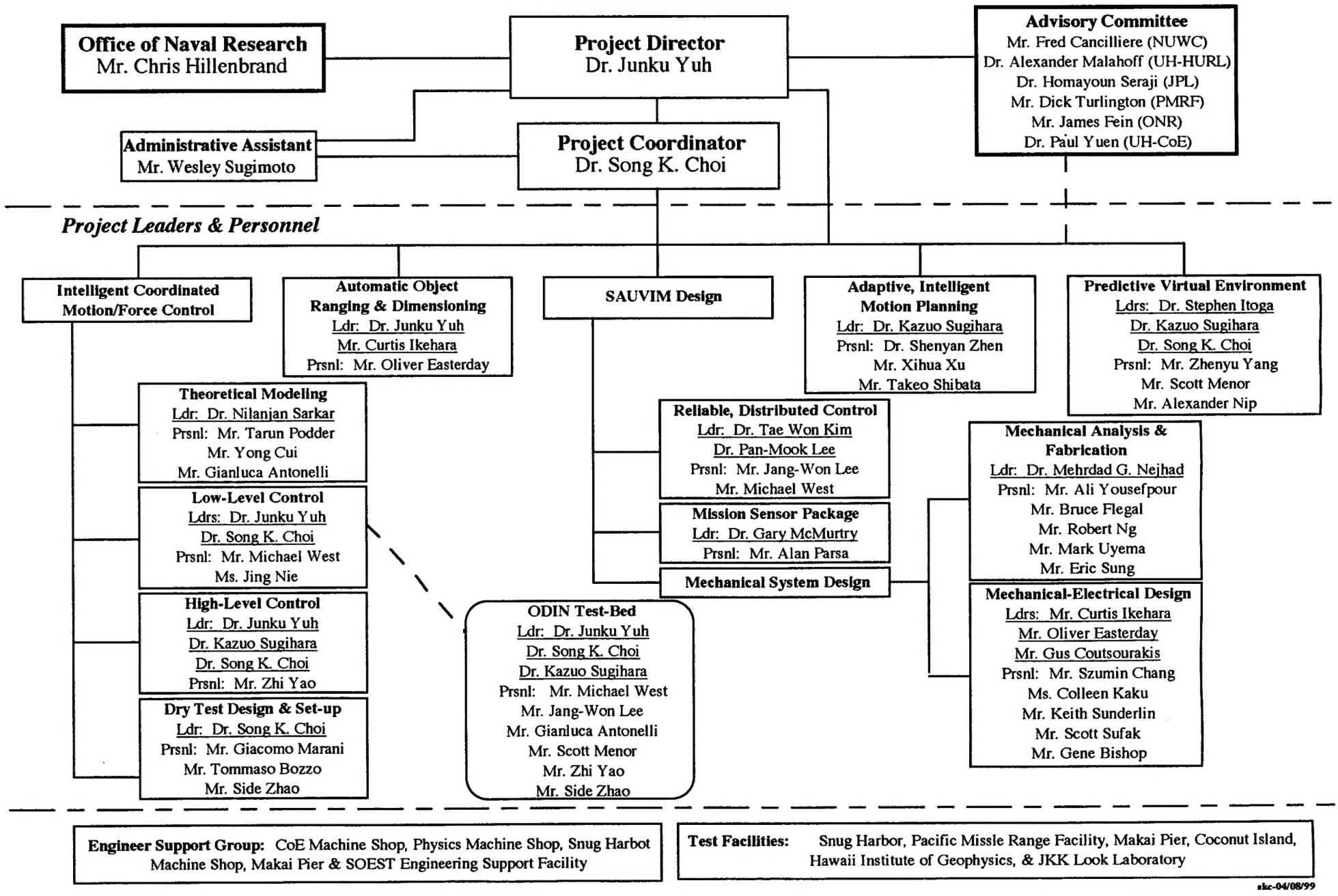

Engineer Support Group: CoE Machine Shop, Physics Machine Shop, Snug Harbot Machine Shop, Makai Pier & SOEST Engineering Support Facility

Test Facilities: Snug Harbor, Pacific Missle Range Facility, Makai Pier, Coconut Island, Hawaii Institute of Geophysics, & JKK Look Laboratory

skc-04/08/99

SAUVIM Schedule

	Activity	Start Date	Finish Date
1	AIMP: Prototype offline genetic algorithm	6/1	9/1
2	AIMP: Conduct simulation of offline GA	9/1	3/1
3	AIMP: Design interface to SAUVIM	10/1	3/1
4	AIMP: Implement offline GA in C/C++	10/1	7/1
5	AIMP: Prepare map data	4/1	10/1
6	AIMP: Redefine the online GA	6/1	9/1
7	AIMP: Prototype online GA	9/1	12/1
8	AIMP: Conduct simulation of online GA	12/1	6/1
9	AIMP: Design interface to SAUVIM	2/1	6/1
10	AIMP: Implement online GA in C/C++	2/1	10/1
11	AIMP: Implement trajectory generation	9/1	2/1
12	AIMP: Integrate C/C++ programs	1/1	10/29
13	AIMP: Test integrated system with VR	4/1	1/31
14	AIMP: Test motion planning with SAUVIM	5/3	1/31
15	PVE: DF: Survey	6/1	9/1
16	PVE: DF: Design software	9/1	6/1
17	PVE: DF: Communication	6/1	1/31
18	PVE: SS: Survey	6/1	9/1
19	PVE: SS: Purchase, customize, or write	9/1	6/1
20	PVE: SS: Revision of VE & interpolation	6/1	11/29
21	PVE: ANN: Study problem & model	6/1	12/1
22	PVE: ANN: Survey related work & compare	10/1	2/1
23	PVE: ANN: Design and implement	2/1	2/1
24	PVE: ANN: Evaluate by simulation & refine	1/1	1/31
25	PVE: ANN: Integrate w/ other components	5/3	1/31
26	PVE: Combine DF, SS, & ANN with VR	5/3	1/31
27	PVE: Test PVE with SAUVIM	6/3	1/31
28	AORD: LR: Survey	3/2	7/3
29	AORD: LR: Design & analysis	6/1	10/2
30	AORD: LR: Fabrication	10/1	6/28
31	AORD: LR: Design test & modify	4/28	1/31
32	AORD: LR: Fixture to SAUVIM	6/3	1/31
33	AORD: HD: Survey	3/2	6/1
34	AORD: HD: Design & analysis	6/1	4/28
35	AORD: HD: Fabricate, test, & modify	10/1	11/19
36	AORD: HD: Attach to dry test setup	4/1	11/19
37	AORD: HD: Modify for SAUVIM & test	5/3	1/31

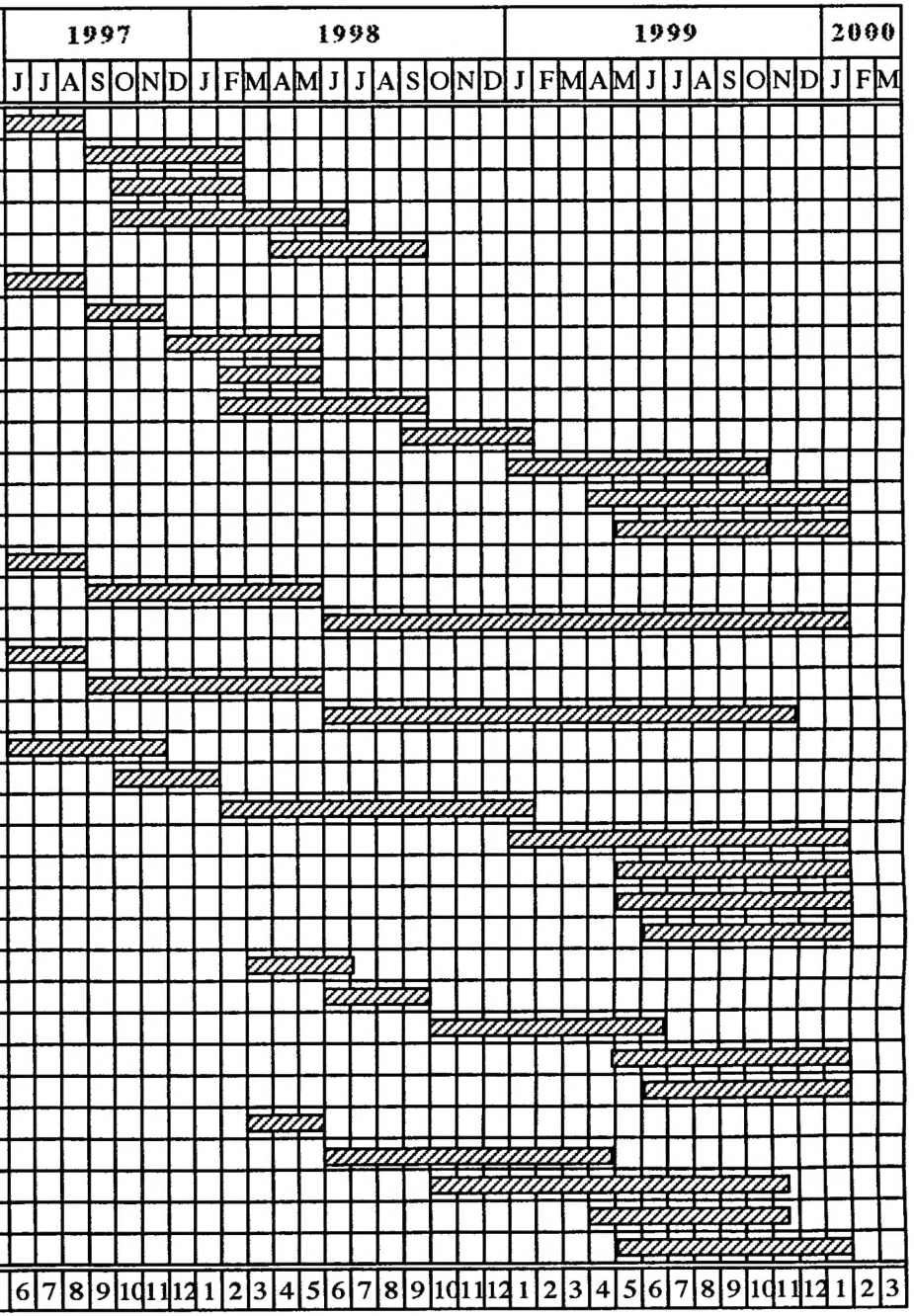

July 31, 1999

skc

SAUVIM Schedule

	Activity	Start Date	Finish Date
38	AORD: HD: Attach to SAUVIM	5/31	1/31
39	AORD: PA: Survey & research	7/1	10/1
40	AORD: PA: Conceptualize & design	9/1	7/1
41	AORD: PA: Fabricate, test, & modify	6/1	7/1
42	AORD: PA: Attach to dry test setup	4/1	1/31
43	AORD: PA: Modify for SAUVIM & test	1/1	1/31
44	AORD: PA: Attach to SAUVIM	6/1	1/31
45	SD: HDCA: Shape optimization	8/1	4/1
46	SD: HDCA: Hydrodynamic coefficient analysis	4/1	10/29
47	SD: HDCA: Hydrodynamic coefficient test	3/1	1/31
48	SD: MAF: Setup ANSYS & DYNA3D	6/1	8/1
49	SD: MAF: Preliminary design	8/1	12/29
50	SD: MAF: Design refinement	1/1	9/28
51	SD: MAF: Frame design & analysis	3/15	9/28
52	SD: MAF: Scaled model: design, fabricate & test	10/1	1/31
53	SD: MAF: Final design	5/1	1/31
54	SD: MAF: Fabricate set-up modification	5/1	1/31
55	SD: MAF: Fairing design	6/1	1/31
56	SD: MAF: Full scale PV & end-cap fabrication	6/1	1/31
57	SD: MAF: Full scale PV test	6/1	1/31
58	SD: MAF: Fairing fabrication	6/1	1/31
59	SD: MAF: Additional PV fabrication	6/1	1/31
60	SD: MED: Setup work space	6/1	1/29
61	SD: MED: Make mock test site	6/16	7/7
62	SD: MED: Design vehicle	6/16	3/30
63	SD: MED: Component identification	8/11	2/26
64	SD: MED: Redesign	9/8	5/29
65	SD: MED: Process purchases	9/29	5/29
66	SD: MED: Frame fabrication	11/17	4/28
67	SD: MED: CPU, I/O, software control	11/17	8/6
68	SD: MED: Install & test sensors	11/18	1/31
69	SD: MED: Install & test video	11/17	1/31
70	SD: MED: Arm modification	5/1	1/31
71	SD: MED: Install & test manipulator	5/1	1/31
72	SD: MED: Test integrated system	8/3	1/31
73	SD: MED: Shallow water system	2/13	1/31
74	SD: MED: Sub-assembly - fabricate, fesign, etc.	2/26	1/31

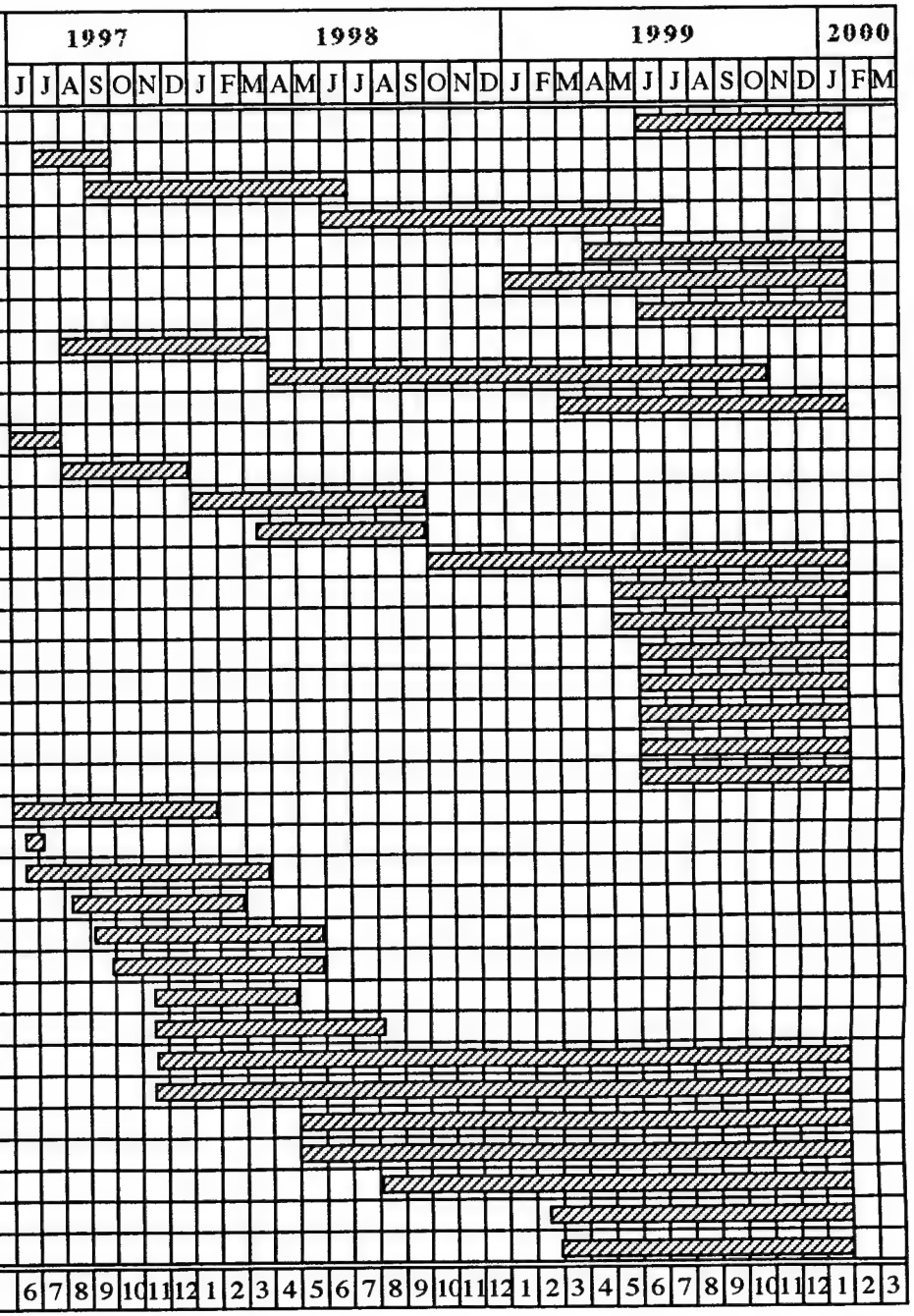

July 31, 1999

skc

SAUVIM Schedule

	Activity	Start Date	Finish Date
75	SD: RDC: Survey	8/1	12/29
76	SD: RDC: Purchase & design	11/3	2/26
77	SD: RDC: Test of VMEbus and boards & I/O	1/1	6/29
78	SD: RDC: Software architecture for vehicle/arm	6/1	9/28
79	SD: RDC: Real-Time OS programming	9/1	4/28
80	SD: RDC: Port software to Tornado PC	2/1	4/2
81	SD: RDC: Graphic simulator for VME system	3/1	12/29
82	SD: RDC: Make device driver for RTW	11/2	1/31
83	SD: RDC: Port software to RTW & debugging	3/29	11/29
84	SD: RDC: System integration	8/31	1/31
85	SD: RDC: System debugging & modification	11/2	1/31
86	SD: MSP: Survey	6/2	10/1
87	SD: MSP: Purchase & design	10/1	2/2
88	SD: MSP: Software development	2/2	6/1
89	SD: MSP: Field test & calibrate	6/1	10/1
90	SD: MSP: Integration with SAUVIM	2/1	1/31
91	SD: MSP: Shallow water test	10/1	1/31
92	ICM/FC: Manipulator survey	6/1	6/1
93	ICM/FC: Manipulator purchase & testing	6/1	1/31
94	ICM/FC: DTDS: Conceptualize & design	9/3	2/26
95	ICM/FC: DTDS: Test & modify setup	3/2	4/1
96	ICM/FC: DTDS: Attach manipulator & modify	3/1	7/29
97	ICM/FC: TM: Kinematics & dynamics	9/1	2/28
98	ICM/FC: TM: Motion coordination algorithms	3/1	7/31
99	ICM/FC: TM: Computer simulation of MC	8/1	1/31
100	ICM/FC: TM: Force control algorithm	11/1	12/31
101	ICM/FC: TM: Computer simulation of FC	1/1	1/31
102	ICM/FC: TM: Test on MC & FC	4/1	1/31
103	ICM/FC: LLC: Survey	6/2	10/1
104	ICM/FC: LLC: Design algorithm	9/1	2/26
105	ICM/FC: LLC: Impletment algorithm on ODIN	12/1	10/1
106	ICM/FC: LLC: Test & modify for SAUVIM	3/1	1/31
107	ICM/FC: HLC: Survey	9/1	1/31
108	ICM/FC: HLC: Design pilot algorithm	10/1	10/29
109	ICM/FC: HLC: Implement pilot algorithm	2/3	1/31
110	ICM/FC: Combine TM, LLC, & HLC w/ veh	12/1	1/31

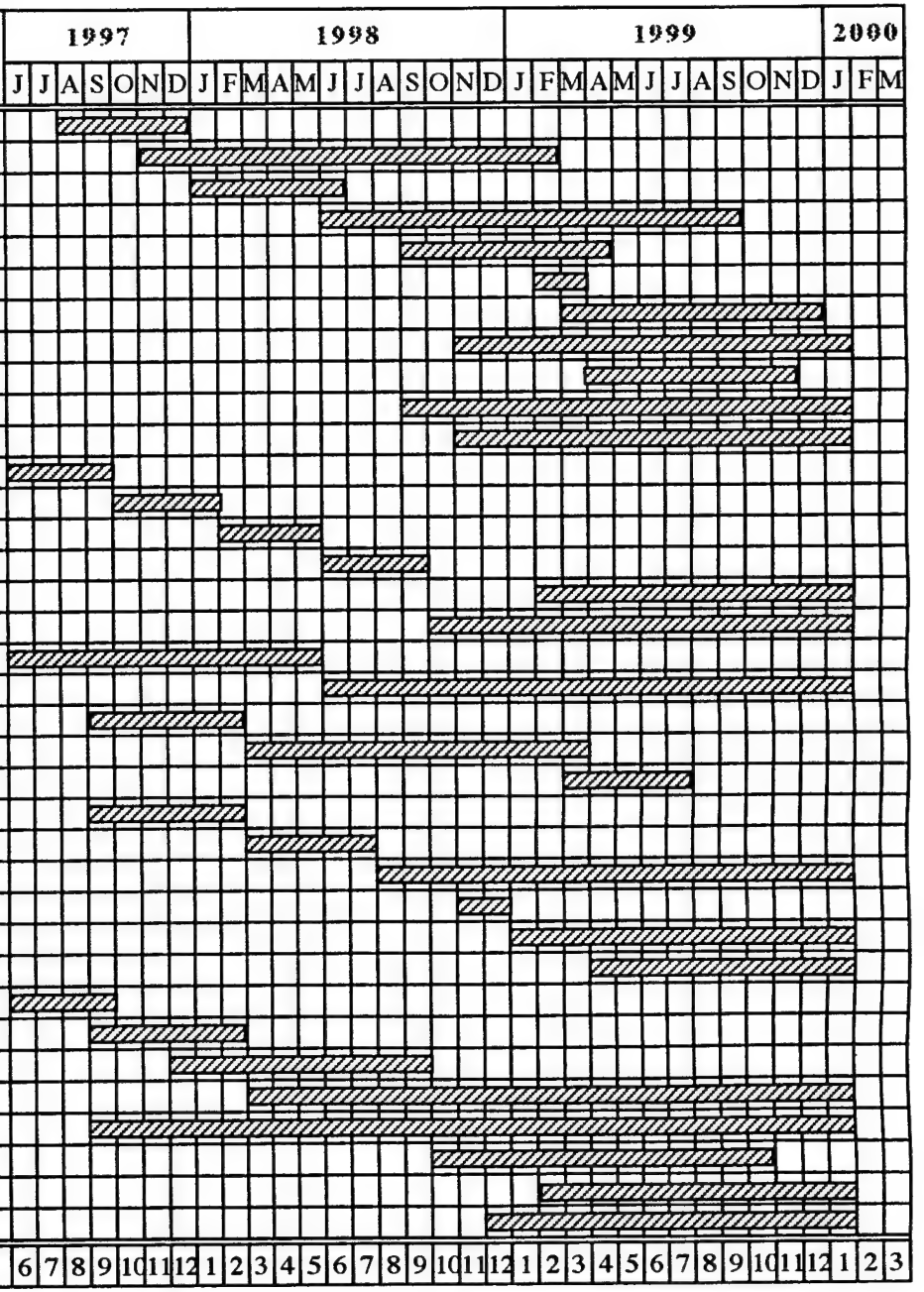

Adaptive, Intelligent Motion Planning (AIMP)

Project Leaders: Dr. Kazuo Sugihara
Personnel: Mr. Haidong Chang, Ms. Hongshi Chen, Mr. Xihua Xu, Mr. Yongcan Zhang & Mr. Shenyan Zhen

Objectives

This sub-project aims at developing the motion planning system for SAUVIM. It is intelligent and adaptive in the sense that the system is capable of decision-making at a task or mission level and can deal with unknown or time varying environment.

Three basic objectives are:

- To develop an off-line 3D motion planning algorithm;
- To develop an on-line 3D motion planning algorithm; and
- To develop an adaptive, intelligent motion planning system by integrating the off-line and the on-line planning algorithms.

Current Status (Tasks Completed During 8/1/98 - 7/31/99):

Introduction

Motion planning of an autonomous underwater vehicle (AUV) can be decomposed into path planning and trajectory generation, although they are not completely independent of each other. Path planning is the computation of a collision-free path in an environment with obstacles and optimizes it with respect to specific criterion. Trajectory generation is the scheduling of movements of an AUV along the planned path over time. This section addresses the path planning in 3D space.

An algorithm for path planning is said to be off-line if an environment is a known, static terrain and computes a path in advance. Otherwise, it is said to be on-line. An on-line algorithm must be capable of modifying a path in response to environmental changes such as a mobile obstacle and detection of an unknown obstacle. We propose a genetic algorithm (GA), which can be used for both off-line and on-line path planning.

The GA-based approach has two advantages. First, it is adaptive in the sense that it can respond to environmental changes and adjust its path "globally" to a new environment. Second, the dimension of space has much less effect on performance in the GA-based approach than others. Since path planning in 3D space is known to be computationally intractable, this makes the GA-based approach more attractive.

These results are presented in Sugihara 1997, Sugihara 1998a, and Sugihara 1998b.

Achievements

In order to clarify the accomplishments of the second year (1998-1999), the achievements of the first year (1997-1998) must be summarized, as follows:

- A 3D path-planning algorithm had been designed which had employed a genetic algorithm (GA) for both off-line and on-line planning.
- The GA-based 3D path-planning algorithm had been evaluated and tuned by simulation.
- The off-line path-planning program had been implemented in both C++ and C.

The major accomplishments of the second year are listed as follows in chronological order:

1. AIMP Software Version 1.0 alpha (December 1998)
   - The off-line and on-line path planning algorithms were implemented together in C;
   - A graphical user interface was implemented by using OpenGL; and
   - The outputs of the path-planning program for both off-line and on-line planning were tested in experiments with the ODIN AUV.

2. AIMP Software Version 1.0 (April 1999)
   - A program for trajectory generation, which generates a smooth curve for a path computed by the path-planning program and schedules the movement of SAUVIM on the curve, was developed in C. Algorithms for trajectory generation is explained below; and
   - The programs for path-planning and trajectory generation were integrated as software for motion planning.

3. AIMP Software Version 1.1 (July 1999)
   - A database of the seafloor mapping data was implemented on the main memory and incorporated into the motion planning software;
   - Major revisions of source code of the AIMP Software Version 1.0 were made which greatly improved the organization and data structures of the Version 1.0; and
   - The documentation was revised in accordance with the ***SAUVIM Software Development Process,*** which is also explained below.

Figures AIMP-1 & 2 show screen snapshots of the demonstration of AIMP Software Version 1.1. The initial terrain used is the submersed volcano, Loihi Seamount, and unknown obstacles are hypothetically added to obstruct the path of the vehicle.

Trajectory Generation

The path-planning program produces a path represented by a sequence of adjacent cubes in a 3D grid structure. Such a path is intuitively viewed as a corridor, which begins at the start, passes intermediate waypoints, and ends at the destination. Once the path is produced, a smooth curve inside the corridor must be generated (Figure AIMP-3).

Input: The path, the start point, the destination, the initial velocity, and the final velocity.
Output: A curve such that it stays inside the path and its tangent lines at the start and the destination are same as vectors of the initial and final velocities, respectively.

The Hermite curve is used to solve this problem as follows. We sequentially produce a curve between two consecutive waypoints including the start and the destination, beginning from the start. Suppose a curve is represented in a parametric form with 4 constants a, b, c and d, so

$$p(t) = a\,t^3 + b\,t^2 + c\,t + d$$

where p(t) denotes a vector of 3 coordinates x(t), y(t) and z(t) such that $0 \le t \le 1$. With the boundary conditions at the first waypoint (t=0) and the second waypoint (t=1), p(t) must satisfy the following, where v1 and v2 are the velocities at the first and second waypoints, respectively.

$$p(0) = d$$
$$p(1) = a + b + c + d$$
$$p'(0) = v1 = c$$
$$p'(1) = v2 = 3a + 2b + c$$

By solving this system of linear equations, we can determine the constant coefficients and hence compute the curve p(t) which is intuitively S-shaped.

Next, the movement of a vehicle on the curve must be scheduled. To develop the first version of software for trajectory generation, we simplify this scheduling problem by assuming that a vehicle's speed changes in the way shown in Figure AIMP-4 and the vehicle's orientation is always same as a tangent line of the curve at the current location.

Input: The generated curve, the initial speed at the start, the final speed at the destination, constant acceleration, constant deceleration, the cruising speed, and the unit time Δ in scheduling.

Output: A sequence of locations for the vehicle to be located on the curve at each time $i\,\Delta$ where i is a natural number.

In general, choices of a curve and a schedule on it are interrelated. Hence the curve generation and scheduling should be solved together in order to optimize them simultaneously. For example, the maximum cruising speed may depend on the curvature and the maneuverability of a vehicle (e.g., minimum turning radius). In addition, the vehicle's dynamics should be taken into account. This is one of the issues to be investigated in future.

Software Development Process

In order to assure the software quality, control version upgrades, and manage the software documentation, we designed and implemented the standardized process of software development described as follows.

Every Week (performed by each member)
Take backup of all the current software and a progress report together with each member's activity log on ZIP disks. The backup hierarchically consists of the following.

```
sw_name/        (software name)
    ver#/       (version number)
    src/        (source code)
```

```
        doc/        (documents)
        data/       (data or examples for testing)
        demo/       (binary files or a compressed file for a demo)
        report/     (progress reports with activity log)

    backup_log      (backup history on the ZIP disk)
```

Once Every One or Two Months (performed by all members)
The latest version of each software is tested by another member, as follows.

1. Try to reinstall the software from the backup;
2. Try to reproduce and run a demo of the software; and
3. Give the author comments/suggestions based on this experience.

The author(s) will revise the software including documentation accordingly.

Upon the End of a Term or Substantial Progress (performed by a supervisor)

1. Compile new documents and/or revise previous documents;
2. Create a new version of software; and
3. Certify it as the latest version on the backup and keep it in duplicate.

A version upgrade should be done as follows.

1. Clean up source code of software.
   - Test whether it works after the cleanup;
   - Write informative imbedded comments; and
   - Add the version number, author(s)' name(s), date, and copyright at the beginning of every source file.

2. Write the following documentation about the software.
   - Requirement Specifications: Objectives, functionality (what to do, especially, input/output relationships), hardware/software environments, etc.
   - Design Specification: Overall architecture of your software, module structure, caller/callee relationships with data flow, algorithms, data structures, etc. Use of diagrams is strongly desired.
   - Reference Manual: Any implementation details, which are important for other programmers to know in order to maintain for correction, improvement and adaptation.
   - User's Manual with README: Instructions for installation and operation. Use of screen snapshots is strongly suggested.
   - Testing Document (optional, but desirable): Methods/tools for debug of the software, input/output data in testing, performance evaluation, etc.

In case of an upgraded version, **Upgrade Note** is also required, which describes what are modifications, why & how the modifications are made, which parts of software and documents have major changes, etc. With the upgrade note, a person who has some knowledge about the previous version can save time to understand the upgraded version.

Future Tasks

- To implement an interface of the mapping database to real-time sensory inputs.
- To integrate the motion planning software into PVE (Predictive Virtual Environment).
- To transport the software to a SAUVIM's on-board CPU.
- The development of AIMP will continue through Phase II, such as an application of fuzzy control to trajectory generation.

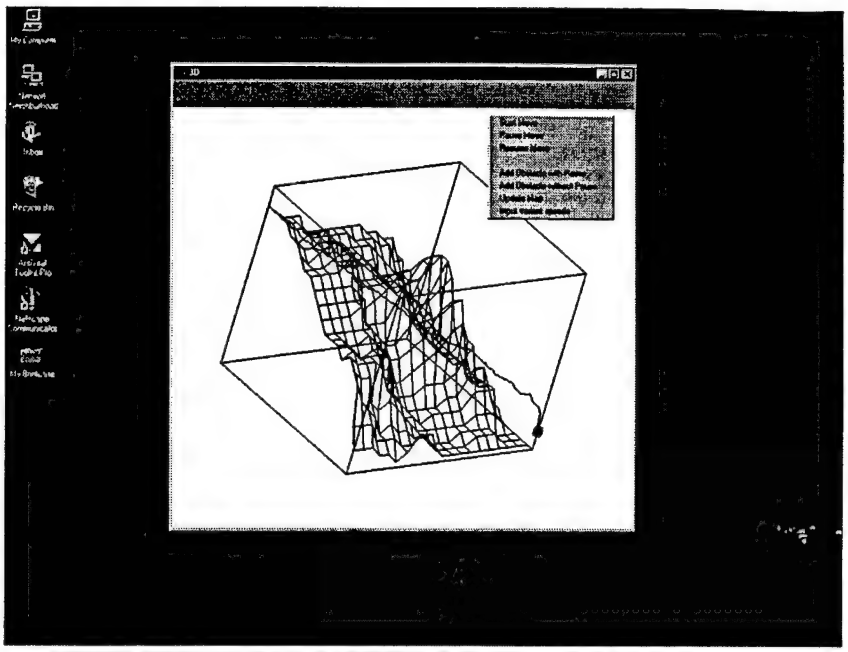

Figure AIMP-1: A Screen Snapshot of Software Version 1.1.

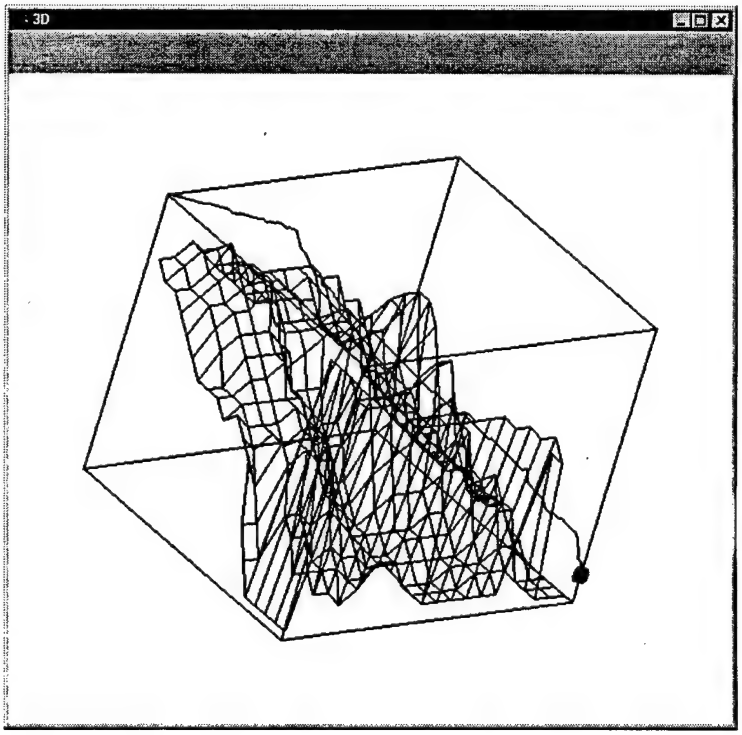

Figure AIMP-2: 3-Dimensional Representation of the Output After Obstacles are Added.

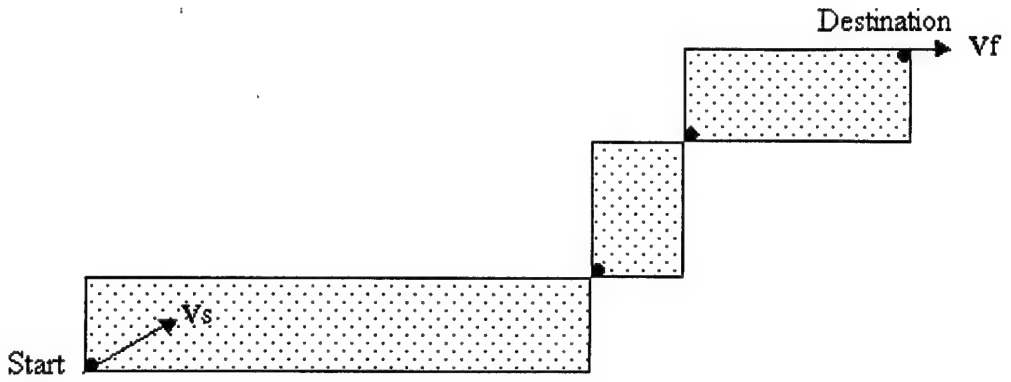

Figure AIMP-3: Inputs for Generation of a Curve from a Path.

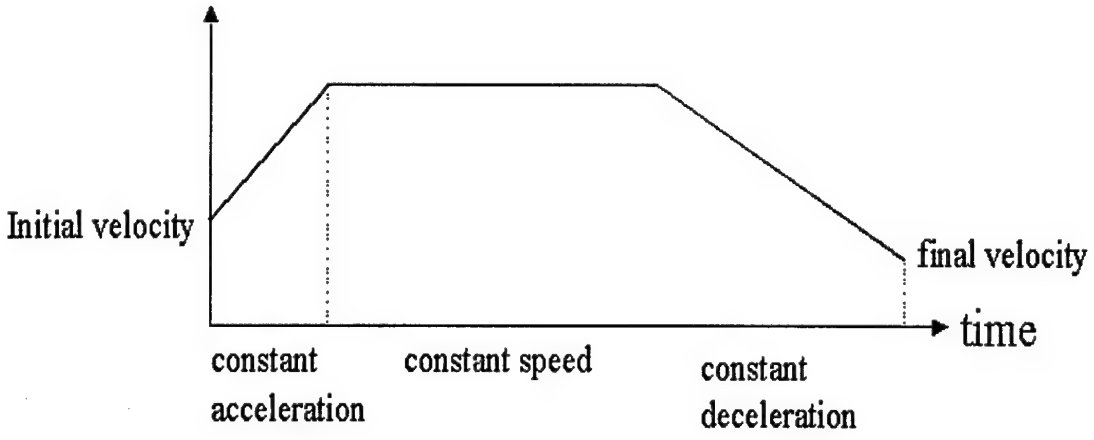

Figure AIMP-4: A Schedule of Speed on the Curve.

Automatic Object Ranging and Dimensioning (AORD)

Project Leaders: Dr. Junku Yuh & Mr. Curtis Ikehara
Personnel: Mr. Oliver Easterday & Mr. Marc Rosen

Objectives

To develop a multiple sensor configuration to be utilized during SAUVIM's intervention mission. The configuration will allow accurate vehicle positioning, workspace dimensioning and ranging, and manipulator homing to the task object.

Methodology

A three-sensor combination has been considered for this task. They are 1) a passive arm sensor system that will provide accurate information for vehicle positioning, 2) a laser ranging sensor system that will provide workspace dimensioning and ranging, 3) a manipulator homing sensor system that will allow accurate homing of the manipulator gripper to workspace location.

Each of the AORD system is described below:

Passive Arm (PA)

The passive arm system (PA) is a multi-jointed mechanical arm that utilizes direct kinematics to sense the proximity and orientation between its two ends; specifically, each axis of each joint senses angular position through the use of a potentiometer. One end of the arm is mounted and fixed within the forward cavity of the SAUVIM vehicle adjacent to the robotic arm. The other end of the arm is designed to temporarily attach to the workstation, by means of an electro-magnet, during intervention tasks. Hence, any changes in the relative proximity between the vehicle and the workstation will be sensed by angular displacements in the joints of the PA. The PA will be stored in a crutched position during non-interventive mission periods. The vehicle's robotic arm will aid in both the crutching and un-crutching of the PA as well as position it for use during interventive tasks.

Laser Ranging System (LRS)

The laser array ranging system is a sensor system designed to provide the vehicle control system with navigation information relative to a predetermined target at the task site. The operational range of this system is between 1-3 meters and is designed to supplement longer-range sonar system.

Manipulator Homing Sensor (MHS)

A camera will be attached to the robotic arm, and will be used to acquire image data for the homing sensor. The homing sensor is tasked to locate and identify shapes. Specifically, it will locate a predetermined target, which will be used as a reference point, and will determine the distance and angles between the robot arm and the target.

Current Status (Tasks Completed During 8/1/98 - 7/31/99):

Passive Arm

As mentioned in the previous report, the prototype PA is shown in Figure AORD-1. The mechanical fabrication of the deep-sea PA is complete (Figure AORD-2 & 3). The fabrication of over forty pieces that locate the seven degrees-of-freedom (dof) of the arm across two, three-axis gimbals and one single-axis hinge joint has been accomplished. Preliminary assembly has established that the backlash and the jitter in the joints are negligible. Most of the components are comprised of aluminum 6061, chosen for both its relatively high resistance to corrosion from seawater and its ease of machining. The bearing surfaces are bronze bushings; these are not exposed to seawater being internal to the arm. The entire structure is filled with white grade No. 9 mineral oil; thus serving as the lubricating medium and compensating fluid.

The original flexibility specified for the PA is preserved in the deep-sea version. The range of swing of the base gimbal allows freedom of movement of the base leg of the PA in a cone that ranges up to 60 degrees off the perpendicular line of the base canister. Redesign of the magnet canister allows the same range of freedom for the lower leg of the PA. The hinge joint in its final configuration can range from a full extension (180 degrees) to a 60 degrees crutched angle.

The procurement of the hardware fittings including wire, joint bellows, clamps, electrical penetrators, etc. are complete and assembly has begun.

In the meantime performance testing has proceeded on the prototype PA setup (Figure AORD-4). This arm, which features identical kinematic topology and connected to a Pentium 60 computer, has established repeatability of surface location and orientation determination.

In the prototype PA, the ranging relative error is within 5%, and the orientation error is also within 5%. At full extension, the relative positioning error due to accumulated angular errors works out to be within 1 cm.

The final step in the deep-sea PA involves completing the wire-up and assembly of the passive arm, performing tuning and calibration of the potentiometers in the arm, and full wet testing of the arm. The software development is to port the C-code for the prototype to the VME system, adjust some of the arm characteristics in the static array, code optimization, and routines to allow velocity tracking of the magnet head relative to the base.

Laser Ranging System

The Laser Ranging System is a parallax-based system consisting of multiple lasers in a regular geometric array, a camera to image the spots formed by the lasers on any intersecting solid surfaces, and a frame grabber/micro-controller to digitize and process the camera image (Figure AORD-5), then compute the range and report the data to the SAUVIM navigation CPU system via a serial link.

The LRS is proceeding towards a full ocean depth version. Completed are the camera vessel housing, array frame, and the sixteen pressure housings for the diode lasers (Figures AORD-6 & 7). The camera housings are aluminum 6061 casings that sit at the center of the array. Opaque methacylate plastic is used for fabrication of the array frame and machining tolerances of ±0.002" were specified to insure a parallel orientation of the tubes.

The proof-of-concept testing was performed using the 4-laser array dry, prototype setup in a darkened room. Laser attenuation experiments were performed also to anticipate operational range. As a result of these tests, two parallel green lasers were added to the array. These lasers are used for self-calibration measure as well as for ranging to greater distances than the red lasers in the seawater medium. Being parallel and paired, the distance between these two lasers can be used as a reference, which in turn is used to determine the distance to an occluding object provided that the given surface is relatively flat.

The immediate future tasks for this system entail completion of the pressure vessels for sealing the lasers and installation of these into the array. The code will be modified to account for the 16-lasers now comprising the array. The following software modifications are called for: (1) reducing code latency by mapping lasers to slots on the frame grabber board, (2) adding a self-calibration routine to exploit the paired green lasers, and (3) adding a moving Brownien-motion filter routine in anticipation of stirred sediment particles in the field of view. Finally, the integration of the completed system into the SAUVIM navigation CPU will be performed.

Manipulator Homing Sensor

The Manipulator Homing Sensor (Figure AORD-8) hardware fabrication is close to complete. The camera has been ordered along with the PC-104 and frame grabbing hardware that will support it. The pressure vessel enclosure for the homing sensor is complete and fabrication of the mounting bracket to fasten to the Ansaldo arm is also complete. The development of the skeletal frame grabbing and storing code for the PC-104 has also been accomplished.

The target that will be used for object recognition and manipulator orientation was changed before the last site visit from basic geometric shapes to a system of circular barcode for a couple of compelling reasons. Among these reasons are: (1) the barcode algorithms and technology are well-established, (2) the barcode targets are radially symmetric resulting in a simplification of the object recognition routines, (3) the targets can now be assigned identification numbers via the barcodes, and (4) the environmental noise tolerance of barcode systems is higher.

The major remaining tasks for this system are the software algorithms ranging from the completion and coding of the barcode recognition to the ranging and target orientation routines. Testing of the homing sensor in the dry lab setup will continue before overall integration to the SAUVIM vehicle.

Future Tasks

- Complete wiring of passive arm, calibrate, wet test, and integrate to SAUVIM Navigation VME CPU and I/O boards.
- Modify PA arm software to allow for first-derivative/velocity determination, and optimize code to remove loop latencies.
- Complete installing leads into laser-array pressure vessels, modify software from dry-test setup from a 4-array to an operational 16-laser array system. Add routines for self-calibration and moving (Brownien) particle rejection routine.
- Install homing sensor camera and vessel on to the Ansaldo arm and add circular barcode detection & tracking logic to skeletal image frame grabbing code.

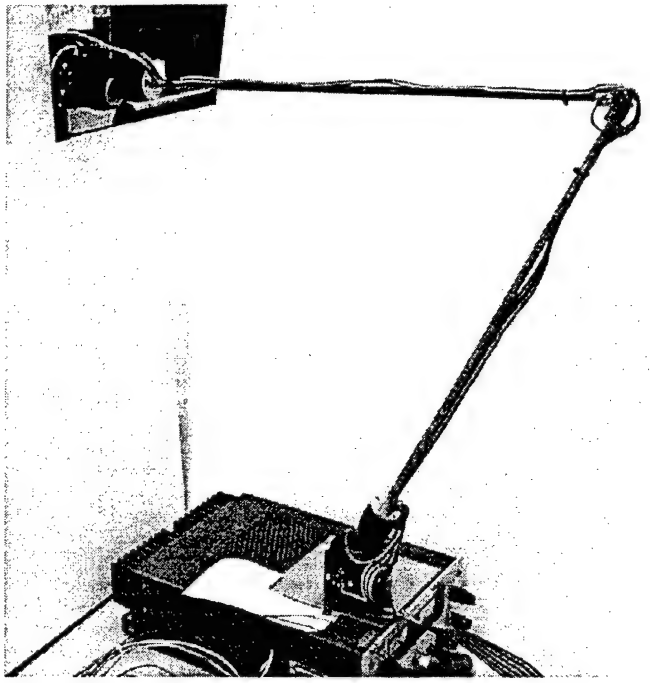

Figure AORD-1: Prototype of Passive Arm Sensor.

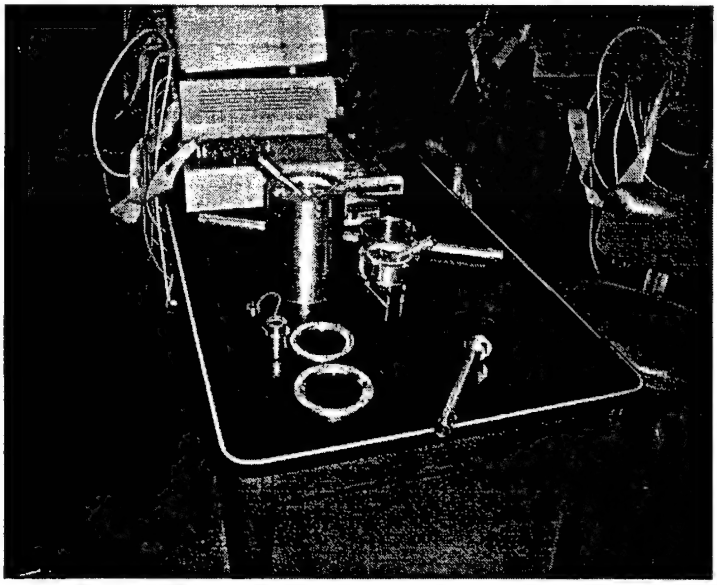

Figure AORD-2: Deep Ocean Passive Arm Disassembled.

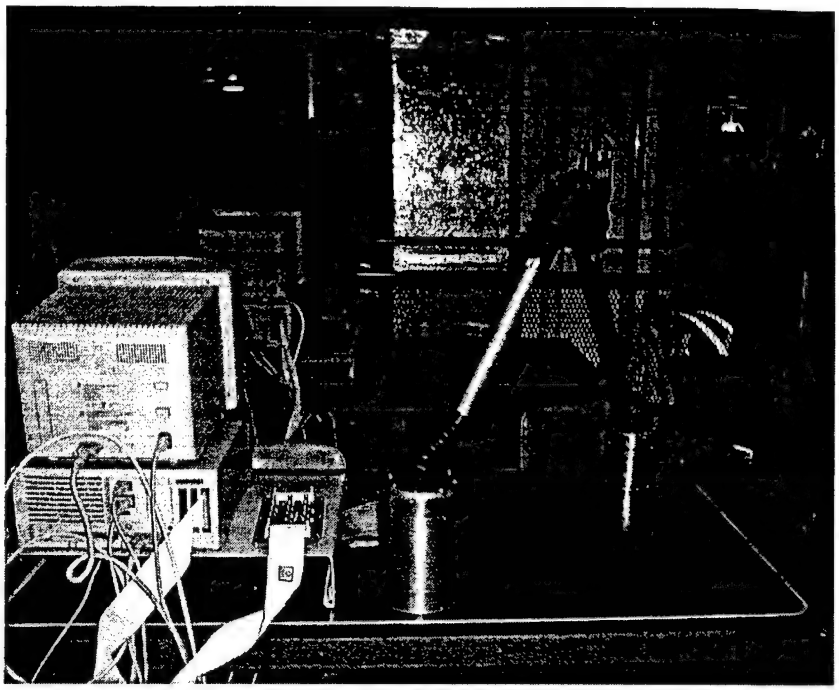

Figure AORD-3: Deep Ocean Passive Arm Assembled

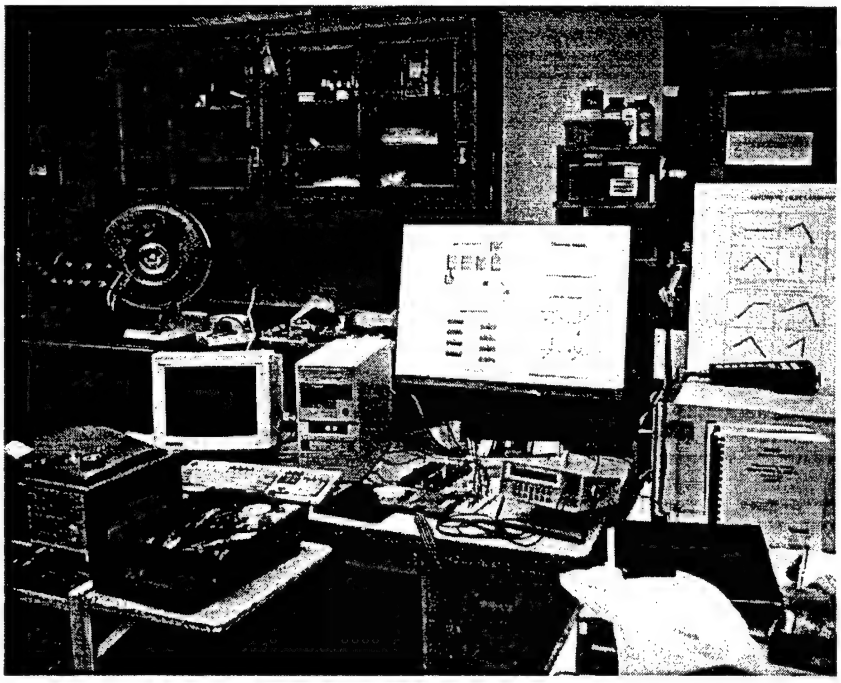

Figure AORD-4: Prototype Passive Arm Set-Up

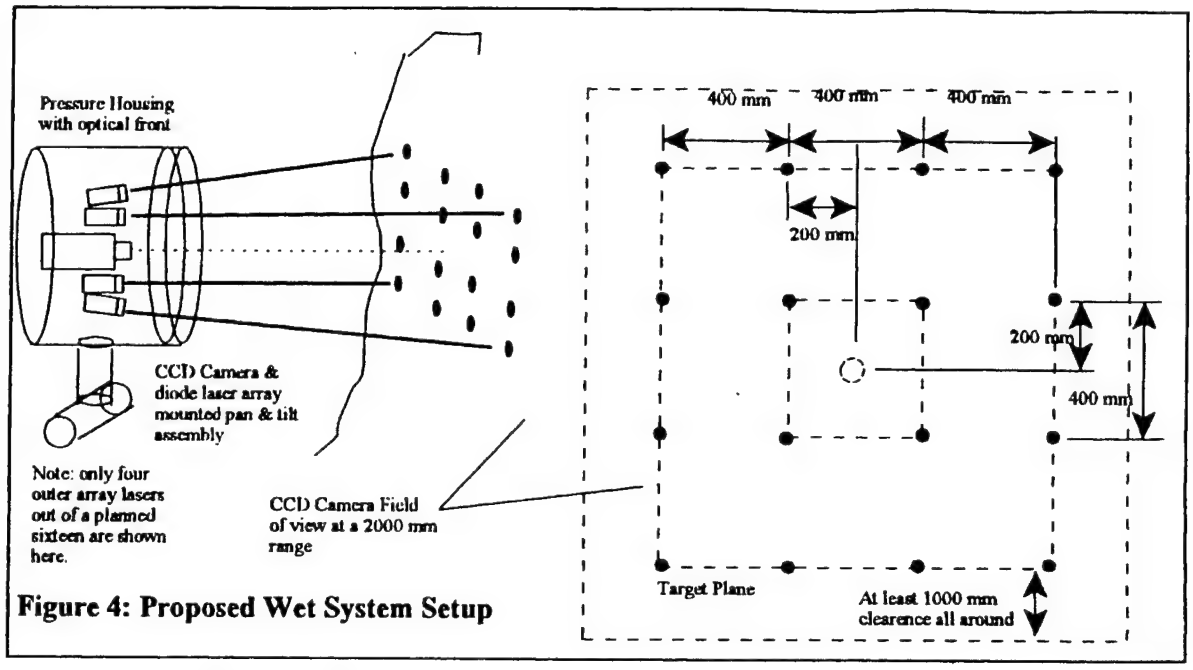

Figure AORD-5: Diagram of Laser Ranging System

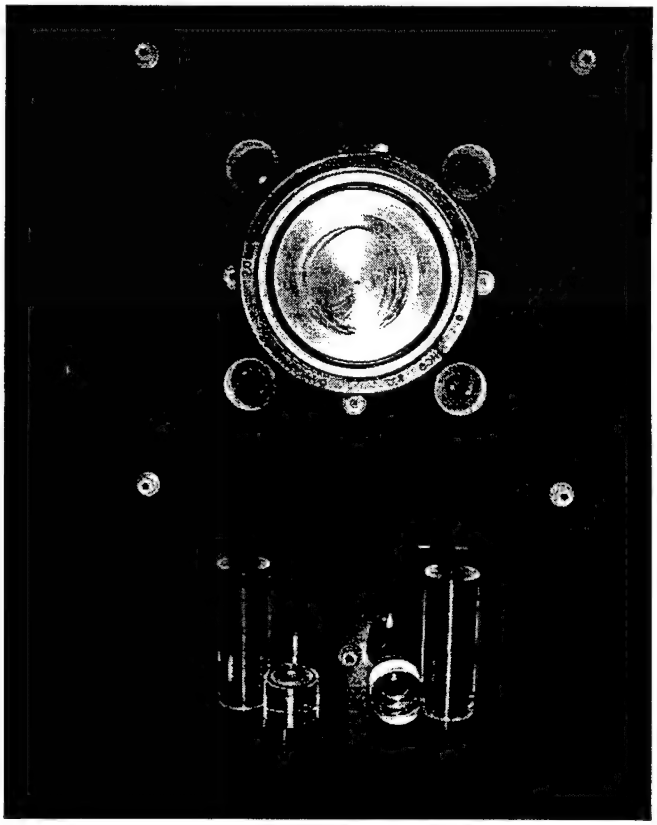

Figure AORD-6: Close-Up of Laser Ranging System with Two, Laser Housing at Bottom.

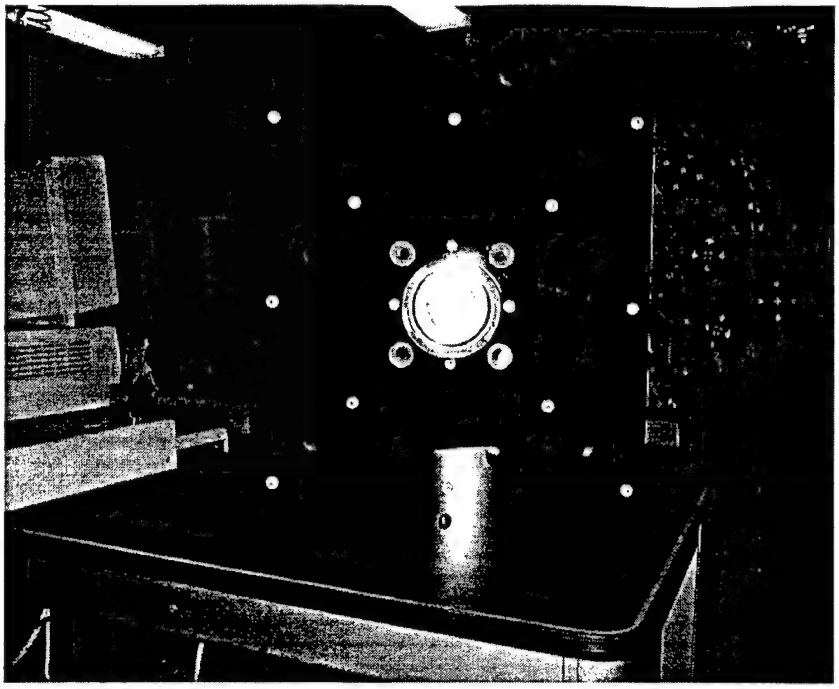

Figure AORD-7: Full View of Laser Ranging System Array

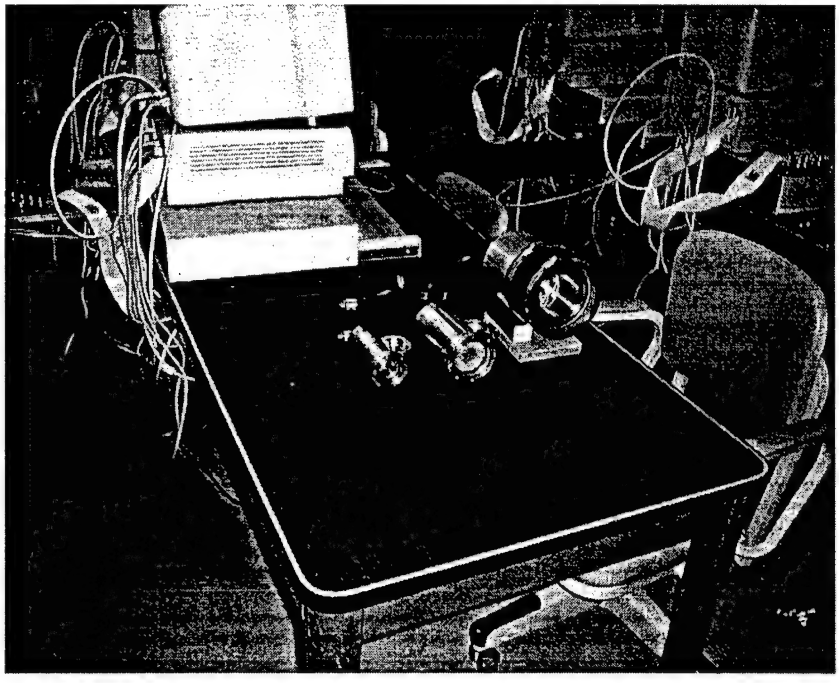

Figure AORD-8: Various Deep Ocean Camera Housing – The Small Housing is for the Manipulator Homing Sensor

Intelligent Coordinated Motion/Force Control (ICM/FC)

Project Leaders: Dr. Nilanjan Sarkar, Dr. Junku Yuh & Dr. Song K. Choi

The main technical progress of the ICM/FC group is described in the following sections: Theoretical Modeling, Low-Level Control, High-Level Control, and Dry Test Design and Setup.

Theoretical Modeling (TM)

Project Leaders: Dr. Nilanjan Sarkar
Personnel: Mr. Tarun Podder, Mr. Yong Cui & Mr. Gianluca Antonelli

Objectives

Theoretical investigations into the dynamics, motion coordination and force control of Underwater Vehicle-Manipulation System (UVMS)

Current Status (Tasks Completed During 8/1/98 - 7/31/99):

Summery of Accomplishments:

We have derived dynamic equations of motion of a general UVMS by using the *Quasi-Lagrange* approach, (2) we have formulated a new drag force optimization algorithm utilizing kinematic redundancy and gradient projection method, (3) we have formulated direct force control scheme and impedance control scheme, and (4) we have performed computer simulation for a 6 degrees of freedom (DOF) vehicle and an onboard 3 DOF robot manipulator for trajectory following tasks using non-regressor based adaptive control and computed torque control techniques.

Introduction

The dynamics of UVMS is highly nonlinear, coupled and time-varying. It also includes hydrodynamic parameter uncertainties. When one or more manipulators are mounted on the vehicle, it becomes a multi-body system and the modeling becomes more complex. Evaluation of hydrodynamic reactions on a rigid body moving unsteadily in an unbounded perfect fluid, which is otherwise at rest, is one of the classical problems in fluid mechanics. The Kirchhoff-Lagrange formulation expresses the forces and moments acting on such a 6 DOF body in terms of velocities and added-mass tensor (Lamb 1945, Kochin 1965, Milne-Thomson 1968).

In the past several years, researchers (Lewis 1984, Sagatun 1992, Healy 1992, Kato 1993, Yuh 1994, Goheen 1990) have investigated the modeling and control of Remotely Operated Vehicles (ROVs) and Autonomous Underwater Vehicles (AUVs). Researchers have also performed modeling and control of underwater vehicle-manipulator systems. Yuh 1994 proposed a neural network control system using a recursive adaptation algorithm with a critic function (reinforced learning approach). Goheen 1990 investigated a controller as an autopilot for underwater vehicles. McMillan 1995 developed a dynamic simulation algorithm based on the articulated-body dynamics for an underwater vehicle with a robotic manipulator. Tarn 1996 developed a dynamic model of an underwater vehicle with a robot manipulator using Kane's method. Experiments conducted at the Monterey Bay Aquarium Research Institute (MBARI) using the OTTER vehicle have shown that dynamic interaction between an arm and a vehicle can be very significant [McLain 1996]. Wit 1998 has designed a robust nonlinear control for an underwater vehicle to compensate the coupling effects due to an onboard robot arm. Mahesh 1991 has derived the dynamic equations of motion for the underwater vehicle and manipulator system using NBOD2 approach. Several researchers [Liegeois 1977, Klein 1983, Chan 1995, Hollerbach 1987, Nakamura 1985] have investigated the merits and demerits of kinematic redundancy of robot manipulators in the light of mechanical design, dexterity measures, multi-criteria optimization, controller design and computational considerations. Most of

these works have been performed for land-based robotic systems and space robotic systems. There are few works [Antonelli 1998, Sarkar 1999a, Sarkar 1999b] where the researchers have exploited the kinematic resolution of redundancy to satisfy secondary performance criteria for underwater robotic systems.

To increase the adaptability of UVMS for underwater environment, such as underwater pipe-line maintenance, cable burial when the end-effector of the manipulator has to interact with the environment, force control must be included into the control system of UVMS. In Dunnigan 1996, a hybrid position/force control scheme was developed and tested on a TA9 hydraulic manipulator mounted on an underwater vehicle. Kajita 1997 presented a method utilizing the restoring force generated by thrusters to compensate the contact force at the endpoint of the manipulator mounted on a floating vehicle. Limiting our attention to elastically compliant, frictionless environments several control schemes have been proposed in the literature. An overview of interaction control schemes can be found in [Canudas 1996, Whitney 1987]. A first strategy is the hybrid force/position control [Raibert 1981]: the force and position controllers are structurally decoupled according to the analysis of the geometric constraints to be satisfied during the task execution. These control schemes require a detailed knowledge of the environment geometry, and therefore are unsuitable for use in poorly structured environments and to the occurrence of unplanned impacts.

To overcome this problem, parallel force/position control can be adopted [Chiaverini]. In this case, position and force loops are closed in all task-space directions, while structural properties of the controller ensure that a properly assigned force reference value is reached at steady state. Since the two loops are not decoupled, a drawback of parallel control is the mutual disturbance of position and force variables during the transient.

Dynamic Equations of Motion

The dynamic equations of motion of the underwater vehicle-manipulator system (UVMS) have been derived using the *Quasi-Lagrange* approach. We have formulated a new algorithm to minimize the total drag effect on the whole system utilizing kinematic redundancy resolution scheme and gradient projection method.

When the base of the manipulator is not fixed in inertial frame, as is the case for underwater robotic vehicle, it is convenient to express the Lagrangian not in terms of the velocities expressed in inertial frame but in terms of velocities expressed in body-attached frame. Moreover, for feedback control, it is more convenient to work with velocity components about body-attached axes, as sensors measure motions and actuators apply torques in terms of components about the body-attached reference frame. But the components of body-attached angular velocity vector cannot be integrated to obtain actual angular displacement. As a consequence of this, we cannot use Lagrange equation directly to derive the dynamic equations of motion in the body-attached frame. However, this problem is circumvented by applying the *Quasi-Lagrange* approach.

The fundamental form of Lagrange's equations of motion in the matrix form is

$$\frac{d}{dt}\left(\frac{\partial T}{\partial \dot{q}}\right)-\left(\frac{\partial T}{\partial q}\right)=Q \qquad (1)$$

where $T = T(q,\dot{q})$=total kinetic energy of the system, q = vector of generalized coordinates expressed in inertial frame, $\dot{q}$ = vector of first time derivative of the generalized coordinates, Q = vector of generalized forces applied to the system.

$$\frac{d}{dt}\left(\frac{\partial \overline{T}}{\partial w}\right) + B^T \gamma \frac{\partial \overline{T}}{\partial w} - B^T \frac{\partial \overline{T}}{\partial q} = \tau \tag{2}$$

This is referred to as *Lagrange's equations for quasi-coordinates*, where the notations $w = A^T \dot{q}$, $\dot{q} = Bw$, $\gamma = \left[w^T B^T \frac{\partial A}{\partial q}\right] - \left[w^T B^T \left[\frac{\partial A}{\partial q}\right]\right]$, $\tau = B^T Q$, $A^T B = I$, $w = [w_1, w_2, ..., w_n]^T$ is the velocity vector expressed in body-attached frame also called as *quasi-velocities* and $\overline{T} = \overline{T}(q,w)$= total kinetic energy of the system in terms of quasi-velocities.

The final form of the dynamic equations of motion of the UVMS is as follows:

$$M_b(q_m)\dot{w} + C_b(q_m, w)w + D_b(q_m, w)w + G_b(q) = \tau_b \tag{3}$$

where the subscript *'b'* denotes the corresponding parameters in body-attached frames of the vehicle and manipulator, $M_b(q_m)$ is the $(6+n)\times(6+n)$ inertia matrix including the added mass inertia matrix, $C_b(q_m, w)$ is the $(6+n)\times 1$ vector of centrifugal and Coriolis forces including terms due to added mass, $D_b(q_m, w)$ is the $(6+n)\times 1$ vector of drag forces, $G_b(q)$ is the $(6+n)\times 1$ vector of gravity and buoyancy forces, τ_b is the $(6+n)\times 1$ vector of forces on UVMS, $q = [q_v, q_m]^T$, $q_v = [q_1, ..., q_6]^T$, and $q_m = [q_7, ..., q_{6+n}]^T$ are the generalized coordinates. Detail derivation of dynamic equations of motion can be found in [29].

Redundancy Resolution

In general, UVMS is a redundant system, because the vehicle is commonly designed to provide motion in six directions; hence, the onboard manipulator adds redundant degrees of freedom. A kinematically redundant system is attractive due to several reasons. This redundancy can be exploited to achieve: (i) greater dexterity in maneuvering in a workspace with obstacles, (ii) configurational singularity avoidance, (iii) optimization of multiple performance criteria. Redundancy can be resolved either kinematically or dynamically (kinetically) to achieve desired goals.

Kinematic Resolution of Redundancy

The task-space and joint-space velocities of a UVMS are related as

$$\dot{x} = J(q)\dot{q} \tag{4}$$

where $\dot{x}$ is the $m\times 1$ vector of task-space velocities, and $\dot{q}$ is the $(6+n)\times 1$ vectors of and joint-space velocities, $J(q) \in R^{m\times(6+n)}$ is the end-effector Jacobian matrix. For a kinematically redundant system $m<(6+n)$. The least-norm (LN) solution to Equation (4) (dropping the dependent variable) is

$$\dot{q} = J^{+}\dot{x} \tag{5}$$

where $J^{+} = J^{T}(J\,J^{T})^{-1}$ is called Moore-Penrose generalized inverse or pseudo-inverse of J. The complete solution to Equation (4) which includes homogeneous solution with Equation (5) can be written as

$$\dot{q} = J^{+}\dot{x} + (I - J^{+}J)\dot{\phi} \tag{6}$$

where $(I - J^{+}J)$ is the projection matrix onto the null-space of J and $\dot{\phi} \in R^{(6+n)}$ is an arbitrary vector.

Dynamic (Kinetic) Resolution of Redundancy

To incorporate the generalized inverse into dynamics, pseudo-inverse must be formulated in terms of acceleration. Differentiating Equation (4) we obtain the task-space and joint-space accelerations relation as

$$\ddot{x} = J\,\ddot{q} + \dot{J}\,\dot{q} \tag{7}$$

The least-norm solution for $\ddot{q}$ is

$$\ddot{q} = J^{+}(\ddot{x} - \dot{J}\,\dot{q}) \tag{8}$$

where $\ddot{x}$ is the $m \times 1$ vector of task-space accelerations and $\ddot{q}$ is the $(6+n)\times 1$ vector of joint-space accelerations, $\dot{J}$ is the first time derivative of Jacobian, J.

The complete solution to Equation (7) can be written as

$$\ddot{q} = J^{+}(\ddot{x} - \dot{J}\dot{q}) + (I - J^{+}J)\ddot{\phi} \tag{9}$$

where $(I - J^{+}J)\ddot{\phi} \in N(J)$ is the null-space solution and $\ddot{\phi} \in R^{(6+n)}$ is an arbitrary vector which can be utilized to stisfy various performance criteria.

A New Drag Minimization (DM) Algorithm

In case of underwater robotic system, a major portion of the energy supplied by the battery is consumed to overcome the hydrodynamic drag effects. Hence, it is an important direction of research to minimize drag effects on the UVMS. Here, we formulate a new algorithm, which is capable of minimizing hydrodynamic drag effects on whole system (i.e. vehicle + manipulator). We resolve the redundancy at acceleration level (given in Equation (9)) and derive a suitable null-space vector by applying Gradient Projection Method (GPM) to minimize drag forces on UVMS. The rationale for choosing GPM is that the negative gradient of a scalar function compute the local minimum of the function in successive iterations. We derive a new algorithm to minimize drag force utilizing dynamic resolution of redundancy and GPM as follows:

We write a positive definite a scalar potential function, $p(q,\dot{q})$, which is a quadratic function of drag forces as

$$p(q,\dot{q}) = D^T(q,\dot{q})W\,D(q,\dot{q}) \tag{10}$$

where $D(q,\dot{q})$ is the $(6+n)\times 1$ vector of drag force and W is a positive definite weighting matrix. This potential function, $p(q,\dot{q})$, captures the total drag force on the whole vehicle-manipulator system. Therefore, the minimization of this function will lead to the reduction of drag effects on the whole system.

Now taking the gradient of the potential function, $p(q,\dot{q})$, we obtain

$$\nabla p(q,\dot{q}) = \frac{\partial p(q,\dot{q})}{\partial q} + \frac{\partial p(q,\dot{q})}{\partial \dot{q}} \tag{11}$$

We take the gradient, $\nabla p(q,\dot{q})$, as the arbitrary vector, $\ddot{\phi}$, of Equation (9) to minimize the hydrodynamic drag effects in the following form:

$$\ddot{\phi} = -\kappa\,\nabla p^T \tag{12}$$

where κ is an arbitrary positive quantity, and the negative sign implies minimization of the performance criteria.

Substituting Equation (12) into Equation (9) with desired parameters we obtain

$$\ddot{q}_d = J^+(\ddot{x}_d - \dot{J}\,\dot{q}_d) - \kappa(I - J^+J)\nabla p^T \tag{13}$$

which includes the performance criteria, drag minimization, as null-space vector.

Computed Torque Method

The dynamic equations of motion (Equation (3)) can be rewritten in the generalized coordinates, q, as follows:

$$M(q)\ddot{q} + C(q,w)\dot{q} + D(q,w)\dot{q} + G(q) = \tau \tag{14}$$

where $M(q) = B^{-T}M_b(q_m)B^{-1}$, $C(q,w) = B^{-T}[C_b(q_m,w) - M_b(q_m)B^{-1}\dot{B}]B^{-1}$, $D(q,w) = B^{-T}D_b(q_m,w)B^{-1}$, $G(q) = B^{-T}G_b(q)$, and $\tau = B^{-T}\tau_b$.

From Equation (14) we can write,

$$M\,\ddot{q} + \xi = \tau \tag{15}$$

where $\xi = C\,\dot{q} + D\,\dot{q} + G$, (dropping the dependent variables).

We write the computed torque as

$$\hat{M}[\ddot{q}_d + K_v(\dot{q}_d - \dot{q}) + K_p(q - q)] + \hat{\xi} = \tau \tag{16}$$

where $\hat{M}$ and $\hat{\xi}$ are estimates of the model parameters, K_p and K_v are positive gains. If $\hat{M} = M$ and $\hat{\xi} = \xi$, then from Equation (15) and Equation (16) we can write

$$\ddot{q} = \ddot{q}_d + K_v(\dot{q}_d - \dot{q}) + K_p(q_d - q) \tag{17}$$

Denoting errors $e = q_d - q$, $\dot{e} = \dot{q}_d - \dot{q}$, and $\ddot{e} = \ddot{q}_d - \ddot{q}$ we can rewrite Equation (17) as

$$\ddot{e} + K_v\dot{e} + K_p e = 0 \tag{18}$$

Equation (18) guarantees asymptotic reduction of the error, *e*.

Simulation Results

The results of DM algorithm are compared with that of conventional pseudo-inverse (PI) method, which is a standard method to resolve kinematic redundancy, to show the efficacy of our proposed algorithm. We have incorporated 10% model inaccuracy in our computer simulation because of the uncertainties involved in unstructured underwater environment. Two basic trajectories chosen for simulation are (i) a circular, and (ii) a straight-line trajectories. We have used the following parameters in computer simulation,

vehicle length = 2.0 m	radius of link 1 = 0.1 m
vehicle width = 1.0 m	radius of link 2 = 0.08 m
vehicle height = 1 m	radius o f link 3 = 0.07 m
vehicle shape: ellipsoidal	mass of link 1 = 32 kg
vehicle mass = 1073 kg	mass of link 2 = 21 kg
radius of link 1 = 0.1 m	mass of link 3 = 16 kg

all the links of manipulator are taken as 1.0 m length, density of water = 1025 kg per cubic meter, radius of circle to be traced = 1.5 m, length of the straight line = 10.0 m, scalar coefficient , κ varies form 1×10^{-4} to 1×10^{-7}.

Initial positions and velocities:

desired position, $q_d = [7,2,0,0,0,0,\frac{\pi}{2},-\frac{\pi}{2},-\frac{\pi}{2}]^T$, desired velocity, $\dot{q}_d = [0,0,0,0,0,0,0,0,0]^T$

actual position, $q = [7,2,0,0,0,0,\frac{\pi}{2},-\frac{\pi}{2},-\frac{\pi}{2}]^T$, actual velocity, $\dot{q} = [0,0,0,0,0,0,0,0,0]^T$

Simulation results for a 6 DOF vehicle and an onboard 3 DOF planar robot manipulator have been presented in Figure TM-1. In Figures TM-1(a), (b) and (c) we have plotted task-space trajectory, norm of drag force and total energy consumed, respectively, for straight-line trajectory. Figures TM-1(d), (e) and (f) show the results for circular trajectory. The desired and actual circular trajectories for pseudo-inverse (PI) method and drag force minimization (DM) method are plotted in Figures TM-1(a) and (d). In both the cases the trajectories are traced with a reasonable accuracy. It is observed from Figures TM-1(b) and (e) that the total drag force (norm of drag force) on the whole UVMS has been reduced significantly in DM method as compared to that of in PI method.

From Figures TM-1(c) and (f) we find that the total energy consumption of the UVMS is less in DM method as compared to that of PI method.

Problems Associated to Underwater Robotic Systems

Underwater Vehicle-Manipulator Systems (UVMS) are complex systems characterized by several strong constraints:

- Uncertainty in the model knowledge, mainly due to the poor knowledge of the hydrodynamic effects;
- Complexity of the mathematical model;
- Structural redundancy of the system;
- Difficulty to control the vehicle in hovering, mainly due to the poor thrusters performance;
- Dynamic coupling between vehicle and manipulator;
- Low bandwidth of the sensor's readings.

Therefore, the motion coordination and force control schemes for an UVMS require taking into account the above characteristics. To circumvent the modeling uncertainties, we have investigated a decentralized adaptive control along with coordinated motion planning approach for the UVMS as follows.

Adaptive Control of UVMS Subject to Kinematic Constraints

We have exploited the kinematic redundancy of the UVMS to satisfy the kinematic constraint (joint limit). The weighted least norm (WLN) solution to Equation (4) can be written as

$$\dot{q}_d = J_w^+ \dot{x}_d \tag{19}$$

where $J_w^+ = W^{-1}J^T(JW^{-1}J^T)^{-1}$ is the weighted pseudo-inverse of J and $W = diag(h_1, h_2, ..., h_{6+n})$. Now, we can write the desired acceleration in joint-space as

$$\ddot{q}_d = J_w^+(\ddot{x}_d - \dot{J}_w\dot{q}_d) \tag{20}$$

The diagonal elements of W are calculated from the joint limits as follows [Chan 1995]:

$$h_i = 1 + \left|\frac{\partial H(q)}{\partial q_i}\right| \tag{21}$$

$$\text{where } H(q) = \sum_{i=1}^{6+n} \frac{1}{C_i} \frac{(q_{i,\max} - q_{i,\min})}{(q_{i,\max} - q_i)(q_i - q_{i,\min})} \tag{22}$$

$$\text{and } \frac{\partial H(q)}{\partial q_i} = \frac{(q_{i,max} - q_{i,min})(2q_i - q_{i,max} - q_{i,min})}{C_i(q_{i,max} - q_i)^2(q_i - q_{i,min})^2} \tag{23}$$

where $q_{i,max}$ and $q_{i,min}$ are the upper and lower limits of ith joint, and C_i is a positive quantity which is determined from the desired degree of stiffness of the i-th joint.

From the above expression (23), we notice that $\partial H(q)/\partial q_i$ is equal to zero when the ith joint is at the middle of its range, and becomes infinity at either limit. Thus, h_i varies from 1 to infinity if the ith joint goes from middle of the range to its limit. If the ith joint approaches its limit, then h_i becomes very large and the corresponding element in W^{-1} goes to zero and ith joint virtually stops.

Consider the following adaptive control law [Sarkar 1999] and [Yuh 1996]:

$$\tau = K_1\ddot{q}_d + K_2\dot{q} + K_3 + K_4\dot{e} + K_5 e = \sum_{i=1}^{5} K_i \Phi_i \tag{24}$$

where $\Phi_1 = \ddot{q}_d, \Phi_2 = \dot{q}, \Phi_3 = \kappa,$ a positive constant vector, $\Phi_4 = \dot{e}, \Phi_5 = e,$ and K_i are control gain matrices.

The tracking error, $e = q_d - q$, will asymptotically converge to zero with the following adaptive controller:

$$K_i = \frac{\hat{\theta}_i \tilde{e} \Phi_i^T}{\| \tilde{e} \| \| \Phi_i \|} \tag{25}$$

$$\dot{\hat{\theta}}_i = f_i \| \tilde{e} \| \| \Phi_i \| \quad i=1,...,5 \tag{26}$$

where f_i are positive constants, $\hat{\theta}_i$ are estimates of θ_i, and

$$\tilde{e} = \dot{e} + \sigma e \tag{27}$$

where σ is a positive constant.

As shown in Figure TM-2, two separate control systems (one for each subsystem) were designed and implemented, based on the adaptive control system described above.

From Equation (24) the control law for the vehicle can be written as

$$\tau_v = K_{1v}\ddot{q}_{dv} + K_{2v}\dot{q}_v + K_{3v} + K_{4v}\dot{e}_v + K_{5v}e_v = \sum_{i=1}^{5} K_{iv}\Phi_{iv} \tag{28}$$

and control law for the robot manipulator is

$$\tau_m = K_{1m}\ddot{q}_{dm} + K_{2m}\dot{q}_m + K_{3m} + K_{4m}\dot{e}_m + K_{5m}e_m = \sum_{i=1}^{5} K_{im}\Phi_{im} \tag{29}$$

The relative influence of each control parameter on the performance of the controller was discussed in detail in [Yuh 1999, Choi 1996].

Simulation Results

We have conducted extensive computer simulations to investigate the performance of the proposed method. We have attached a 3 DOF planar robot manipulator (working in the vertical plane) with a 6 DOF ODIN type vehicle [Tarn 1996], which is spherical in shape having radius of *0.3m*, mass of

125kg. Limits of the position variable are: $surge = \pm 10m$, $sway = \pm 10m$, $heave = \pm 10m$, $roll = \pm 5^o$, $pitch = \pm 10^o$, $yaw = \pm 30^o$, $jo\,\text{int}\,1 = \pm 90^o$, $jo\,\text{int}\,2 = \pm 100^o$ and $jo\,\text{int}\,3 = \pm 120^o$.

The computer simulation results are plotted in Figures TM-3 & 4. Top view and side view of the configuration of UVMS are graphically represented in Figure TM-3. Since the vehicle is spherical in shape, we have taken mid-plane cross-section (circular) to represent the vehicle in 2D. From these figures (Figures TM-3(a) & (b)), we see that the circular shape of the vehicle for both the views are gradually becoming elliptical in case of without joint limits and also the vehicle and manipulator are aligning with the direction of task-space motion. It results large surge, pitch and yaw motions. The UVMS, specially the vehicle, moves optimally when joint limits are imposed (Figures TM-3(c) & (d)).

In Figure TM-4, we have plotted task-space position and its error for two cases. *Case 1:* without imposing joint limits (drawn in dashed line), and *case 2:* with joint limits (drawn in solid line). It is observed in Figure TM-4 that for both cases the end-effector follows the desired trajectory. However, the end-effector trajectory for case 2 is more accurate as compared to that of case 1. In both the cases, the end-effector gradually adapts task-space trajectory as time passes and the steady state error is small.

The redundancy resolution method can be extended further to incorporate other performance criteria such as drag optimization, energy minimization, and obstacle avoidance.

Force Control

Force control schemes for UVMS have been investigated aimed at handling the strong limitations that we have to face in case of underwater systems. Based on the schemes proposed in [Ferretti 1997] and [D'egoulange 1994], two force control schemes will be analyzed that do not require exact dynamic compensation; however, the knowledge of part of the dynamic model can always be exploited when available. Extension of the original schemes to redundant systems is achieved via a task-priority inverse kinematics redundancy resolution algorithm [Chiverini 1997] and suitable secondary tasks are defined to exploit all the degrees of freedom (DOF) of the system.

Mathematical formulation

The mathematical model of a UVMS in contact with the environment is strongly non-linear and coupled [Sarkar 1999]. The force/moments at the tip of the manipulator are projected on the whole system by the transpose of the Jacobian, this projection, thus, is non-linear and configuration dependent.

If the end-effector of a robotic system is in contact with the environment the force/moment at the tip of the manipulator acts on the whole system according to the equation

$$M_b(q_m)\dot{w} + C_b(q_m, w)w + D_b(q_m, w)w + G_b(q) = \tau_b - J^T f \quad (31)$$

where f is the force vector at the end-effector expressed in the inertial frame.

Contact between the manipulator and the environment is usually difficult to model. In the following cases we will resort to the simple model constituted by a frictionless and elastically compliant plane.

The force at the end-effector is related to the deformation of the environment by the following simplified relation

$$f = K(x - x_e) \tag{32}$$

where x is the position of the end-effector expressed in the inertial frame, x_e is the constant position of the unperturbed environment expressed in the inertial frame and

$$K = k\upsilon\upsilon^T \tag{33}$$

with k>0, is the stiffness matrix being υ the vector normal to the plane.

Three different force control schemes have been developed to overcome the problems that arise with the implementation of the existing schemes. These force control schemes do not require dynamic compensation of the system and allow it to exploit its kinematic redundancy. The difference between the schemes is mainly on the projection of the force error in the task space onto the joint space that is obtained in different ways:

- The force error gives a reference position in the task space that is added to the motion reference position and further projected in the joint space via a suitable Inverse Kinematic algorithm; this approach is known as External force control, stability analysis for a redundant manipulator has been provided.
- The force error gives is projected as a reference velocity at the joint space by the use of the transpose of the Jacobian;
- The force error is projected at the joint torques by the use of the transpose of the Jacobian. The latter are known as explicit force control.

The major drawback of hybrid control is that it is not robust to the occurrence of an impact in a direction where motion control has been planned. In such a case, in fact, the end-effector is not compliant along that direction and strong interaction between manipulator and environment is experienced. This problem has been solved by resorting to the parallel approach [Chiaverini 1993], where the force control action overcomes the position control action at the contact.

The proposed schemes (Figure TM-5, 6, 7) show the same feature as the parallel approach. If a contact arises along a motion direction, the force controller guarantees that a null force error at steady state is achieved while a non-null position error is obtained. This implies that, in the direction where a null desired force is commanded, the manipulator reacts to unexpected impacts with a safe behavior. Moreover, in the directions in which a desired force is commanded, the desired position is overcome by the controller. This is a nice feature for manipulation tasks in unstructured environments.

Due to the floating base and the possible occurrence of external disturbances (such as, e.g., ocean current), it can happen that the end-effector looses the contact with the environment during the task fulfillment. In such a case the control action might become unsuitable. A way to handle this problem has been proposed and successfully simulated.

To practical implementation of the proposed force control schemes some implementation issues have been outlined:

- Different control bandwidth between vehicle and manipulator, due to the different inertia and actuator performance. Moreover limit cycles in underwater vehicle are usually experienced due to the thruster's characteristics. A modification in the original Inverse Kinematics (IK) algorithm [Chiaverini 1994] has then been implemented.
- Force control task require accurate positioning of the end-effector. The vehicle, i.e. the base of the manipulator, is characterized by large errors and difficulty in positioning; a different velocity decomposition between manipulator and vehicle has been obtained by further modification of the Inverse Kinematics algorithm.
- The UVMS are usually highly redundant, if a 6 DOF manipulator is used this means that 12 DOF are available. We can then define more tasks to be iteratively projected on the null space of the higher priority tasks. An example of 3 task could be: (1) motion/force control of the end-effector, (2) manipulability measure of the manipulator, (3) roll and pitch orientation of the vehicle.
- To decrease power consumption it is possible to implement IK algorithms with bounded reference values for the secondary tasks. Using some smooth functions, or fuzzy techniques, it is possible to activate the secondary tasks only when the relevant variables are out of a desired range. For the roll and pitch vehicle's angles, for example, it is sufficient to implement an algorithm that keeps them in a range, e.g., 10^{o}.
- The regressor of an underwater vehicle does not depend on the actual position. If a model based adaptive control law is applied, then, it cannot compensate for disturbances or model mismatching that will affect the vehicle position. For example, if a linear constant ocean current acts on the vehicle, at steady state a non-null position error will be experienced. A suitable integral action might be added to the desired control law to take into account this possibility.
- Force/moment sensor readings are usually corrupted by noise. The use of a derivative action in the control law, thus, can be difficult to implement. With the assumption of a frictionless and elastically compliant plane we can observe a linear relation between the force and the end-effector's position. The force derivative action can then be substituted with a term proportional to the end-effector velocity. The latter will be computed by differential kinematics from the system velocities that are usually available directly from sensor readings or from the position via a numerical filter.

Simulation Results

To prove the effectiveness of the proposed force control schemes several simulations have been run under Matlab 5.2, Simulink 2.0 environment. The UVMS simulated has 9 DOF, 6 DOF of the vehicle plus a 3link manipulator mounted on it [Podder 1998]. The model takes into account all the main dynamic and hydrodynamic effects. The controllers have been implemented with a sampling frequency of 200 Hz. The vehicle is a box of dimensions (2x1x0.5m), and the vehicle fixed frame is located in the geometrical center of the body. The manipulator is a 3 link planar manipulator with rotational joints.

The first task is to exert a force along a certain direction while moving in the other directions. At the same time, two secondary tasks have been defined: (1) keep the manipulator manipulability in a safe range and (2) keep the roll and pitch vehicle angle in a safe range.

To simulate a non-perfect hovering of the vehicle we decided to implement a control law with *lower* gain for the vehicle; the performance of the simulated vehicle, thus, has an error that is of the same magnitude of a real vehicle in hovering. In all the simulations the secondary tasks have to be fulfill only when the relevant variable is outside of a desired bound.

Where a dynamic compensation has been performed the initial value of the parameters has been chosen such that the gravity compensation at the beginning is different from the real one, adding an error bounded in 10% for each parameter.

Several simulations have been run in different operative conditions, unexpected impacts or poor thrusters behavior have also been simulated. In Figure TM-8, some plots of the force at the end-effector are shown.

Impedance Control

The dynamic interaction between the UVMS and the environment is neither zero nor negligible. The control strategies, which aim to control a quantity, such as position, velocity or force, cannot meet this requirement. The aim of impedance control is to control mechanical impedance of the manipulator and the environment instead of controlling position or force alone. For UVMS, the motion of the end-effector is usually slow. So the torque-based impedance method is suitable to meet the requirement and will be used here.

$$M(q)\ddot{q} + \xi(q,\dot{q}) = \tau - \tau_e \tag{34}$$

From Equations (8) and (34), we can write

$$M(q)J^{+}(\ddot{x} - \dot{J}\,\dot{q}) + \xi(q,\dot{q}) = \tau - \tau_e \tag{35}$$

where τ_e is a $(6+n)\times 1$ vector of external disturbance joint torque.

We define $$\widetilde{J} = J^{T} \tag{36}$$

The UVMS dynamic equation now is written by

$$\widetilde{J}^{+} M\, J^{+}(\ddot{x} - \dot{J}\,\dot{q}) + \widetilde{J}^{+}\xi = F - F_e \tag{37}$$

Now we can write the vehicle and manipulator dynamic equation model in Cartesian space as

$$\widetilde{M}\,\ddot{x} + \widetilde{\zeta} = F - F_e \tag{38}$$

where $\widetilde{M} = \widetilde{J}^{+} M\, \widetilde{J}^{+}, \widetilde{\zeta} = \widetilde{J}^{+}\xi - \widetilde{M}\,\dot{J}\,J^{+}\dot{x}$.

Now we design the torque-based impedance control scheme based on UVMS model expressed in Cartesian space. The control law is

$$F = \hat{\widetilde{M}}U + \hat{\widetilde{\zeta}} + F_e \tag{39}$$

where $\hat{\widetilde{M}}, \hat{\widetilde{\zeta}}$ are estimates of $\widetilde{M}, \widetilde{\zeta}$ and F_e is the exerted force on the environment.

$$F_e = P\ddot{E} + B_d\dot{E} + KE \tag{40}$$

The impedance control block diagram is shown in Figure TM-9. The actual UVMS is subjected to unpredictable dynamics behavior and it is difficult to obtain the accurate model. $\Delta\tilde{M}, \Delta\tilde{\zeta}$ are not equate to zero. Details are given in [Cui 1999]. To improve the robustness, learning control or adaptive control methods can be employed.

Simulation Results

To investigate the effectiveness of the proposed method, extensive computer simulations have been performed for an UVMS comprising of a 6 DOF vehicle and a 3 DOF robot manipulator. We have considered a solid environment like a vertical wall having stiffness $K_e = 10{,}000N/m$ at a distance of $x=3.59m$. The desired contact force (200 N in our simulation) can be obtained by designing X_r (reference end-effector trajectory) properly. Other specifications are same as previous cases.

We have plotted the simulation results in Figures TM-10 to 11. From Figure TM-10, it is observed that the impedance controller performs reasonably well while tracing the desired task-space trajectory and imparting desired force on the environment. We have introduced noise in force measurement as Gaussian distribution with mean equal to 1 and standard deviation equal to 0.1. The results with the noise are plotted in Figure TM-11. We assumed that there is no error in position and velocity measurement. The plot in Figure TM-11(b) show that the position error is small and it is decreasing gradually even in the presence of measurement noise.

In this simulation, we have not incorporated the null-space solution of Equation (9). It can be utilized to satisfy various performance criteria such as singularity avoidance, joint limit avoidance, obstacle avoidance, energy minimization and different other criteria.

Conclusions

We have derived dynamic equations of motion of the UVMS using *Quasi-Lagrange* approach to investigate different control algorithms. A new drag force minimization algorithm has been developed utilizing kinematic redundancy and gradient projection method. The kinematic redundancy has also been exploited to satisfy various performance criteria such as joint limits, manipulability measure, and force control. We have implemented a non-regressor based control approach where we integrate a centralized planner with decentralized control scheme consisting of two different controllers - one for the 6 DOF vehicle and the other for the onboard n DOF robotic manipulator. Here, the reference trajectories are computed considering the whole UVMS with $6+n$ DOF. But each controller follows only the part of the reference trajectory that is applicable to the individual subsystem, i.e., either the vehicle or the manipulator. Thus, this approach overcomes the difficulty in designing and adjusting the gains for one high dimensional controller. We have investigated several force control schemes and impedance control scheme. The results from the computer simulation demonstrate the effectiveness of proposed methods.

Future Tasks

- Include model of Ansaldo Arm in the simulation codes.
- Test the motion coordination and for control algorithms for SAUVIM in the simulation package.

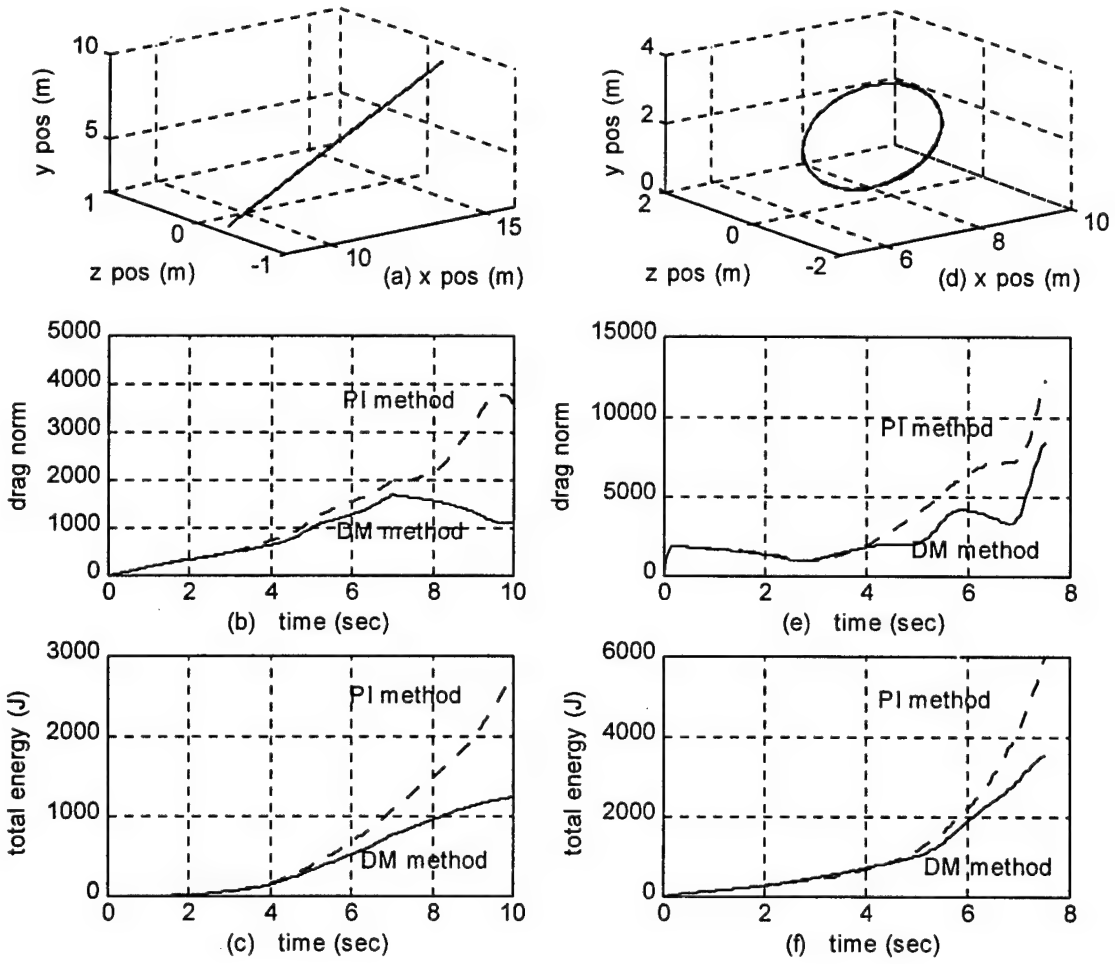

Fig. TM-1: Task-space (XYZ) trajectory, norm of drag forces and total energy consumption; (a),(b),(c) for straight line trajectory and (d),(e),(f) for circular trajecto

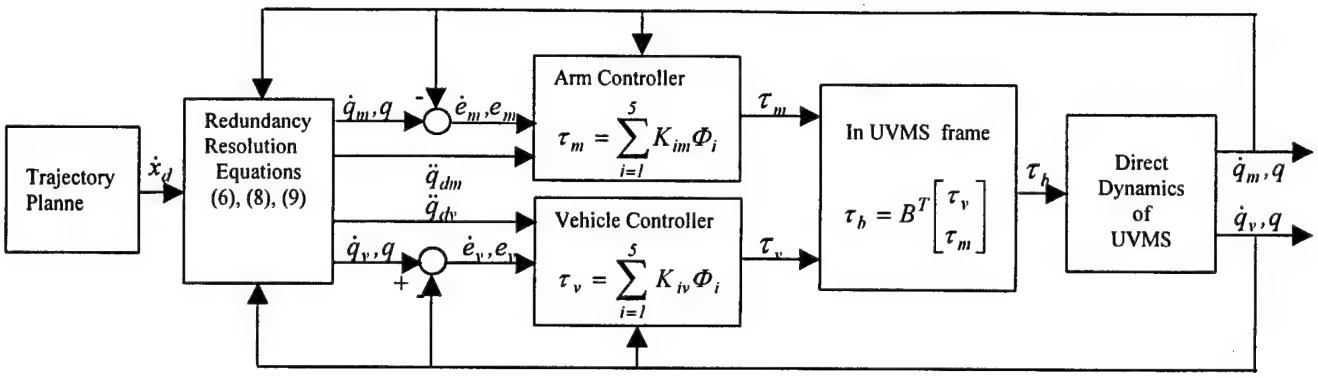

Figure TM-2: Block diagram of redundancy resolution and adaptive control.

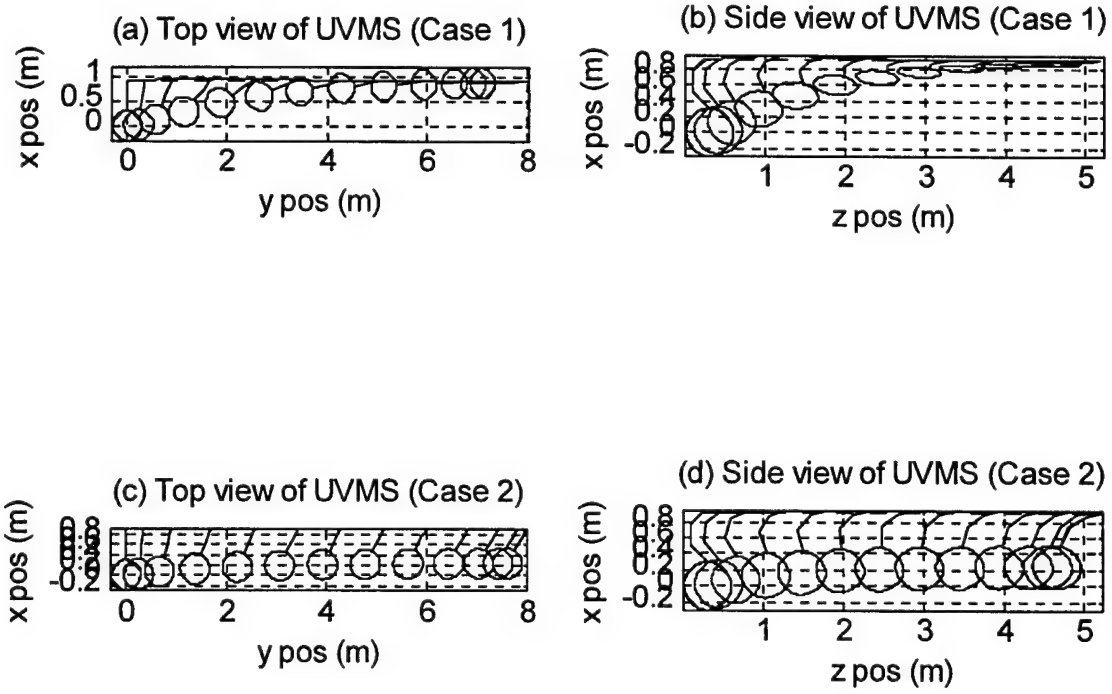

Figure TM-3: Graphical representation of configuration of the UVMS for Case 1 (without joint limits) and Case 2 (with joint limits).

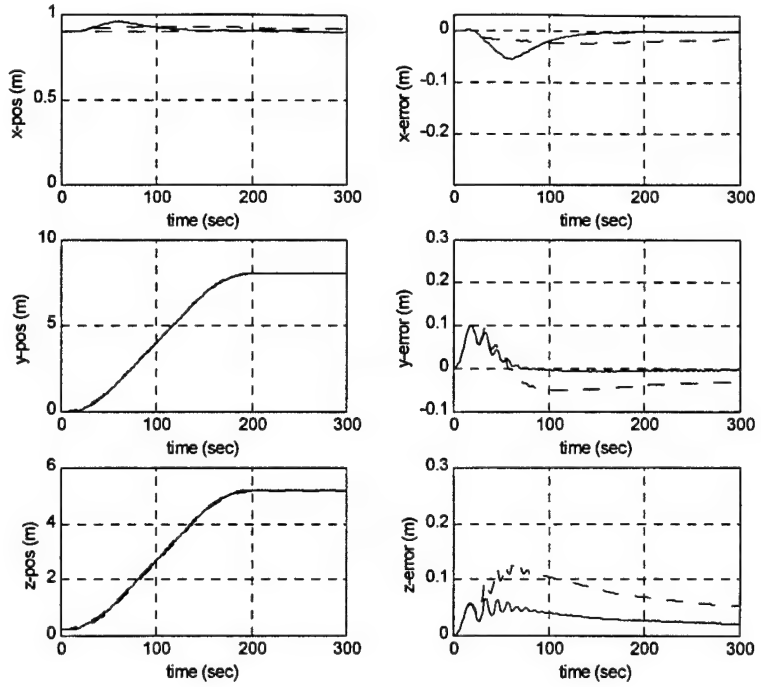

Figure TM-4: X,Y,Z (task-space) position and its error – solid line denotes position/error with joint limits, dashed line denotes position/error without joint limits; position plots (left column) include desired position curves (dashed line).

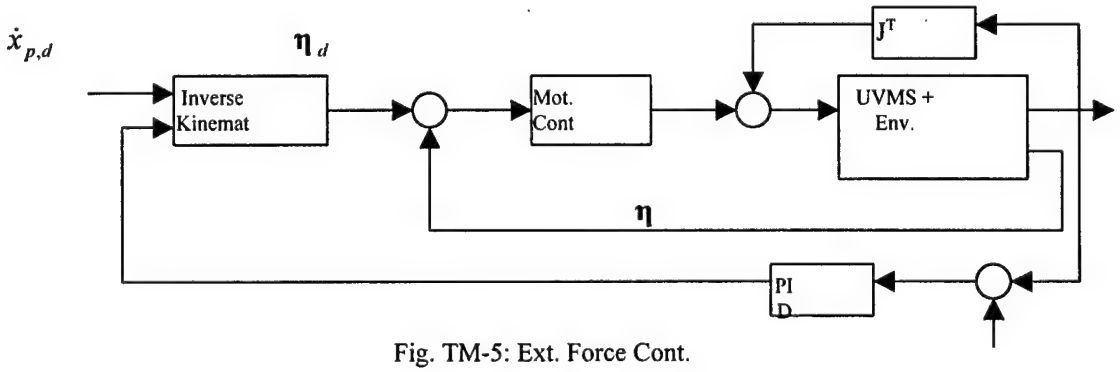

Fig. TM-5: Ext. Force Cont.

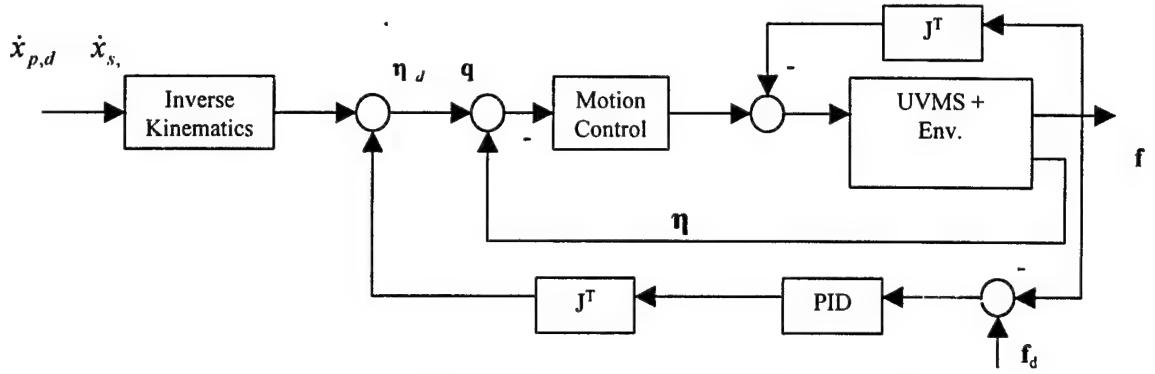

Fig. TM-6: Explicit Force Control, 1st Scheme

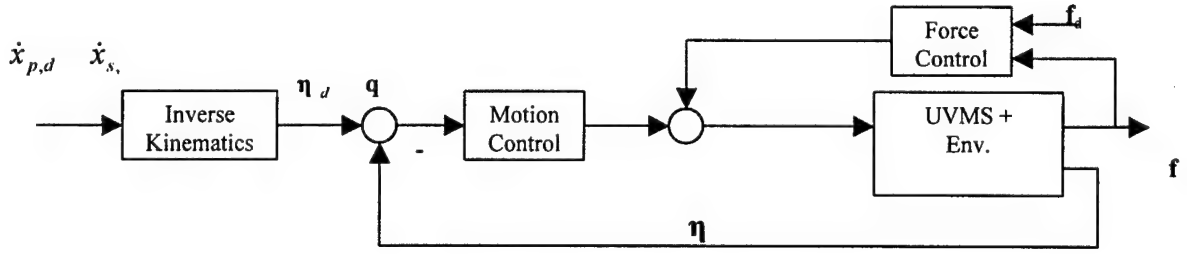

Fig. TM-7: Explicit Force Control, 2nd Scheme

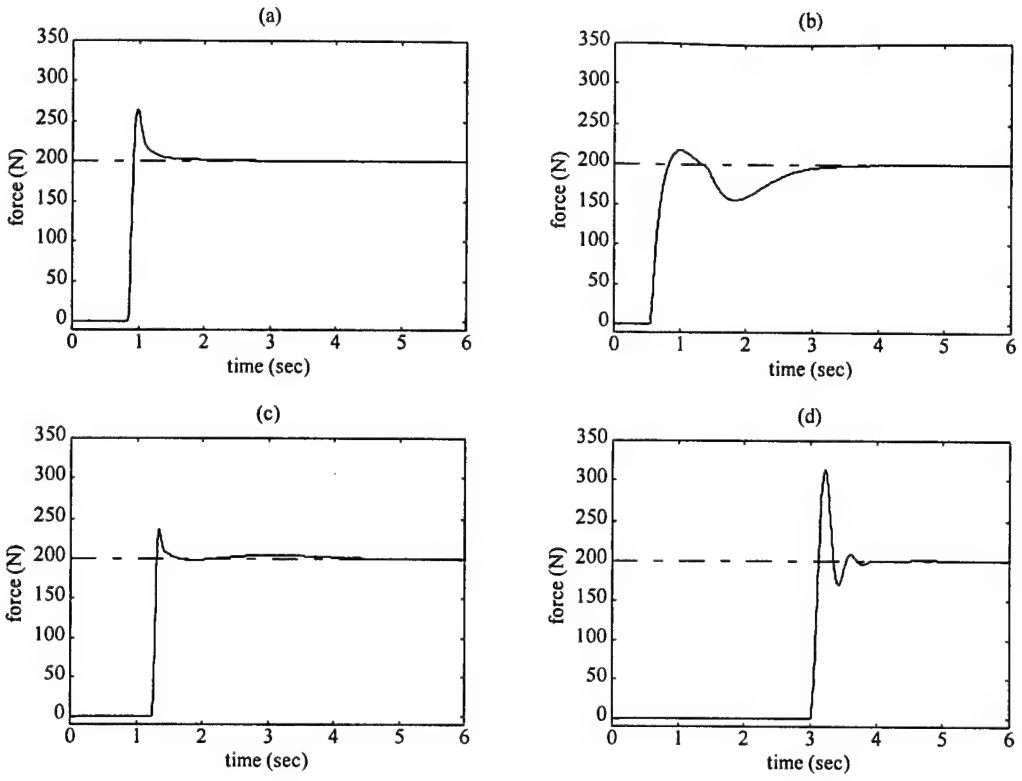

Fig. TM-8: Environmental force for different operative conditions and different control schemes. Redundancy has been exploited to achieve the secondary tasks, a wrong knowledge of the sole restoring force has been assumed for dynamic compensation: (a) force control in Fig. TM-7, (b) force control in Fig. TM-6, (c) and (d) force control in Fig. TM-5 for two completely different initial configurations.

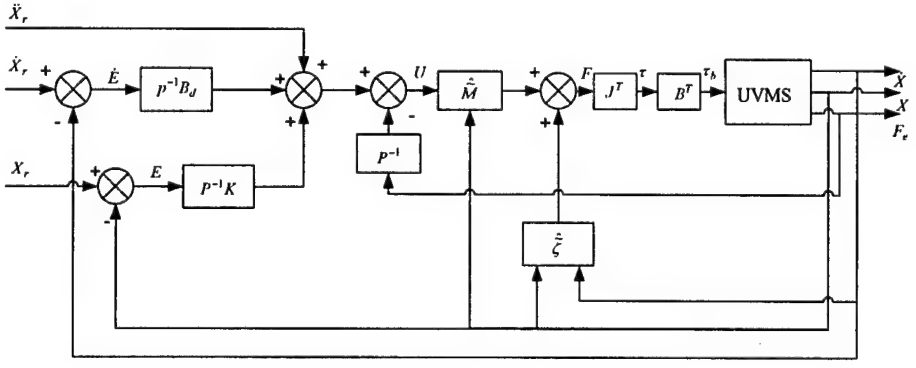

Figure TM-9. Impedance control block diagram.

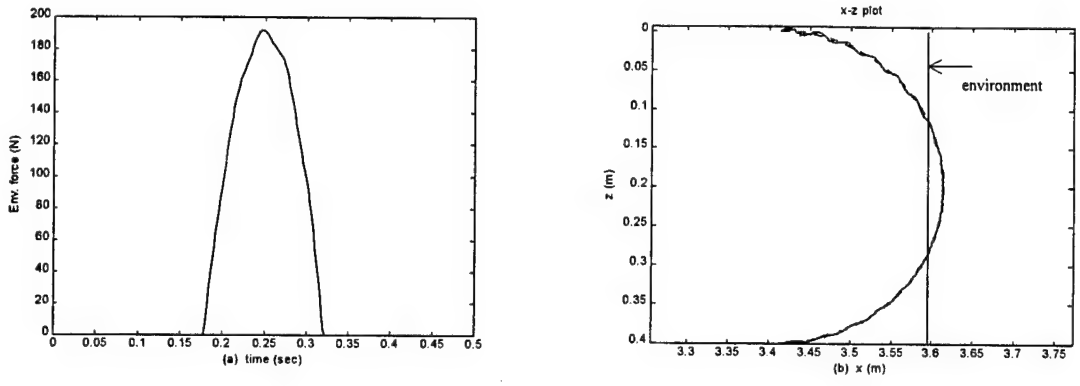

Fig. TM-10: Force and position trajectory response.

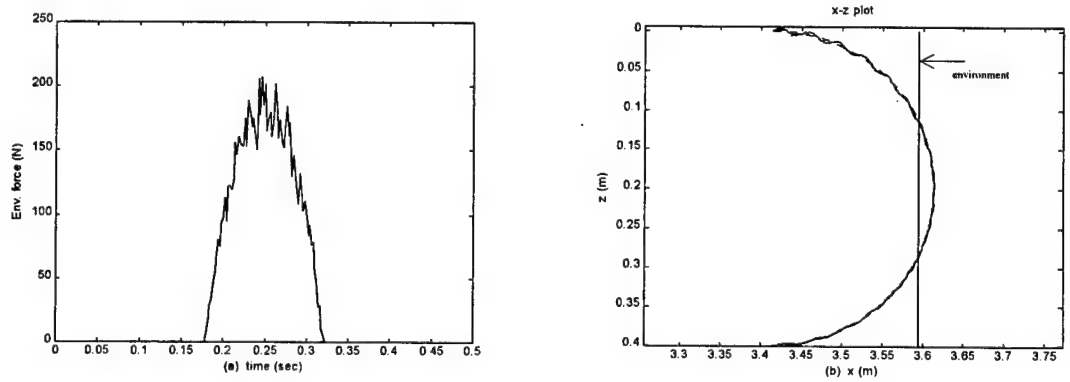

Fig. TM-11: Force & position trajectory response with noise.

Low-Level Control (LLC)

Project Leaders: Dr. Junku Yuh & Dr. Song K. Choi
Personnel: Ms. Jing Nie & Mr. Michael West

Objectives

- To design an advanced vehicle control for navigation and hovering; and
- To design an advanced coordinated motion/force control of the vehicle and manipulator during the intervention mode.

Current Status (Tasks Completed During 8/1/98 - 7/31/99):

Accomplishments

- Development of a non-regressor based adaptive control system algorithm for AUVs;
- Extensive simulation and testing on ODIN AUV with sonar-based position measurements;
- Development of methodology to transport algorithm and code to SAUVIM;
- Introduction of a localization technique using certainty grids; and
- Initial simulation and testing of the localization techniques.

Non-Regressor Based Adaptive Control

Introduction

Several advanced controllers for underwater robots have been proposed in the literature. Among them are sliding mode control [Cunha 1995, Healey 1993, Dougherty 1990], neural network based control [Ishii 1994], fuzzy logic control [DeBitetto 1994], and hybrid adaptive control [Tabaii 1994]. Cunha 1995 presented an adaptive control scheme for dynamic positioning of remotely operated vehicles (ROV) based on a control algorithm called Variable Structure Model-Reference Adaptive Control (VS-MRAC). In this scheme, each degree of freedom of interest is controlled by a single loop VS-MRAC controller. Healey 1993 used the sliding mode method to control the underwater vehicle and separated the system into non-interacting (or lightly interacting) subsystems, grouping certain key motion equations together for separate functions of steering, diving, and speed control. The design and testing of the flight control system of an advanced unmanned underwater vehicle (UUV) also using sliding mode methods with several single-input single-output (SISO) controllers was presented in [Dougherty]. Ishii 1994 proposed a neural network based control system called "Self-Organizing Neural-Net-Controller System" (SONCS) for autonomous underwater vehicles (AUV) and examined its effectiveness through application to heading keeping control of an AUV called "Twin-Burger." In their study, a quick adaptation method of the controller called "Imaginary Training" was used to improve the time-consuming adaptation process of SONCS. A simple 14-rule fuzzy logic controller was developed and simulated for the depth control of a UUV in the study of Debitetto 1994. In the hybrid adaptive control (suggesting that the procedure is a mixture of continuous and discrete operations) of AUV done by Tabaii 1994, the control system was simulated in the continuous domain while the control and identification section was discrete.

In this study, a new adaptive control scheme for underwater robots was experimentally implemented on the Omni-Directional Intelligent Navigator (ODIN) (Figure LLC-1). ODIN is a 6 degrees-of-

freedom, autonomous underwater robot with 8 thrusters; various navigation sensors such as sonar, a pressure sensor, and an inertial navigation system (INS); and an on-board CPU with VxWorks OS in VMEbus. A detailed description is available at in reference [Kawaguchi 1996] or at the laboratory website "http://www.eng.hawaii.edu/~asl/odin.html website."

The presented control scheme is different from conventional adaptive control schemes in that it estimates a set of combinations of unknown bounded constants of system parameter matrices rather than estimating each parameter individually. And the presented adaptive law adjusts the controller gains based on the performance of the system instead of the knowledge of the dynamic model. Its computational requirement does not depend on the number of unknown system parameters. Therefore, the presented adaptive control system is structurally simple and computationally efficient. Stability analysis by the Lyapunov method proves that the tracking error can asymptotically converge to zero. Results from wet experiments show that the controller can achieve high-performance trajectory tracking in the presence of model uncertainties, measurement noises, and external disturbances.

Navigation and Control

Figure LLC-2 shows a general overview of an underwater robot's (vehicle) navigation and control systems. The task/motion planning and trajectory generator module provides the desired vehicle position as a function of time. The controller then computes desired vehicle force/torque, by comparing the desired vehicle position with the current position estimate based on the sensor measurements. The corresponding value of each thruster force to provide the desired vehicle force/torque is computed using a thruster control matrix (TCM). TCM's elements are geometry dependent and can be computed in advance for each vehicle. Then, the desired input voltage to each thruster driver can be computed by using a thruster model. Input to the thruster model is the input voltage to the thruster driver and its output is the thruster force. A thruster system has highly nonlinear dynamics. Therefore, a simple thruster static model (TSM) is often used to compute the desired input voltage to each thruster driver, assuming that a time constant of the thruster system is much smaller than a time constant of the overall control system. In this study, a simple linear TSM of ODIN, which was experimentally obtained, was used. A pressure sensor was used to measure its position in z and its velocity was estimated by Kalman filter. Eight sector sonars on ODIN were used to determine its position in x and y coordinates defined in a water tank. As shown in Figure LLC-2, the raw sonar measurements were processed through the pre-processing filter to remove false readings; the function filter was used to estimate x and y position with INS outputs; and the Kalman filter was used to estimate velocities in x and y. These estimates were used in the control system. As this paper focuses on the control system, detailed description of the navigation system is omitted here. Detailed information about the navigation systems and filters used on ODIN is available in ref. [Nie 1999]. Figures LLC-3a, b & c show effectiveness of the navigation system with three filters shown in Figure LLC-2. Figure LLC-3a shows input signals to the navigation system, which are raw data of one sonar with lots of false readings and noise; Figures LLC-3b & 3c show position and velocity estimates of the Kalman filter, respectively, which are outputs of the navigation system.

Adaptive Control System

The presented control system is based on the adaptive control with bound estimation developed by Yuh (Yuh 1996, Choi 1996). In general, underwater vehicles can be represented by the following vector equation:

$$\mathbf{M}_v\dot{\mathbf{v}} + \mathbf{C}_v(\mathbf{v})\mathbf{v} + \mathbf{D}_v(\mathbf{v})\mathbf{v} + \mathbf{g}_v(\eta) = \tau_v \qquad (1)$$

$$\dot{\eta} = \mathbf{J}(\eta)\mathbf{v} \qquad (2)$$

where $\mathbf{v}$ = the linear and angular velocity vector with coordinates in the body-fixed frame, η = the position and orientation vector with coordinates in the earth-fixed frame, $\mathbf{M}_v = \mathbf{M}_{RB} + \mathbf{M}_A$, $\mathbf{C}_v(\mathbf{v}) = \mathbf{C}_{RB} + \mathbf{C}_A$, $\mathbf{M}_{RB}$ = rigid body inertia matrix, $\mathbf{M}_A$ = added inertia matrix; $\mathbf{C}_{RB}(\mathbf{v})$ = rigid body Coriolis and centripetal matrix, $\mathbf{C}_A(\mathbf{v})$ = hydrodynamic Coriolis and centripetal matrix, $\mathbf{D}_v(\mathbf{v})$ = hydrodynamic damping and lift matrix, $\mathbf{g}_v(\eta)$ = gravitational forces and moments vector, τ_v = control inputs (forces and moments) vector, and $\mathbf{J}$ = transformation matrix between vehicle and fixed frames.

Equation (1) can also be written in earth-fixed coordinates as follows:

$$\mathbf{M}\ddot{\eta} + \mathbf{C}(\mathbf{v},\eta)\dot{\eta} + \mathbf{D}(\mathbf{v},\eta)\dot{\eta} + \mathbf{g}(\eta) + \mathbf{u}_d = \tau \qquad (3)$$

where $\mathbf{M}(\eta) = \mathbf{J}^{-T}\mathbf{M}_v\mathbf{J}^{-1}$, $\mathbf{C}(\mathbf{v},\eta) = \mathbf{J}^{-T}[\mathbf{C}_v(\mathbf{v}) - \mathbf{M}_v\mathbf{J}^{-1}\dot{\mathbf{J}}]\mathbf{J}^{-1}$, $\mathbf{D}(\mathbf{v},\eta) = \mathbf{J}^{-T}\mathbf{D}_v(\mathbf{v})\mathbf{J}^{-1}$, $\mathbf{g}(\eta) = \mathbf{J}^{-T}\mathbf{g}_v(\eta)$, and $\mathbf{u}_d$ represents a class of unmodeled effects which are bounded by

$$\|\mathbf{u}_d\| \le d_0 + d_1\|\dot{\mathbf{e}}\| + d_2\|\mathbf{e}\| \qquad (4)$$

where d_i i=0, 1, 2 are positive constants and the tracking error vector $\mathbf{e}$ is defined as

$$\mathbf{e} = \eta_d - \eta \qquad (5)$$

where η_d is a desired value of η.

The system matrices of the vehicle are assumed to be bounded by

$$\|\mathbf{M}^{-1}\| \le \alpha, \quad \|\mathbf{M}\| \le \beta_1, \quad \|\mathbf{C}+\mathbf{D}\| \le \beta_2, \quad \|\mathbf{g}\| \le \beta_3, \quad \lambda_{min}(\mathbf{M}^{-1}) \rangle \gamma \qquad (6)$$

where α, β_i, and γ are positive constants.

Instead of mathematically proving Eq. (6), we will show how to estimate

$$\theta_i = \frac{\alpha(\beta_i + d_{i-3})}{\gamma} \quad i = 1, ..., 5 \qquad (7)$$

where $\beta_4 = \beta_5 = \frac{\varepsilon}{\alpha}$, ε is a positive constant, and $d_i = 0$ for $(i-3) < 0$.

Consider the following control law:

$$\tau = \mathbf{K}_1\ddot{\eta}_d + \mathbf{K}_2\dot{\eta} + \mathbf{K}_3 + \mathbf{K}_4\dot{\mathbf{e}} + \mathbf{K}_5\mathbf{e} = \sum_{i=1}^{5}\mathbf{K}_i\Phi_i \qquad (8)$$

where $\Phi_1 = \ddot{\eta}_d$, $\Phi_2 = \dot{\eta}$, $\Phi_3 = \mathbf{1}$, $\Phi_4 = \dot{\mathbf{e}}$, $\Phi_5 = \mathbf{e}$, and $\mathbf{K}_i$ are control gain matrices.

From Eqs. (3) and (8), the error equation can be obtained as follows

$$\ddot{\mathbf{e}} = \mathbf{M}^{-1}(\mathbf{M}-\mathbf{K}_1)\ddot{\eta}_d + \mathbf{M}^{-1}(\mathbf{C}+\mathbf{D}-\mathbf{K}_2)\dot{\eta} + \mathbf{M}^{-1}(\mathbf{g}-\mathbf{K}_3) + \mathbf{M}^{-1}\mathbf{u}_d - \mathbf{M}^{-1}\mathbf{K}_4\dot{\mathbf{e}} - \mathbf{M}^{-1}\mathbf{K}_5\mathbf{e}$$
$$= \mathbf{M}^{-1}\sum_{i=1}^{5}(\mathbf{P}_i - \mathbf{K}_i)\Phi_i + \mathbf{M}^{-1}\mathbf{u}_d \qquad (9)$$

where $\mathbf{P}_1 = \mathbf{M},\ \mathbf{P}_2 = \mathbf{C}+\mathbf{D},\ \mathbf{P}_3 = \mathbf{g},\ \mathbf{P}_4 = \mathbf{P}_5 = 0.$

Theorem: The tracking error **e** will asymptotically converge to zero with the following adaptive controller:

$$\mathbf{K}_i = \frac{\hat{\theta}_i \tilde{\mathbf{e}}\Phi_i^{\mathrm{T}}}{\|\tilde{\mathbf{e}}\|\|\Phi_i\|} \qquad (10)$$

$$\dot{\hat{\theta}}_i = \mathbf{f}_i\|\tilde{\mathbf{e}}\|\|\Phi_i\| \quad i=1,...,5 \qquad (11)$$

where $\mathbf{f}_i$ are positive constants, $\hat{\theta}_i$ are estimates of θ_i, and

$$\tilde{\mathbf{e}} = \dot{\mathbf{e}} + \sigma\mathbf{e} \qquad (12)$$

where σ is a positive constant.

Proof: Consider the following Lyapunov function candidate:

$$\mathbf{V} = \frac{1}{2}\tilde{\mathbf{e}}^{\mathrm{T}}\tilde{\mathbf{e}} + \frac{1}{2}\sum_{i=1}^{5}\mathbf{f}_i^{-1}\gamma(\theta_i - \hat{\theta}_i)^2 \qquad (13)$$

Differentiating Eq. 13 along Eq. 9 with respect to time yields

$$\dot{\mathbf{V}} = \tilde{\mathbf{e}}^{\mathrm{T}}\ddot{\mathbf{e}} + \sigma\tilde{\mathbf{e}}^{\mathrm{T}}\dot{\mathbf{e}} - \sum_{i=1}^{5}\mathbf{f}_i^{-1}\gamma(\theta_i - \hat{\theta}_i)\dot{\hat{\theta}}_i$$
$$= \left[\tilde{\mathbf{e}}^{\mathrm{T}}(\mathbf{M}^{-1}\sum_{i=1}^{5}\mathbf{P}_i\Phi_i + \mathbf{M}^{-1}\mathbf{u}_d) + \sigma\tilde{\mathbf{e}}^{\mathrm{T}}\dot{\mathbf{e}} - \sum_{i=1}^{5}\mathbf{f}_i^{-1}\gamma\theta_i\dot{\hat{\theta}}_i\right] + \left[-\tilde{\mathbf{e}}^{\mathrm{T}}\mathbf{M}^{-1}\sum_{i=1}^{5}\mathbf{K}_i\Phi_i + \sum_{i=1}^{5}\mathbf{f}_i^{-1}\gamma\hat{\theta}_i\dot{\hat{\theta}}_i\right] \qquad (14)$$

With the adaptive controller Eq. (10), Eq. (11) and $\varepsilon > \sigma$, the equation in the first bracket of (14) becomes

$$\tilde{\mathbf{e}}^{\mathrm{T}}(\mathbf{M}^{-1}\sum_{i=1}^{5}\mathbf{P}_i\Phi_i + \mathbf{M}^{-1}\mathbf{u}_d) + \sigma\tilde{\mathbf{e}}^{\mathrm{T}}\dot{\mathbf{e}} - \sum_{i=1}^{5}\mathbf{f}_i^{-1}\gamma\theta_i\dot{\hat{\theta}}_i$$
$$= \tilde{\mathbf{e}}^{\mathrm{T}}\sum_{i=1}^{3}\mathbf{M}^{-1}\mathbf{P}_i\Phi_i - \sum_{i=1}^{3}\alpha\beta_i\|\tilde{\mathbf{e}}\|\|\Phi_i\| + \sigma\tilde{\mathbf{e}}^{\mathrm{T}}\dot{\mathbf{e}} - \varepsilon(\|\tilde{\mathbf{e}}\|\|\dot{\mathbf{e}}\| + \|\tilde{\mathbf{e}}\|\|\mathbf{e}\|) + \tilde{\mathbf{e}}^{\mathrm{T}}\mathbf{M}^{-1}\mathbf{u}_d - \alpha(d_0\|\tilde{\mathbf{e}}\| + d_1\|\tilde{\mathbf{e}}\|\|\dot{\mathbf{e}}\| + d_2\|\tilde{\mathbf{e}}\|\|\mathbf{e}\|)$$
$$\le \sum_{i=1}^{3}(\|\mathbf{M}^{-1}\|\|\mathbf{P}_i\| - \alpha\beta_i)\|\tilde{\mathbf{e}}\|\|\Phi_i\| + (\sigma-\varepsilon)\|\tilde{\mathbf{e}}\|\|\dot{\mathbf{e}}\| - \varepsilon\|\tilde{\mathbf{e}}\|\|\mathbf{e}\| + (\|\mathbf{M}^{-1}\| - \alpha)(d_0 + d_1\|\dot{\mathbf{e}}\| + d_2\|\mathbf{e}\|)\|\tilde{\mathbf{e}}\| \le 0 \qquad (15)$$

and the equation in the second bracket becomes

$$-\tilde{\mathbf{e}}^T\mathbf{M}^{-1}\sum_{i=1}^{5}\mathbf{K}_i\Phi_i+\sum_{i=1}^{5}f_i^{-1}\gamma\hat{\theta}_i\dot{\hat{\theta}}_i=\sum_{i=1}^{5}(-\frac{\tilde{\mathbf{e}}^T\mathbf{M}^{-1}\tilde{\mathbf{e}}}{\tilde{\mathbf{e}}^T\tilde{\mathbf{e}}}+\gamma)\|\tilde{\mathbf{e}}\|\|\Phi_i\|\hat{\theta}_i\ \le\sum_{i=1}^{5}(-\lambda_{min}(\mathbf{M}^{-1})+\gamma)\|\tilde{\mathbf{e}}\|\|\Phi_i\|\hat{\theta}_i\ \le 0 \quad (16)$$

From Eqs. (14), (15) and (16), we can conclude that $\dot{V}<0$ for all $\tilde{e}\neq 0$. Therefore, the tracking error e will asymptotically go to zero from Eq. 10.

The adaptive controller is described by Eqs. (8), (10) and (11). However, the direct use of the controller of Eq. (10) would generate large control input signals at near zero values of the denominator. To avoid this problem, the following modified controller is used:

$$\mathbf{K}_i=\frac{\hat{\theta}_i\tilde{\mathbf{e}}\Phi_i^T}{\|\tilde{\mathbf{e}}\|\|\Phi_i\|}\quad \text{for } \|\tilde{\mathbf{e}}\|\|\Phi_i\|>\delta_i$$
$$\mathbf{K}_i=\frac{\hat{\theta}_i\tilde{\mathbf{e}}\Phi_i^T}{\delta_i}\quad \text{for } \|\tilde{\mathbf{e}}\|\|\Phi_i\|\le\delta_i \qquad (17)$$

where i = 1,...,5 and δ_i is a positive constant.

The modified controller of Eq. (17) may not guarantee asymptotic stability; however, tracking errors are bound by small values of δ_i. To reduce the error, a term $k_I\int e dt$ is added to Eq. (8), where k_I is a small constant.

Influence and Control parameters

There are four parameters that affect the performance of the adaptive controller: adaptation gain (f) in Eq. (11), sigma (σ) in Eq. (12), threshold (δ) in Eq. (17), and I-control gain (k_I). One can note the following, σ affects the time constant of the overall control system. The adaptation gain f affects the adaptation period. Appropriate values of the threshold δ would keep the denominator in Eq. 17 from becoming the near zero value that may cause high gain values and large control signals beyond saturation limits. Appropriate small values of the I-control gain k_I would help reduce the steady state errors due to δ without affecting the overall stability.

Effects of these parameters were investigated by experiments on ODIN. The desired path for ODIN has three segments. Segment 1: ODIN moves down from the surface with the position control in the z direction only (Z: 0 to 2 m). Segment 2: ODIN then moves in the y direction with position control in all 6 dof, tracking in y (y: 2.5 to 4.5 m) and regulation in x at 2.5 m, z at 2 m, pitch at zero degree, roll at zero degree, and yaw at zero degree. Segment 3: ODIN then moves in the x direction with position control in all 6 dof, tracking in x (x: 2.5 to 4.5 m) and regulation in y at 4.5 m, z at 2 m, pitch at zero degree, roll at zero degree, and yaw at zero degree. The desired trajectory for each segment of the path was generated using a trapezoidal velocity profile. Since there was no position control in the x and y directions during segment 1, ODIN was usually away from the desired initial location of segment 2 at (x, y)= (2.5m, 2.5m) after segment 1. As can be seen from experimental results in Figures LLC-4 to 6, ODIN tried to move to the desired x and y location (2.5m, 2.5m) as soon as segment 2 started with control in all 6 dof. During experiments, all control gains were initially set to zero.

Case 1: Effect of σ was tested with three different values of σ = 1, 2 and 3. The same values of (f, δ, k_I)=(0.9,55,0.008) were used for each σ. It can be seen from Figure LLC-4 that the tracking in the x-y plane is much better when sigma = 2 (Figure LLC-4b) than when sigma = 1 (Figure LLC-4a). However, when sigma increases to sigma = 3, the performance degrades. This is because when sigma is too large, it leads to very large voltage input, reaching the saturation limit of the motor. Oscillation is observed in Figure LLC-4c.

Case 2: Effect of f was tested with three different values of f = 0.2, 0.5, and 0.9. The same values of (σ, δ, k_I)=(2,55,0.008) were used for each f. Figure LLC-5 shows that the performance gets better when adaptation gain f increases from f = 0.2 (Figure LLC-5a) to f = 0.5 (Figure LLC-5b) and to f = 0.9 (Figure LLC-5c).

Case 3: Effect of δ was tested with three different values of δ = 55, 60, and 65. The same values of (σ, f, k_I)=(2,0.9,0.008) were used for each δ. As shown in Figure LLC-6, tested values of δ provide almost the same performance even though it was observed during the wet experiment that δ=0 caused instability of the system.

Case 4: During wet tests to investigate effect of k_I, the following values for other parameters were used: (σ, f, δ)=(2,0.9,55). The influence of I-control gain k_I is shown in Figure LLC-7. It was observed in earlier tests that there were almost no steady state errors in x, y and other angles with or without k_I but large steady state errors in the z direction without k_I. Therefore, k_I was used only for the z direction. Figure LLC-7 shows that the steady state errors are reduced significantly with k_I = 0.008 (Figure LLC-7b) compared to steady state errors with k_I = 0 in (Figure LLC-7a).

Conclusion

This section described a new multi-input multi-output (MIMO) adaptive controller using bound estimation for underwater robots and presented experimental results of the control system on ODIN. Results show that the control system did not require any prior information about the system dynamics and yet could provide high performance in the presence of noise and unmodeled dynamics. Even though a very simple static thruster model was used as part of the control system, the adaptive controller could still provide good performance. No information about the ODIN's hydrodynamics was required in the adaptive controller design, yet it still provided good performance. Conventional linear controller with zero or poorly tuned gains cannot provide good performance and may even result in instability while the presented adaptive control performed well with gains initially set to zero. The fine-tuning of PID-type controller gains for the underwater robot system is very difficult if not impossible. It is not only due to the robot's highly nonlinear and time-varying dynamics but also because the operator may not have full access to the robot's on-board control unit while the robot is in water.

Based on a theoretical model and experimental results, ODIN's dynamic model was obtained and computer simulator software for ODIN, *OdinSim* was also developed in Matlab as well as in C language, including all modules shown in Fig. 2. Future research will be on integration of a GA-based motion planner [Sugihara 1998] with the presented navigation and control system and its implementation on ODIN.

Localization using Certainty Grids

Introduction

A largely unexplored area of underwater navigation is the ability to estimate the autonomous underwater vehicles' (AUV) position given an a priori map of the vehicles working space. In other words, the AUV must be able to determine from a small number of sensor readings its current position given a map made previously from a large set of readings. We will explore this problem of localization of the vehicle using the certainty grid technique developed by Elfes 1987 and Moravec 1989.

Currently, most AUV localization techniques are "geometric" based and require constructing point, line, or other surface descriptions from sense data at an early stage of processing [Faugeras 1993]. Leonard 1997 uses a technique called concurrent mapping and localization (CML), which tracks the vehicle and a set of proposed features through time. Leonard's system theoretically will produce very accurate results even without an a priori map of the environment; however, the technique requires the use of very expensive underwater navigation sensors (such as the Navy's high resolution array (HRA) imaging sonar [Nussbaum 1996]). The technique also suffers with the lack of features to reference, ie. a sandy bottom. Healey 1996 and McLain 1996 have investigated other "geometric-based" techniques for AUV localization. However, they have the disadvantage of having to process a tremendous amount of data about the geometric extensions in a very short amount of time. Thus, the technique is susceptible to errors if the underwater sensors are not clean.

The technique that we wish to demonstrate uses the evidence grid approach. The technique allows the use of fairly inexpensive wide beam angle sonar's. These underwater sensors are known for having transient mis-readings. Instead of registering objects, the grid method accumulates occupancy evidence from an array of spatial locations and slowly resolves the ambiguities as the AUV travels [Moravec 1996]. It has proved tremendously successful for land based mobile robots. Stewart 1988 considered concurrent mapping and positioning of underwater vehicles using a grid-based technique. Aramaki 1996 used a grid-based technique with their "Twin Burger" underwater vehicle.

Mathematical Approach for Certainty Grid

Certainty grids (or occupancy grids) are mapped regions of space divided into cells, where each cell represents the probability of being occupied or empty. The implementation of the certainty grid algorithm requires a sensor map (Figure LLC-8) and an update rule. The update rule assigns a value between 0 and 1 based on the probability that the grid is occupied.

In order to determine the occupancy probability, Moravec 1996 used a Bayesian model updating formula. The Bayesian sequential update formula may be written as

$$p(A \mid B_k) = \frac{p(b_k \mid A \wedge B_{k-1})}{p(b_k)} \times p(A \mid B_{k-1})$$

Now, let's substitute o for A, which corresponds to the current certainty value of the cell. Next, let B_k correspond to R_k, the sequence of all the range reading obtained so far. Finally, let b_k correspond to r_k, a single range reading. The Bayesian update rule is rewritten as the following

$$p(o \mid R_k) = \frac{p(r_k \mid o)}{p(r_k)} \times p(o \mid R_{k-1})$$

The quantity $p(r_k \mid o)$ determines the probability of getting a given range reading given the cell is occupied. This is the sensor model, which was shown in figure 1. The quantity $p(r_k)$ is the probability of getting a range reading independent of the occupancy of the cells.

Future Tasks

- Continue testing of control systems on the ODIN AUV before porting to SAUVIM.
- Continue the development of the localization algorithm.
- Test the localization algorithm to the ODIN AUV and test.
- Refine and combine the vehicle control and manipulator software.
- Import software to SAUVIM.

Figure LLC-1: ODIN AUV

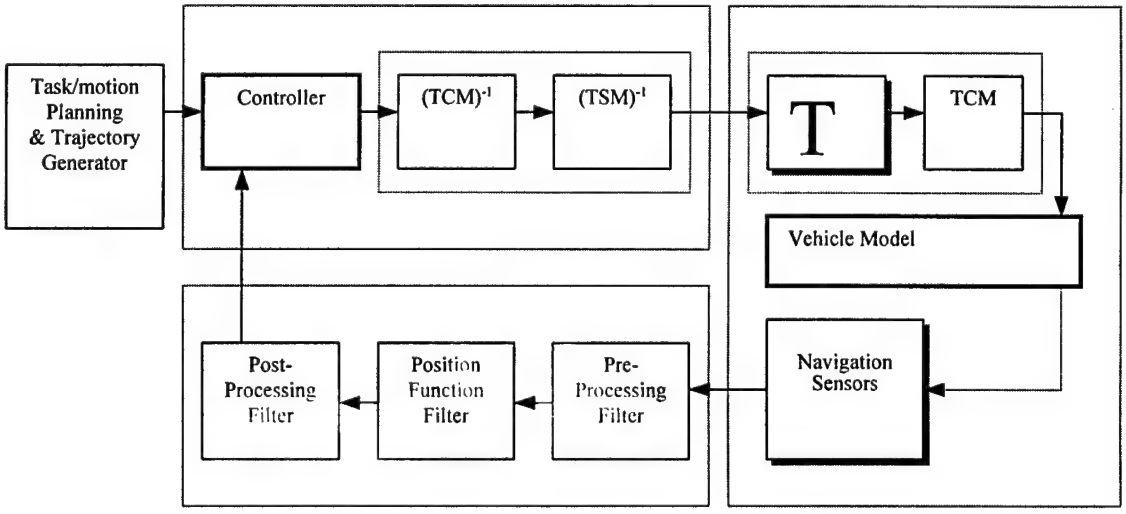

Figure LLC-2: Block diagram of navigation and control system

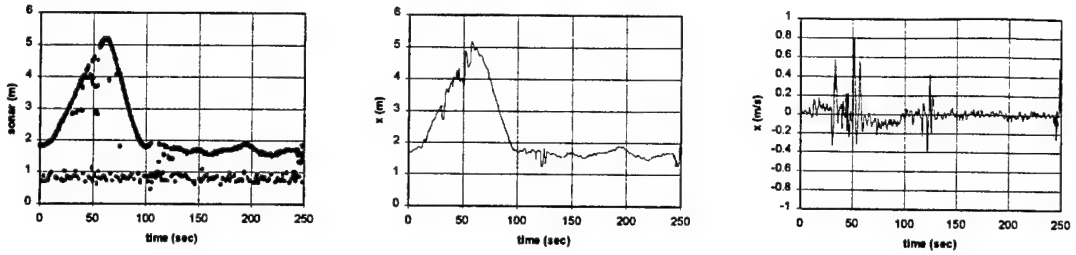

(a) (b) (c)

Figure LLC-3: (a) Unfiltered sonar signal, (b) Position from Kalman filter, (c) Velocity from Kalman filter.

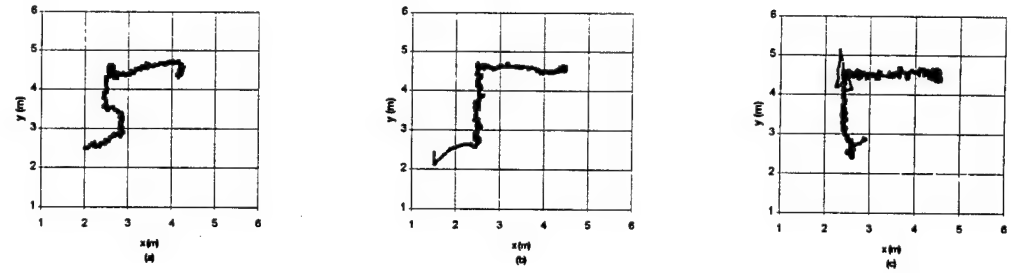

Figure LLC-4: Influence of control parameter sigma. (a) sigma =1, (b) sigma =2, (c) sigma=3.

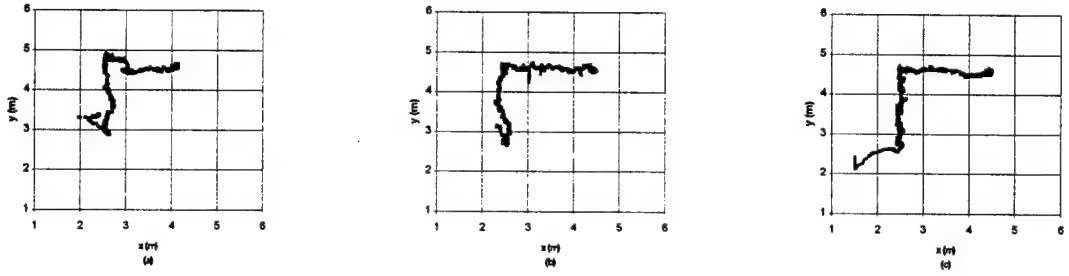

Figure LLC-5: Influence of control parameter f. (a) f=0.2, (b) f=0.5, (c)=0.9.

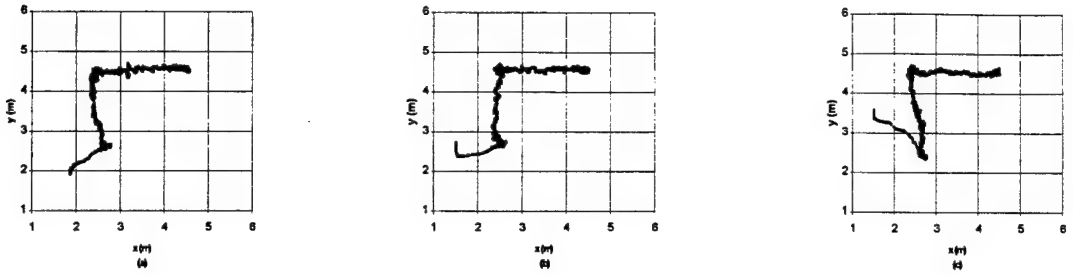

Figure LLC-6: Influence of control parameter threshold: (a) threshold=55, (b) threshold=60, & (c) threshold=65.

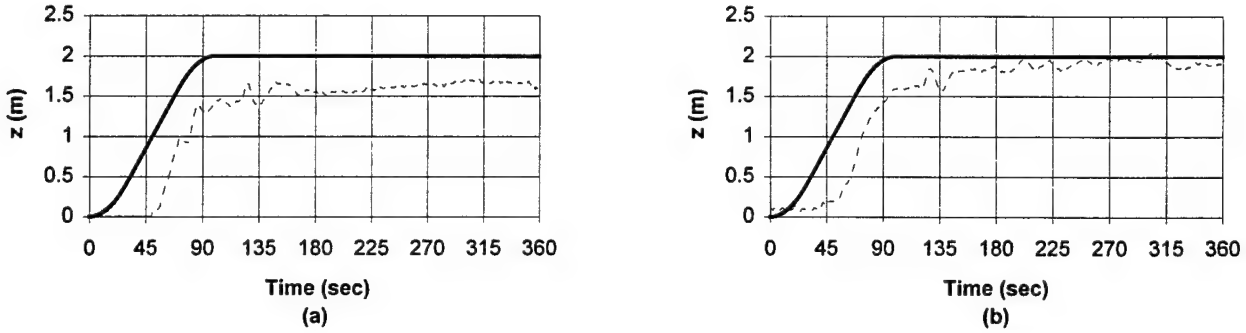

Figure LLC-7: Influence of control parameter k_I in z direction. (a) k_I=0, (b) k_I = 0.008.
(__ Desired trajectory -- Actual trajectory)

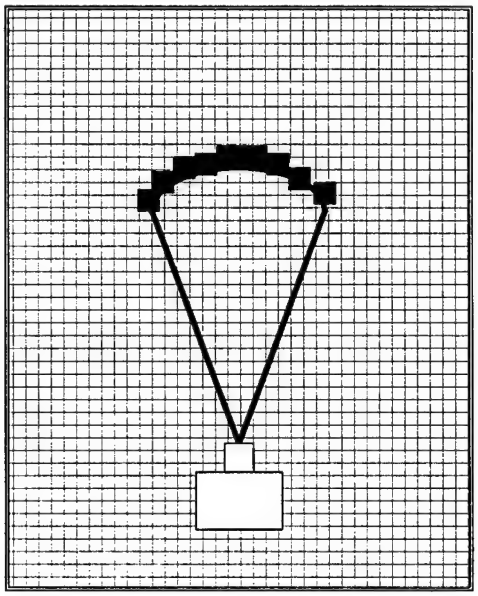

Figure LLC-8: Sonar Senor Model

High-Level Control (HLC)

Project Leaders: Dr. Junku Yuh, Dr. Kazuo Sugihara & Dr. Song K. Choi
Personnel: Mr. Zhi Yao

Objectives

To develop an event-driven supervisory control module that minimizes human involvement in the control of underwater manipulation tasks.

Current Status (Tasks Completed During 8/1/98 - 7/31/99):

From a human viewpoint, a mission is always composed of two parts: the goal and the method of accomplishment. Other words, "what do I need to do" and "how do I do it". Following this strategy, a new architecture of vehicle control, named Intelligent Task-Oriented Control Architecture (ITOCA), is developed for SAUVIM. ITOCA is an effective and efficient operation running on the VxWorks real-time operating system (RTOS) environment. ITOCA is four layers: Planning Layer; Control Layer; Execution Layer and Evaluation Layer. Every mission is broken into many smaller missions, and the simplest mission is considered a task. The combination of different tasks in different sequences accomplishes various missions.

The planning layer consists of the plan supervisor and task supervisor. The plan supervisor decomposes the given mission into the sequence of several sub-goals. The task supervisor sequences task modules for each sub-goal. Common sub-goals and task modules are pre-programmed in database along with a world model that is continuously updated using sensor data. The control layer handles various control actions, such as the adaptive and intelligent motion control and the manipulator force/position control, based on the sequence of tasks. The execution layer includes permanent tasks independent of specific missions. These tasks are interrupt handling, shared memory control, navigation sensor handling, servo control, and communication. The evaluation layer checks the status of the vehicle/manipulator performance by comparing actual performance based on sensor feedback with desired performance given by the plan supervisor and task supervisor. This layer makes a decision for the modifications of sub-goal planning and task sequences or the suspension of the mission from fatal errors.

Advancements, in the SAUVIM software modules of motion planning and control, include: off-line and on-line motion planning modules based on GA; a low-level control module using a new non-regressor based adaptive control scheme; and a redundancy resolution control module for the vehicle and manipulator system.

Future Tasks

- Refinement of ITOCA and development of generic ITOCA command language.
- Software implementation of preliminary version of ITOCA.
- Testing of ITOCA and refinement..
- Implementation in to the SAUVIM software.

Dry Test Design and Set-Up (DTDS)

Project Leaders: Dr. Song K. Choi
Personnel: Mr. Tommaso Bozzo & Mr. Giacomo Marani

Objectives

To design and fabricate a manipulator-vehicle dry test-bed, which will allow high-level, manipulator force/position control algorithm developments. The test-bed will have a fully functional manipulator mounted on a free-moving base, thus allowing translational (x-axis and y-axis) and rotational (roll and pitch) motions.

Test-Bed Description:

The test-bed will have a generic manipulator – kinematically proportional or identical to the SAUVIM manipulator – residing on a free-moving base which will allow dampened translational and rotational motions closely emulating the translational, pitch and roll motions of a submerged underwater vehicle. The free-moving base may be subjected to input motions via a pneumatic, hydraulic or human interaction and will be housed in a fiberglass water tank. A force/torque sensor will be attached to the manipulator wrist to measure the tip contact force, and a prototype passive arm sensor will be attached to the free-moving base to measure its position changes.

Current Status (Tasks Completed During 8/1/98 – 7/31/99):

Since the primary goal of the DTDS is to provide a simple, algorithm development platform, the overall design and its fabrication are simplified. Instead of an identical SAUVIM manipulator, a PUMA 560 arm – a standard, tutorial robot – and a simple, spring and damper free-moving base combination is used. The PUMA arm is fixed to a 3-foot circular, metal plate and suspended in air by eight springs and four pneumatic/hydraulic actuators, which act as dampers. The eight springs have a spring stiffness value capable of sustaining an overall load of 250-lbs (total weight of PUMA arm, free-moving base, and relevant components). The pneumatic/hydraulic actuators are adjustable to create a desired dampening effect. For example, it will be ideal to begin the force/torque/position algorithm developments with a completely stationary base (actuators are in a fixed position) then proceed to an increase in movements (actuators pressures are released to allow movement). A six degree-of-freedom (dof), JR3 force/torque sensor is attached to the PUMA arm at its wrist to obtain force/torque readings. The PUMA arm and base are placed in a fiberglass tank. Currently, the base unit is being fabricated. (Craig 1996, Unimate 1981, Unimate 1984)

The DTDS is controlled by a combination of an Intel 586 PC. The passive arm sensor provides the base position data to the PC. The JR3 sensor provides the PUMA arm force/torque information to the PC. Both the base position and arm force/torque data will be furnished to the PUMA controller via a RS232 connection. These simple connections create crude but sufficient feedback system for the arm. The overall system can be seen in Figure DTDS-1.

With the arrival of the 7-dof, Ansaldo manipulator, the original DTDS development has been suspended, and the new DTDS utilizing the Ansaldo has commenced. The current setup consists of the Ansaldo manipulator connected to a VME bus with motor control I/O boards and a VxWorks

CPU board (Figure DTDS-2). The software for the overall system utilizes the Matlab and Simulink software packages. The software development is expected to proceed in conjunction with the TM Group.

Future Tasks

- Completing the wiring of the Ansaldo manipulator setup;
- Establishing the software and hardware synchronization;

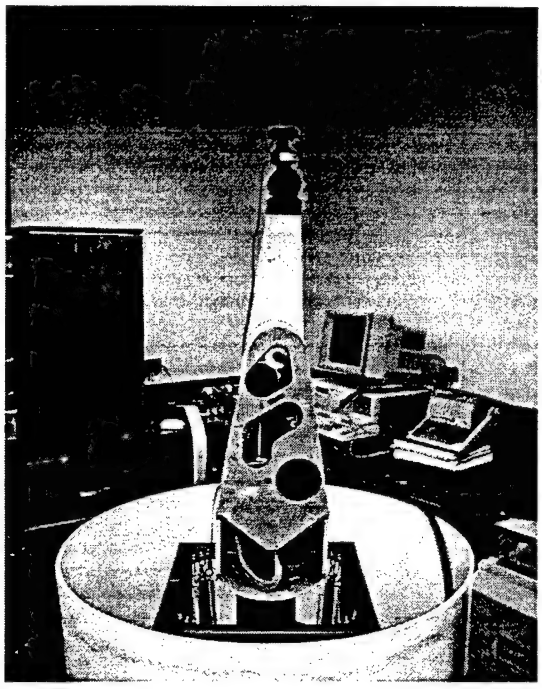

Figure DTDS-1: Original DTDS Utilizing the PUMA Arm.

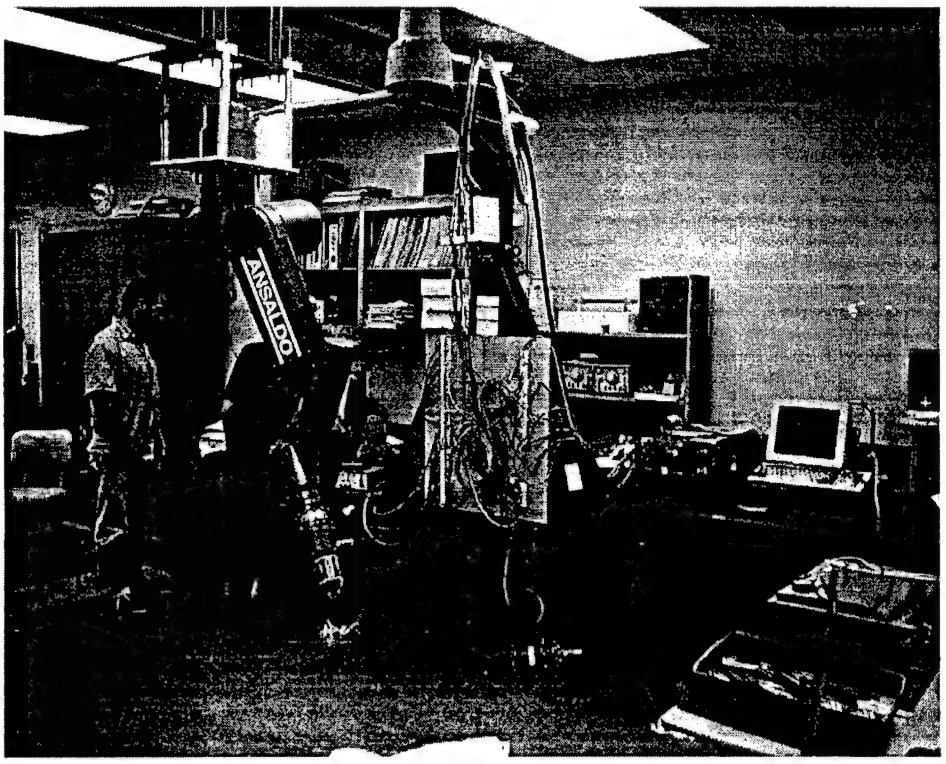

Figure DTDS-2: The New DTDS Utilizing the Ansaldo Manipulator

Predictive Virtual Environment (PVE)

Project Leader: Dr. Stephen Itoga, Dr. Kazuo Sugihara & Dr. Song K. Choi
Personnel: Mr. Scott Menor, Mr. Alexander Nip & Mr. Zhenyu Yang

Objectives

This sub-project aims at applying virtual reality (VR) to the construction of the predictive virtual environment that presents a supervisor with the current situation of SAUVIM as accurately and realistically as possible.

The basic four objectives are:

- To develop software for data fusion of map data and online sensory information;
- To develop software to smooth out a jerky virtual environment due to delayed information from limited bandwidth of communication;
- To develop a learning algorithm for prediction of the current situation from the delayed information acquired by SAUVIM; and
- To integrate the above software modules and interface them with SAUVIM communication for the PVE.

Current Status (Tasks Completed During 8/1/98 - 7/31/99):

In order to clarify what have been accomplished in the second year, the achievements of the first year (8/01/97 - 7/31/98) are summarized as follows.

- A graphic simulation program with the primitive functionality had been implemented in C by using the WorldToolKit (WTK) software from Sense8.
- A virtual instrumentation panel had been implemented in Java so that it runs on any platform by using a Web Browser, such as Netscape or Internet Explorer.
- A program for generating a 3D model of seafloor from real geometric data had been implemented so that the seafloor could be displayed on WTK.

The major achievements of the second year (8/1/98-7/31/99) are the following:

1. SAUVIM Simulation Software Version 1.0, upgraded to Version 1.1 (shown in Figure PVE-1)

    - A Magellan, space-ball mouse has been added to the previous simulation program.
    - An accurate, 3-D graphic model of SAUVIM with the Ansaldo manipulator was created and incorporated.
    - A simple, scene-smoothing technique was implemented by applying the interpolation to the movement of SAUVIM in PVE.
    - An easy-to-use graphic user interface (GUI) was implemented to control the movement of SAUVIM and the Ansaldo manipulator, to change a viewpoint of the virtual environment, to record a simulation run, and to play the simulation back and forth.

2. Video Overlay Software Version 1.0 (shown in Figure PVE-2)

- A program for overlaying video images to the graphic seafloor within the PVE was implemented. It takes a 2D image from a camera of SAUVIM and overlays the image on the surface of a 3D terrain presented in PVE.
- The program was demonstrated by using simulated data for a terrain and an image.

3. Communication Software Version 1.0 for Multiple Vehicle System (MVS, shown in Figure PVE-3)

   - A program, which enables PVE to communicate with vehicles for data fusion, was implemented.
   - The program was tested by experiments, which involved the use of a cellular phone communicating to a modem between the ODIN AUV and SGI Indy (workstation where the MVS software resides).

4. Preliminary design and experiments of ANN (Artificial Neural Network) for prediction of the movement of objects in PVE (shown in Figure PVE-4)

   - Different types of ANNs were surveyed. A 3-layered neural network using backpropagation as a learning algorithm was chosen in order to predict the current situation of SAUVIM based on the delayed information sent from SAUVIM through a communication channel (i.e., acoustic link) of limited bandwidth.
   - The ANN for prediction was designed and implemented in C, provided that input video data was preprocessed to extract the position of target objects in the video frames.
   - The ANN was empirically evaluated, and it was found reasonable in terms of accuracy (limited to within 5% on the average) and computational time (a few ms per frame).
   - For prediction of the movement of multiple objects, two methods based on the ANN were compared. One method uses one instance of the ANN for predicting all the moving objects, and the other uses one instance of the ANN for each of the moving objects. There was no noticeable difference in accuracy. Since the second method is more flexible and easier to implement by software, the second method is preferable to the first method.

Future Tasks

- To implement graphic-scene prediction software based on the designed ANN.
- To integrate various software modules in the overall PVE system.
- The development of PVE will continue through Phase II.

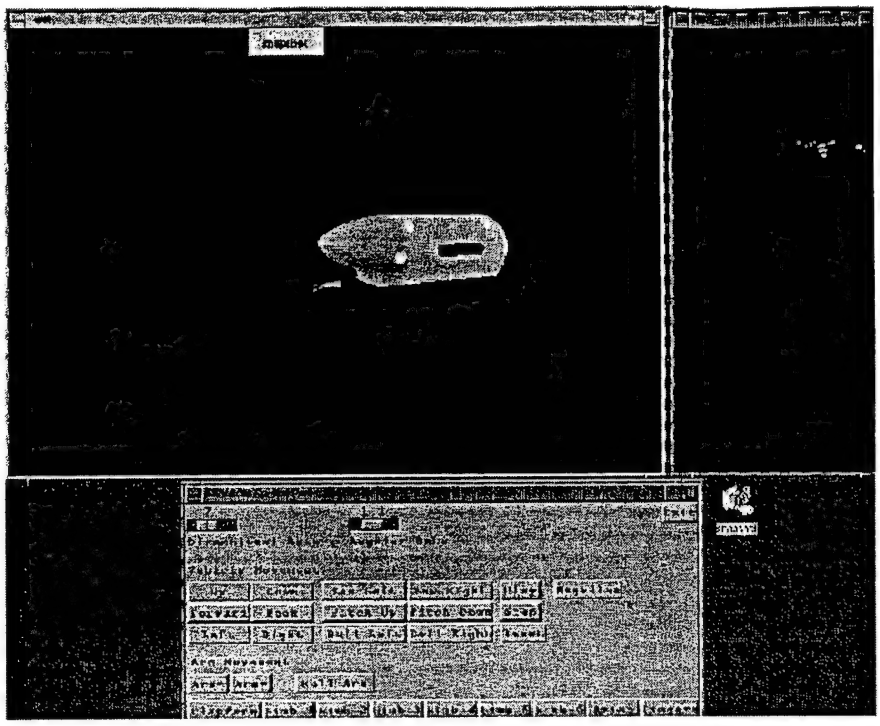

Figure PVE-1: SAUVIM simulation software.

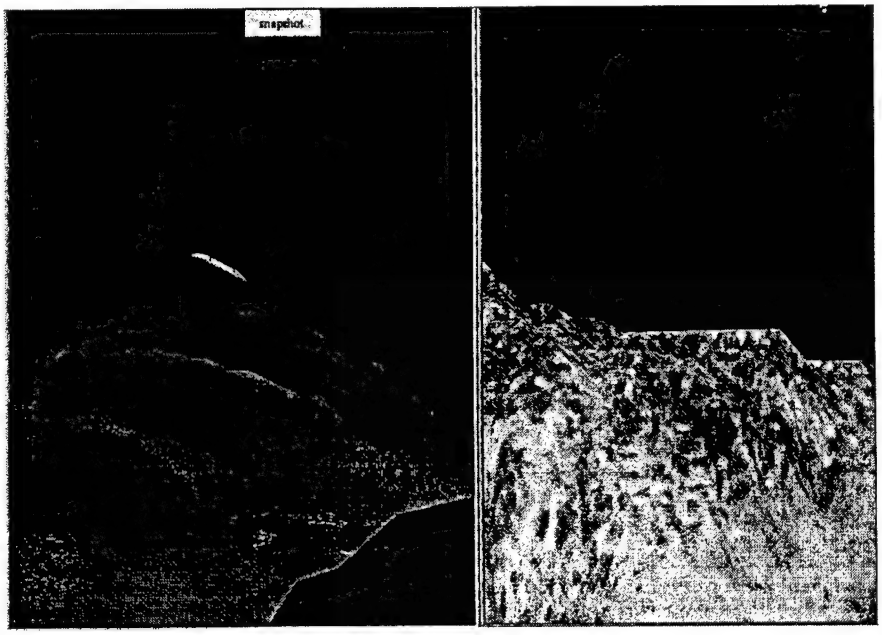

(a) 3D presentation in PVE (b) Video image

Figure PVE-2: Video overlay software.

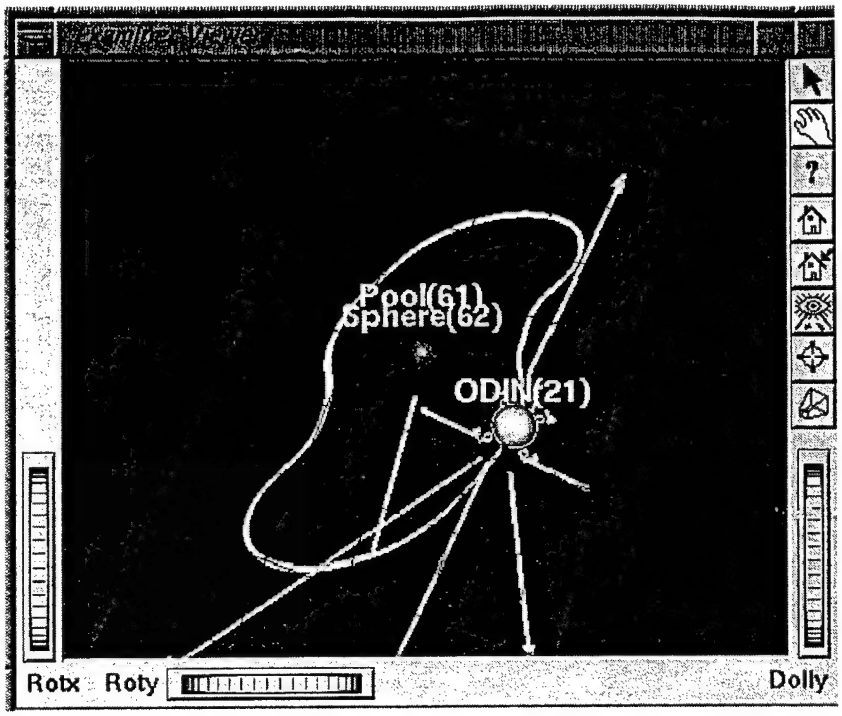

Figure PVE-3: MVS communicating with a vehicle.

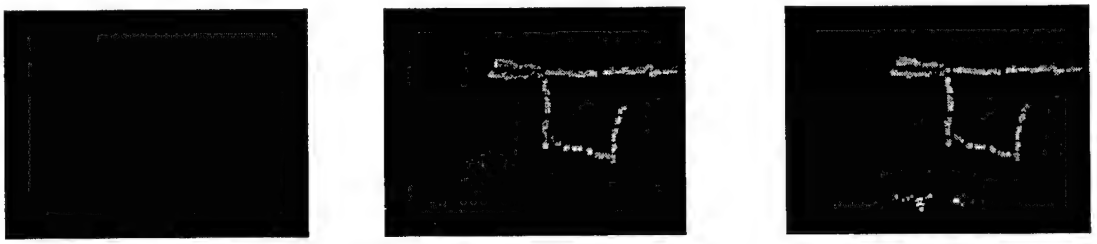

(a) Actual Motion (b) Predicted Motion (c) Overlap of (a) & (b)

Figure PVE-4: An Experiment for Prediction of Two Moving Objects by ANNs.

SAUVIM Design (SD)

Project Leaders: Dr. Tae W. Kim, Dr. Pan-Mook Lee, Dr. Gary McMurtry, Dr. Junku Yuh, Dr. Song K. Choi , Dr. Mehrdad Ghasemi Nejhad & Mr. Curtis Ikehara.

The main technical progress of the SD group is described in the following sections: Reliable, Distributed Control, Mission Sensor Package, Hydrodynamic Drag Coefficient Analysis, Mechanical Analysis & Fabrication, and Mechanical-Electrical Design.

Reliable, Distributed Control (RDC)

Project Leaders: Dr. Pan-Mook Lee & Dr. Tae Won Kim
Personnel: Mr. Jang-Won Lee & Mr. Michael West

Objectives

Develop a reliable and efficient computing architecture for signal and algorithmic processes of the entire SAUVIM system.

Current Status (Tasks Completed During 8/1/98 - 7/31/99):

- The overall control system architecture has been modified and major hardware components were purchased and tested.
- The basic software architecture was designed and hardware driver functions were designed and tested.

Structure of SAUVIM Control System

As shown in Figure RDC-1, the SAUVIM controller consists of multiple CPU boards and I/O boards to distribute tasks among the components. The structure was designed for the boards to work together and perform specific tasks. The boards are connected via VME buses or Ethernet lines depending on the time dependencies of tasks. The entire controller system will be installed in two separate pressure vessels based on control objects. The first pressure vessel will contain hardware components for navigation of the vehicle. The second pressure vessel will house underwater manipulator controller and related components. These two pressure vessels are connected with Ethernet cables. Though Ethernet link can have a little delay in communication, the communication between two systems is not time-critical.

Navigation Control System Hardware

Navigation control system consists of three CPU boards and multiple I/O boards. Two of CPU boards are Motorola MC68060 CPU based Force Computer SYS68K-60Ds. The other board is Pentium MMX processor based PC104 board. Two MC68060 CPU boards are connected with VME bus. The PC104 board communicates with other CPU boards via Ethernet link. Two multifunctional AD/DA/DIO boards are used for interfacing vehicle hardware. One intelligent serial communication board is installed to handle communication between CPU chassis and sensors that have RS-232 or RS-485 interfaces.

The Force SYS68K-60D board has a shard DRAM onboard. The shared memory is used for task synchronization and data exchanges of two navigation CPUs. These two boards are connected via VME bus and Ethernet, but VME bus communication will be used extensively. A small network hub will be installed in the pressure vessel for Ethernet communications among the CPU boards.

The PC 104 board is based on Intel Pentium MMX CPU. A frame grabber card is installed on the board. Up to 4 cameras can be connected to the frame grabber. One of serial ports in the board will be used to receive data from scan sonar. The scan sonar transmits acquired data at 115.2Kbps via RS-

485 interface. Because the serial ports of the board are RS-232 type, a RS-485 to RS-232 converter will be installed.

Each multifunctional analog and digital I/O board, MD-DAADIO, has 32 ADCs, 8 DACs, and 48 digital I/O channels. The ADC and the DI port A (8 bits) of the MD-DAADIO can be driven with an interrupt service routine. The DI port A will be used for the emergency interrupt routines, e.g. leakage detecting routine. Compared to the previous configuration, another multifunctional I/O board has been added to expand capacity. Specific pin layout is under fine-tuning as the vehicle is constructed.

The intelligent serial communication board, MVC16, has 16 serial communication channels. These channels can be set up as RS-232, RS-422 or RS-485 using jumpers. In our configuration, MVC16 board has 12 RS-232 channels and 4 RS-485 channels. This board has own processor with 128Kbyte buffer memory. It does not require main CPU board's processor time to handle communication.

Manipulator Control System

Similar with navigation control system, manipulator control system has its own pressure vessel and power supply. The robot controller uses one Force SYS68K-60D processor board. Two PC 104 boards are used for laser ranger and homing devices. The manipulator control system communicates with the navigation control system via Ethernet. As mentioned earlier, there can be delay in Ethernet communication, but the delay can be neglected. The same multifunctional analog and digital I/O board is used to control brushless DC servo motors of the manipulator. Two IP quadrature counters are installed on a carrier board in the VME bus for detecting seven resolver signals from the motors and one encoder signal from hall sensor in the gripper. A 6 degrees-of-freedom force/torque sensor, JR3, is mounted at the wrist of the robot manipulator, and its controller is installed in the VME bus.

Figure RDC-1 shows the I/O boards and the external components for the manipulator controller. The homing sensor is interfaced with the RS-232 ports of the manipulator controller. The laser ranger is controlled by one of PC104 boards. The acquired information is transmitted to MVC16 intelligent serial communication board in the navigation control system via RS232 interface, because there are not enough serial ports in the manipulator control system and the system can not follow the bandwidth of the signal.

The manipulator control architecture is under development by the Theoretical Modeling and Low Level Control group and in cooperation with University of Genoa in Italy.

Attitude Heading Reference System: AHRS-BA303

AHRS is a low-cost reference navigation sensor. It uses a solid-state gyro system for an attitude gyro and a slaved heading gyro. It corrects errors with a closed loop system and adjusts biases from earth rotation and instrument offsets automatically. The attitude and heading signals are compared with two vertical reference pendulums and a tri-axial fluxgate magnetometer to derive short-term absolute errors. The detailed specification of AHRS-BA303 is provided in Table RDC-1.

Altimeter: Tritech PA200

SAUVIM will be equipped with four range sonar sensors, Tritech PA200. One is for altitude (vertical) and the others are for range measuring. These sensors have RS-458 serial communication interfaces. Table RDC-2 shows the specification of PA200 sensors.

Electronic Compass Sensor: TCM2

TCM2 is an electric compass sensor module. It has a three-axis magnetometer and two-axis tilt sensor. In addition to compass heading, the TCM2 supplies pitch, roll, magnetic field data and temperature information. This sensor can be used as a backup sensor for the AHRS-BA303 sensor. The TCM2 specifications are in Table RDC-3.

Scan Sonar: Imagenex 881 High Resolution Imaging Sonar

The Imagenex sonar is an image scanning sonar. It will provide scanned images around the vehicle. The scanned images can be used for object avoidance or target detecting. However, actual implementation will be done in the future. The sonar consists of two parts. One is a sonar module with a rotating sonar head. The other is a digital signal processing module, which processes sonar signal and transmits processed data via RS-485 interface. Two modules are connected with an oil-filled underwater cable. The processing module is connected to the pressure vessel of the navigation control system with a 4-conductor underwater cable. Table RDC-4 shows specification of the Imagenex 881 sonar.

Software Architecture

There are several objective of software design for the SAUVIM. First, the whole software system is designed to be modularized so that anyone can implement his or her own control algorithm easily and additional functions can be easily added. Second, the tasks should be distributed among processor boards. The tasks should be performed in harmony with other tasks. Third, the system should provide fault-tolerant and/or fault-recovery functions to guarantee return of the vehicle in case of emergency.

Navigation Control System Software

The entire software is being developed on commercial 32-bit real-time operating system, VxWorks. As shown in Figure RDC-2, tasks are distributed in processor boards based on hierarchical software architecture.

The primary CPU board has several main functions. First, it handles the communication between the navigation control system and the manipulator control system. For example, when the manipulator control system requests the navigation control system to move the vehicle after failing to reach an object within arm range, it responds to the request and determines what to do. Second, it reports status of vehicle to the supervisor using Ethernet. Third, it performs high-level control like path planning and task planning It plans tasks based on predefined rules and sends commands to the second navigation CPU. High-level task routines are under development by related groups.

The second navigation CPU has shared memory onboard to synchronize tasks of two processor boards and communicate with other boards. It collects and keeps data required to operate vehicle in

shard memory and provides the data in response to the request from internal tasks or external request from other processor boards. The second CPU has device driver and data handling routines. It communicates with external devices using I/O device drivers for specific hardware. Current status of external devices is saved in the shared memory in the second CPU board for the first navigation CPU.

Manipulator Control System Software

The control software is under development by cooperation with University of Genoa in Italy and the Theoretical Modeling and Low-Level Control group. In the case of failure in the navigation control system, some redundant critical functions are implemented in the software. For example, weight drop task will be implemented in the manipulator control system.

Communication of Two Systems

The communication between the navigation control system and the manipulator control system is under development. The protocol between two systems is still under revising for reliability and integrity.

The overall VME bus system connected to a development server is shown in Figure RDC-3.

Future Tasks

- Revising the software structure and hardware configuration.
- Merging software components into the software architecture.
- Testing and debugging.

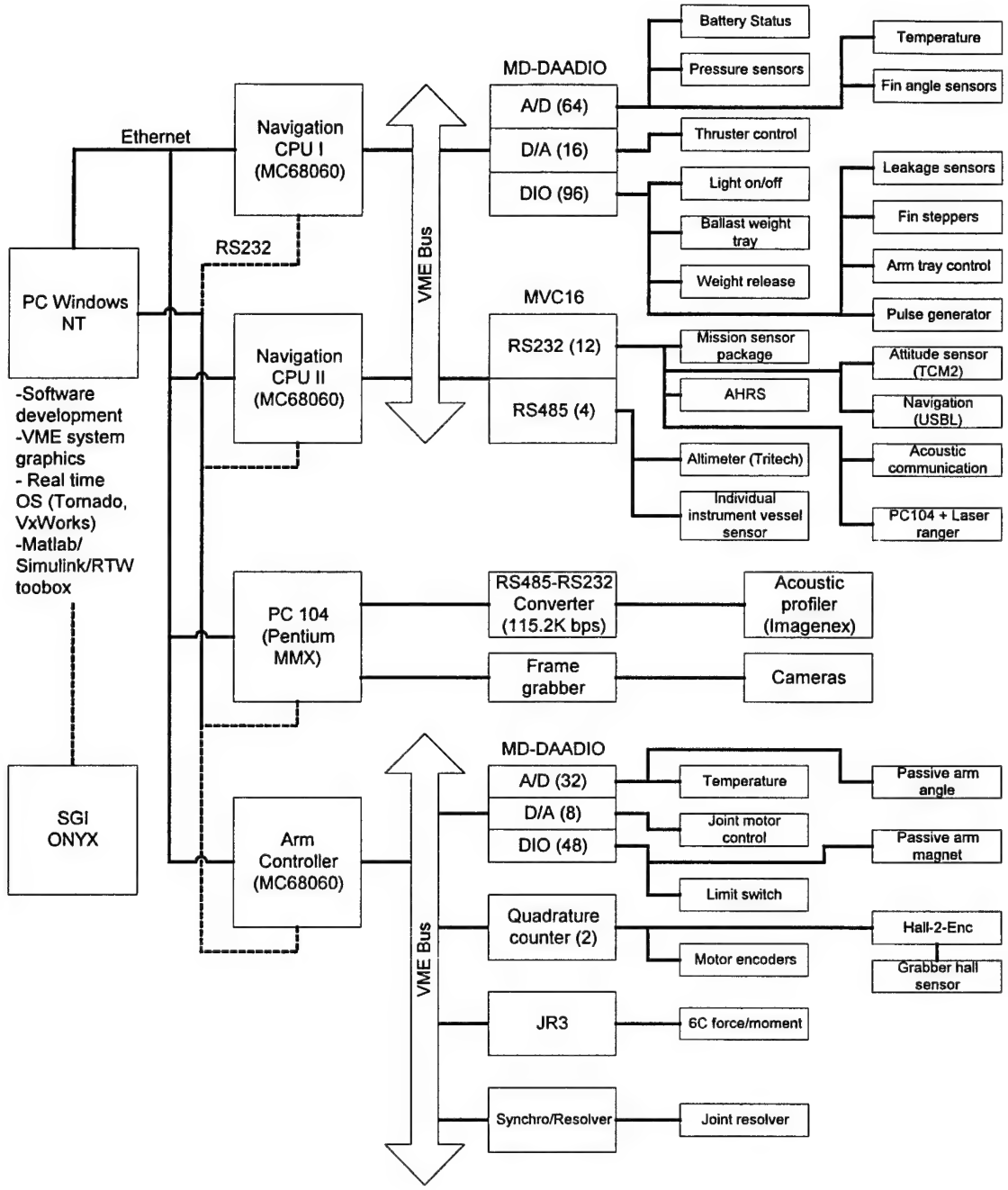

Figure RDC-1: System Diagram of SAUVIM.

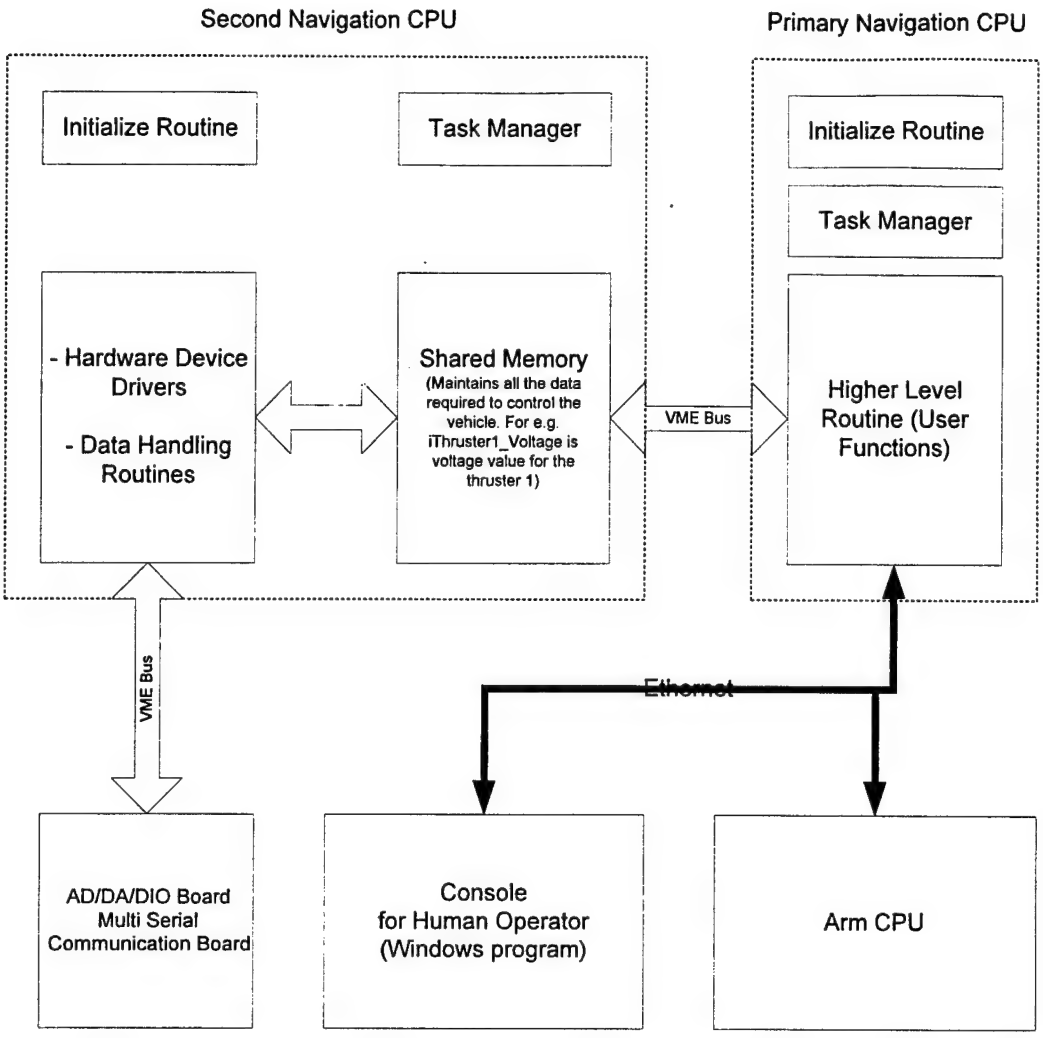

Figure RDC-2: Software Architecture of the Navigation Control System.

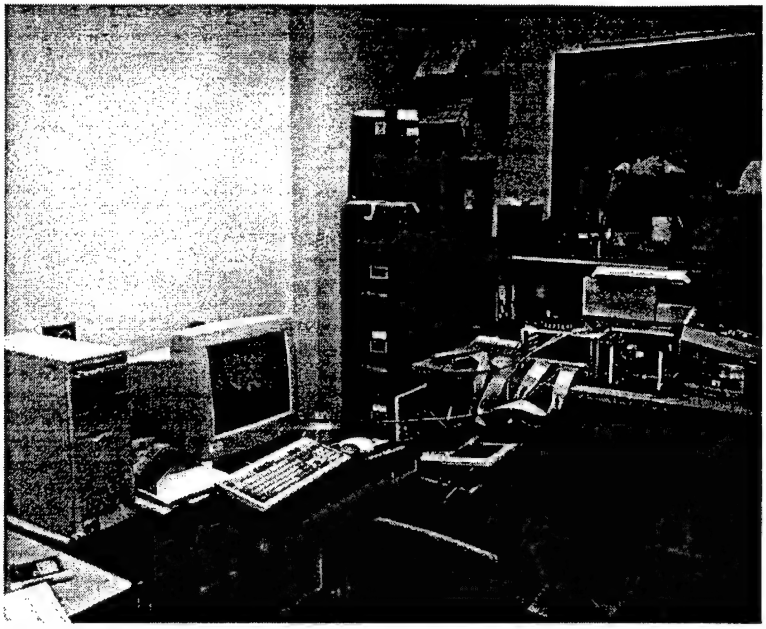

Figure RDC-3: SAUVIM VME Bus System Connected to the PC Development Server.

Table RDC-1: Specification of AHRS-BA303

Item	Range	Accuracy	Sensitivity	Remarks
Pitch rate	±100°/s	Static: ±0.2°/s Dynamic: ±2% digital ±6% analog	10 °/s/V	Positive for nose up
Roll rate	±100°/s			Positive for roll to right
Yaw rate	±100°/s			Positive for right turn
Heading rate	±100°/s			Positive for right turn
Bank	±180°	Static: ±0.5°/s Dynamic: ±2%	18 °/V	Positive for bank to right
Elevation	±90°			Positive for nose up
South heading	0 - 360°	Static: ±1°/s Dynamic: ±2%		S=0V, E=-5V, W=5V, N=±10V
North heading	0 - 360°			N=0V, E=5V, W=-5V, S=±10V
Velocity input	-400 – 400 Km/hr		40 Km/hr/V	Forward velocity
Error correction time		15 seconds		

Table RDC-2: Specification of Tritech PA200

Frequency and beam width	200 kHz and 20 degrees
Measurement range	100 meters
Operating depth	6800 meters
Input voltage	12 VDC
Interface	RS-485, 9600 bps, 8 data bits, 1 stop bit, no parity
Head RS-485 Termination	220 Ω (Sensor A only)
Command	*, or 'A', 'B', 'C', 'D'

Table RDC-3: Specification of Precision Navigation TCM2

Heading information	Accuracy when level	±0.5° RMS
	Accuracy when tilted	±1° RMS
	Resolution	0.1°
	Repeatability	±0.1°
Tilt information	Accuracy	±0.2°
	Resolution	0.1°
	Repeatability	±0.2°
	Range	±20°
Magnetic field information	Accuracy	±0.2 μT
	Resolution	0.01 μT
	Repeatability	±0.2 μT
	Range	±80 μT
Temperature information (sensor is uncalibrated)	Accuracy after calibration	±1°C, ±2°F
	Resolution	1°C, 2°F
	Range	-20°C to 70°C
Power requirement	Supply voltage	+5 VDC regulated 6 to 18 VDC unregulated
	Current	Standard mode: 15-20 mA Low-power mode: 7-13 mA Sleep mode: 2.5 mA
Interface	Digital	RS-232C, NMEA0183
	Analog	0-5V linear, 19.53 mV resolution (256 discrete levels), 0-5 quadrature (sine and cosine)

Table RDC-4: Specification of Imagenex 881

Frequency	675 kHz
Transducer	Imaging/profiling
Power supply	22 – 48 VDC at 1 Amp max.
Interface	RS-485 (115200 bps, 8 data bits, 1 stop bit, no parity)
Operating range	5 – 200 meters (15 – 600 feet); Default: 50m (150ft)
Sector size	Scan with angle Sector mode: 0 to 180° in 3° increments; Default: 180° Polar mode: 0 to 360° in 3° increments; Default: 360°
Speed	Step size angle Slow: 0.3°/step Med: 0.6°/step Fast: 0.9°/step Faster: 1.2°/step Fastest: 2.4°/step Default: fast
Transmit pulse length	0 to 255 μs in 5 μs increments

Mission Sensor Package (MSP)

Project Leaders: Dr. Gary McMurtry
Personnel: Mr. Alan Parsa

Objectives

The SAUVIM Mission Sensor Package for Phase 1 is designed to provide semi-continuous records of AUV water depth (pressure), water temperature, conductivity, computed salinity, dissolved oxygen, pH and turbidity for at least eight hours. These parameters as well as the magnetic signature of the seafloor can be acquired by the SAUVIM in survey mode. In intervention mode, the Mission Sensor Package will provide AUV water depth (pressure), water temperature and compositional parameters at a selected seafloor target, including pumped samples from submarine seeps or vents.

Current Status (Tasks Completed During 8/1/98 - 7/31/99):

All of the components for the mission sensor package have been acquired and most have been either bench or field-tested. The system layout is presented in figure X, and a wiring diagram is presented in figure X+1. A photograph of the package on the seafloor during a brief test deployment on Loihi Seamount in October 1998 is also available. Ambient seawater or submarine vent/seep waters enter the Teflon sensor plenum through a short length of Teflon tubing, which contains a tributal tin marine antifoulant. The Teflon entry nozzle is screened and will face the forward direction of the AUV, allowing waters to passively enter the sensor housing when the AUV is running, or to be pumped across the sensors when the AUV is station keeping. Otherwise, the Sea Bird Electronics impeller pump will remain off to conserve power.

The Ocean Sensors CTD is compact and low power; the sensor head is 2.25 inches in diameter and houses the conductivity cell, thermistor temperature probe, pressure, pH and dissolved oxygen sensors. The CTD and sensor electronics are housed in a 2.25-inch OD anodized aluminum pressure housing that is 6000-m capable. The ranges for the sensors are: pressure, 0 - 6000 decibars; temperature, -2 - 100° C; conductivity, 0.5 - 65 mS/cm; salinity (computed), 2 - 42 PSU; pH, 0 - 14 pH units; dissolved oxygen, 0 - 15 ml/l. All sensors are rated to 6000 m. The Ocean Sensors CTD electronics has been modified to slave to our CPU (via RS-232 link) and will allow up to eight additional analog inputs. Particle concentrations or turbidity levels are measured by a high-gain (to 33 mg/l) SeaTech light scattering sensor (LSS). The LSS or nephelometer will be externally mounted so that the light emitting diodes are not obstructed by the AUV frame.

The magnetic signature of the seafloor will be measured with an Applied Physics Systems model 544 miniature angular orientation sensor. The unit contains both a 3-axis fluxgate magnetometer and a 3-axis accelerometer. These sensors are sampled by an internal ADC and microprocessor subsystem, which outputs 16-bit digital data representing the magnetometer and accelerometer readings via an RS-232 cable to the CPU. Ideally, to minimize the AUV magnetic background, this small (0.75" x 0.75" x 4.6") sensor should be placed as far away from magnetic-field generating devices (e.g., motors, spinning propellers, circuit boards, hard disks) as practicable. To date, we plan placement of this sensor in the nose faring of the AUV. The angular orientation sensor is housed within a 2.5-inch OD cylindrical pressure vessel (6000-m capable) made of high-purity, grade 2 titanium.

For a 6000-m depth capability, we constructed a 7.5-inch OD titanium pressure housing for the sensor electronics, CPU and associated electronics. Currently, we use PC/104 card stacks for the CPU and a ≥500 MB Quantum hard drive for program and data storage. System power will be provided at 12 VDC via rechargeable NiCd batteries within the main body of the AUV. Communications (system command uploads/data downloads) to the surface and other AUV CPUs will be via a light-isolated RS-232 link. We plan for the mission sensor package to be located within the fiberglass faring under the AUV between the two forward battery pods, with the exception of the battery cache and magnetometer that will reside elsewhere within the AUV body. When station keeping, the AUV manipulator will be able to pull the nozzle out toward any vent or seep for better sampling.

Future Tasks

- Continue bench and shallow-water field tests.
- Acquisition of rechargeable NiCd batteries.
- Development of survey and intervention mode software routines.
- Integration of the MSP to SAUVIM software.

Hydrodynamic Drag Coefficient Analysis (HDCA)

Project Leader: Dr. Junku Yuh & Dr. Song K. Choi
Personnel: Mr. Brian Lau & Mr. Oliver Easterday

Objectives

- Determination of the hydrodynamic coefficient via numerical solution of full Navier-Stokes equations using commercial CFD code, PHOENICS.
- Provide design recommendations for the vehicle fairing from the hydrodynamic results.
- Perform experiments to verify and confirm the CFD results.

Current Status (Tasks Completed During 8/1/98 - 7/31/99):

The CHAM PHOENICS software generated various hardware and software errors when an attempt was made to numerically obtain a reasonable drag number for a known object. Further testing of the software will have to be conducted to confirm and verify other standardized numerical results with empirical data in references.

However, using standardized methods to calculate the coefficient of drag (C_d) of an object or a vehicle, the formula,

$C_d = F/0.5*\rho*A*V^2$,

where F is the force in the direction of the flow direction being tested, ρ is the fluid density, A is the frontal area of an object or vehicle, and V is the fluid velocity was used. For the SAUVIM, a coarse grid of *10x10x10* as provided by CHAM was used, and setting ρ as 998 kg/m^3, V = 3m/s, and SAUVIM frontal area of 10 m^2, the software generated a drag coefficient of 0.40.

Future Tasks

- Compare PHOENICS CFD results with other commercial CFD software.
- Fabricate SAUVIM model for testing.
- Compare CFD results to actual test data.
- Correct and modify CFD codes for future use.

Mechanical Analysis and Fabrication (MAF)

Project Leaders: Dr. Mehrdad Ghasemi-Nejhad
Personnel: Mr. Ali Yousefpour, Mr. Eric Sung, Mr. Bruce Flegal, Mr. Robert Ng & Mr. Mark Uyema

Objectives

- Design and manufacture composite pressure vessels with end caps and openings for an operating depth of 6000 meters taking stress, buckling, hygrothermal effects, and fatigue analysis into account.
- Design and manufacture a composite flooded fairing taking impact and crash analysis into account.
- Design an aluminum framing taking joint design into account.

Current Status (Tasks Completed During 8/1/98 - 7/31/99):

C-Ring Testing and Modeling

Mechanical performance of AS4/PEEK thermoplastic composite C-ring samples with different processing conditions was investigated, using in-situ thermoplastic composite filament winding, and the experimental results were compared with numerical results using Finite Element Method (FEM). Mandrel/substrate preheating was found to be necessary for good quality manufacturing. Scanning Electron Microscopy (SEM) was used for quality control. C-ring tests were performed to evaluate failure stress, strain, and deflection of C-rings at room temperature. Samples failed in compression at mid-section and inner radius. Samples made with 70, and 110 lb/linear-inch consolidation pressure and tape preheating below glass transition temperature yielded best results. ANSYS non-linear FEM was employed to simulate the C-ring experiment using shell, target, and contact elements. Figure MAF-1 shows the Finite Element Analysis (FEA) modeling of the C-ring test.

The experimental deflection to failure was applied to the model and the failure stress, strain, and load were determined. The results from non-linear numerical analysis were in a good agreement with the experimental C-ring results. Table MAF-1 gives the comparison of the failure compressive stress, strain, and load determined from FEA and the C-ring test.

Scaled Pressure Vessel Design And Testing

An AS4/PEEK scaled pressure vessel with steel the end-caps were designed and fabricated. Also, an initial pressure test was performed on the scaled pressure vessel with the end-caps. The length and inner diameter of the scaled pressure vessel were chosen to be approximately one-third of the main pressure vessel for the SAUVIM. The length and inner diameter of the scaled pressure vessel were 6.25" and 4.18", respectively. Thickness of the scaled pressure vessel was fixed and chosen to be 0.24" in order to have a thick-walled pressure vessel. A symmetric sub-laminate configuration of $[90/90/0/0/90/90]_S$ was chosen for the composite scaled pressure vessel. The results of Finite Element Analysis (FEA) revealed that the structure could sustain pressures up to 7,000 psi with a

factor of safety of around two. For the initial test, aluminum end-caps were designed and made to sustain a pressure of 3,500 psi with a factor of safety of around two. The end-caps had both radial and axial O-rings for sealing. The initial test was performed at 2,500 psi and no structural damage or leak was observed. Stainless steel end-caps were designed for 7,000 psi with a factor of safety of two. The steel end-caps are currently being manufactured. The scaled pressure vessel with the steel end-caps will be tested up to 7,000 psi. Figure MAF-2 gives a photograph of the scaled pressure vessel its the aluminum end-caps and tie-rods.

Shallow Water Pressure Vessel Design

Shallow water pressure vessels were designed using ANSYS FEA and E-glass/Epoxy. The length and inner diameter of the shallow water pressure vessels are 19.5" and 13", respectively. The design pressure of 165 psi was considered. A symmetric sub-laminate configuration of $[90/0/90/0/90/0]_S$ was chosen for the composite shallow water pressure vessel with [90/0] representing a plain weave cloth. Finite element analyses were performed to design the shallow water pressure vessel. The result of linear buckling analysis, with end-caps in place (modeled as boundary conditions), revealed that the buckling pressures were 220 psi and 450 psi for the thickness of 0.228" and 0.285", respectively. The thickness of 0.285" was chosen to satisfy the desired factor of safety of around two for buckling pressure. Non-linear buckling analysis was performed on the structure to investigate the stability of the shallow water pressure vessel up to 450 psi pressure, with end-caps in place (modeled as boundary conditions with radial constraint in place of the end-caps), and the corresponding pressure-displacement curve is shown in Figure MAF-3. It was found that the shallow water pressure vessel would not lose its stability up to 320 psi. Buckling pressure factor of safety of 1.9 was achieved. Due to axially symmetric geometry, loading, and boundary conditions, ten degrees wedge of the circular cylinder with symmetric boundary conditions was modeled for the stress analysis. Modeling the pressure vessel as a symmetric wedge reduces the computational time and memory requirements, significantly. The stress analysis revealed that the model, with end-caps (modeled as boundary conditions with radial constraint in place of the end-caps), could sustain pressures up to 165 psi with a stress factor of safety of about ten using Tsai-Wu failure criterion. Figures MAF-4, 5, and 6 show the stresses in radial, axial and hoop directions, respectively, which are under 165 psi. It should be noticed that the structure will first fail due to buckling and not stress; therefore, the factor of safety for the pressure vessel is 1.9. The stress analyses were performed to demonstrate that the failure mode of the shallow water pressure vessel was buckling and not stress.

Shallow Water End-Cap Design

End-caps are required to close the ends of the shallow water pressure vessel. Under ocean hydrostatic pressure, the pressure vessel and end-caps are under radial and axial pressure, respectively, and they mutually affect each other. Finite element analysis was performed to study the stress distribution in metallic end-caps with six holes for connectors and one hole for a vacuum valve. Due to axially symmetric geometry, loading, and boundary conditions, 30 degrees wedge of the end-cap was modeled in the FEA. Von-Mises failure criterion was considered for the design of the metallic end-cap. The end-cap was made of aluminum and designed for 165 psi with a factor of safety of about 3.4. The effect of composite pressure vessel on the end-caps appeared in the boundary conditions in form of radial and axial constraints. Figure MAF-7 shows the Von-Mises stress distribution of the end-cap. The dimensions of the end-cap are shown in Figure MAF-8. The end-caps have two radial O-rings for sealing.

Fabrication of Shallow Water Pressure Vessel

Six E-glass/Epoxy shallow water pressure vessels were manufactured using tube role-wrapping technique. In this process, the fabric, i.e., E-glass plain weave, was laid on the table and a mixture of resin and curing agent was poured and spread-even on it. The resin epoxy 331 and Ancamin 1770 curing agent were mixed with a 4:1 ratio. Then, the impregnated fabric was rolled and pressed onto a mandrel. The mandrel was made of aluminum. After reaching the required thickness, the uncured tube was wrapped by a high temperature shrink-tape. The purpose of using shrink-tape was, for the tape, to shrink tightly on the rolled impregnated fabric and squeeze excess resin and air entrapped in the material out from the ends. The part and mandrel were placed in the autoclave for curing. The curing temperature profile for E-glass/Epoxy started from 70°F to 176°F at a rate of 10°F/min, held at 176°F for 2 hours, heated from 176°F to 300°F at a rate of 10°C/min, then held for 2 hours at 300°F. The temperature was then lowered from 300°F to 70°C at a rate of 10°F /min. The sample was slipped off the mandrel and sent to the machine shop to cut to the size. Figure MAF-9 shows the E-glass/Epoxy shallow water pressure vessel with its aluminum end-caps and tie-rods.

Shallow Water Pressure Vessel Testing

One E-glass/Epoxy thermoset composite shallow water pressure vessel with aluminum end-caps in place was tested under hydrostatic pressure up to 165 psi and held for half an hour in the Hawaii Institute of Geophysics Laboratory Pressure Chamber. The pressure vessel was intact and no leak was observed.

Future Tasks

- Develop optimum processing windows for the manufacture of thermoplastic composite pressure vessel.
- Investigate the effects of ring stiffen on the performance of the structure.
- Investigate the effects of end caps on the structure.
- Design and fabricate desirable end caps.
- Design and fabricate a flooded composite fairing for the vehicle.
- Manufacture a scaled pressure vessel with ring stiffeners and end caps.
- Modify the in-situ thermoplastic filament-winding set-up for the manufacture of full-scale pressure vessels.
- Fabricate full-scale pressure vessels.

Table MAF-1: Comparison between FEA and Experimental Results of the C-ring test

	OD (in)	Thickness (in)	Width (in)	Strength (psi)	Failure Load (lb)	Displacement (in)	Compressive Strain (in/in)
Experiment	4.43	0.1151	0.26	97,555	-27.0	0.56	-0.00474
FEA	4.43	0.1150	0.26	97,162	-28.9	0.56	-0.00496
% Difference	0.00	0.11	0.00	0.40	-6.67	0.00	-4.33

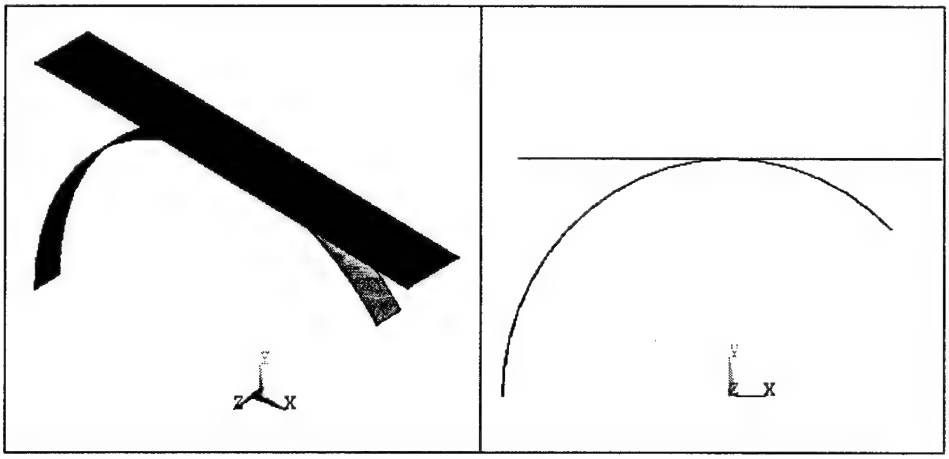

Figure FAM-1: Finite Element Modeling of C-ring Test

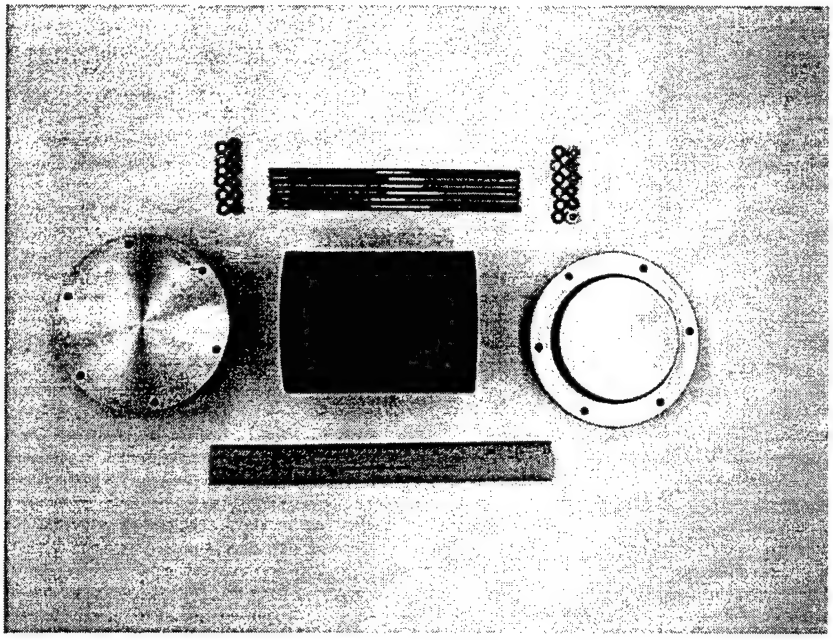

Figure MAF-2: Photograph of the Scaled Pressure Vessel with its End-caps and Tie-rods

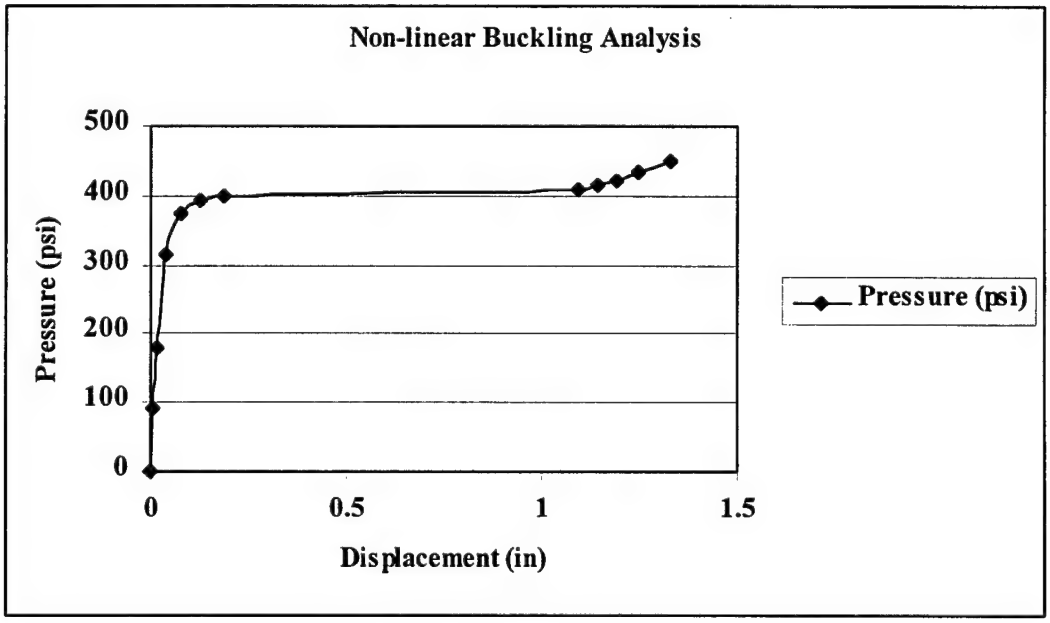

Figure MAF-3: Pressure-Deflection (Mid-length) Curve of Shallow water Pressure vessel Using ANSYS Non-Linear Buckling FEA

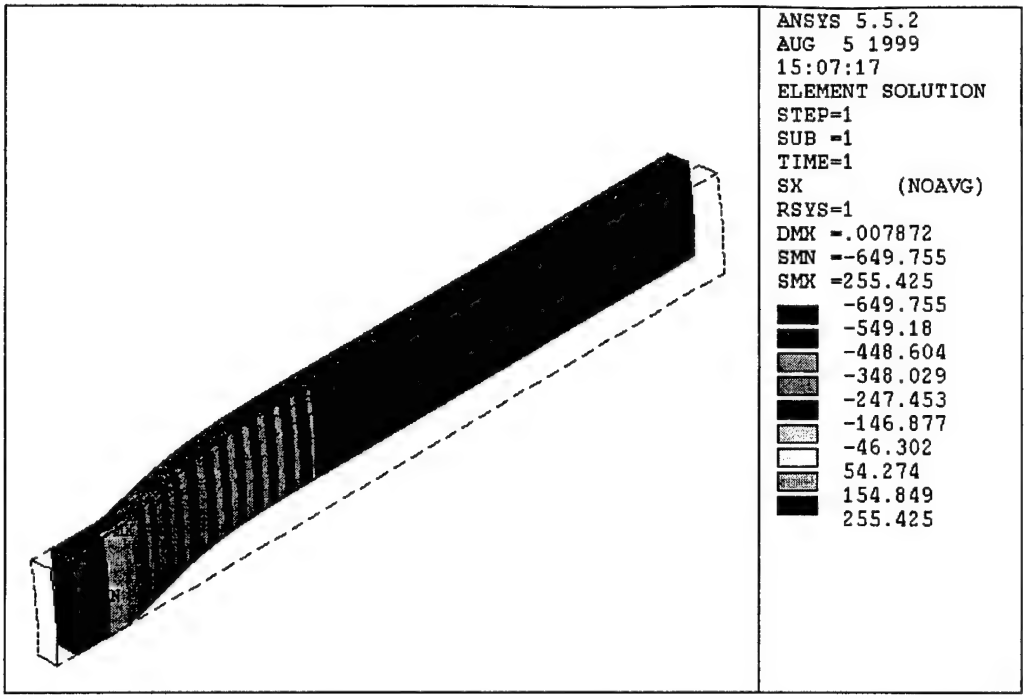

Figure MAF-4: Radial Stress Distribution of Shallow Water Pressure Vessel under 165 psi

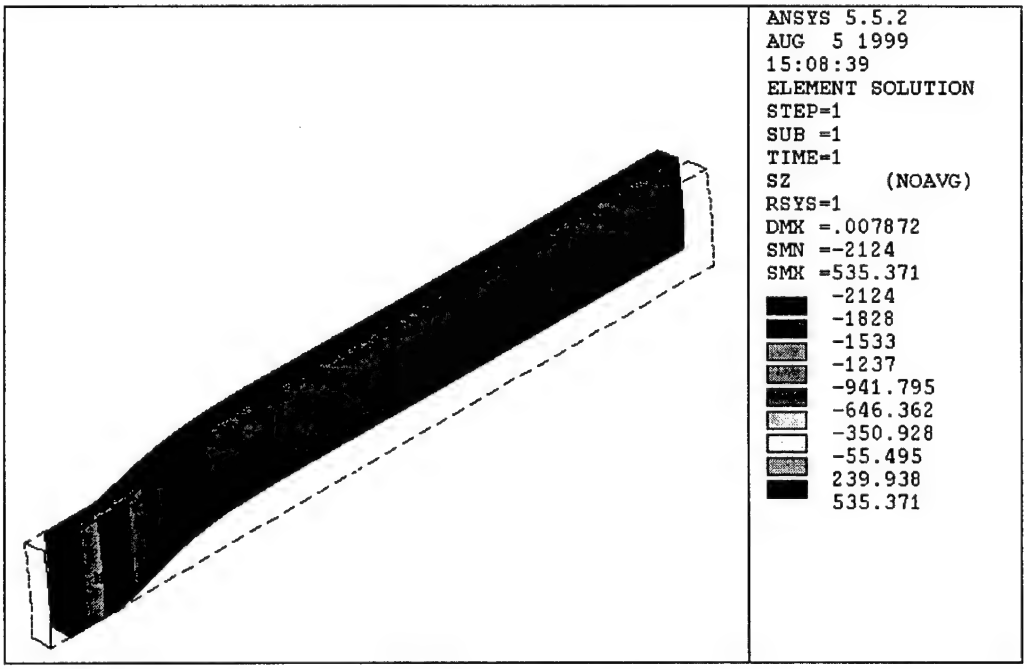

Figure MAF-5: Axial Stress Distribution of Shallow Water Pressure Vessel under 165 psi

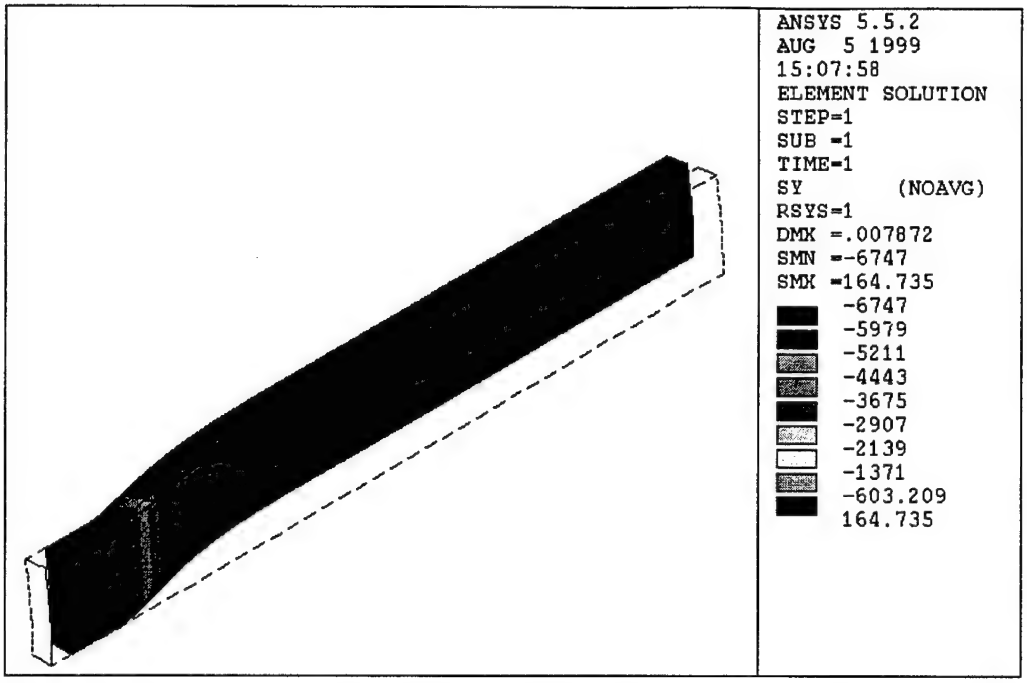

Figure MAF-6: Hoop Stress Distribution of Shallow Water Pressure Vessel under 165 psi

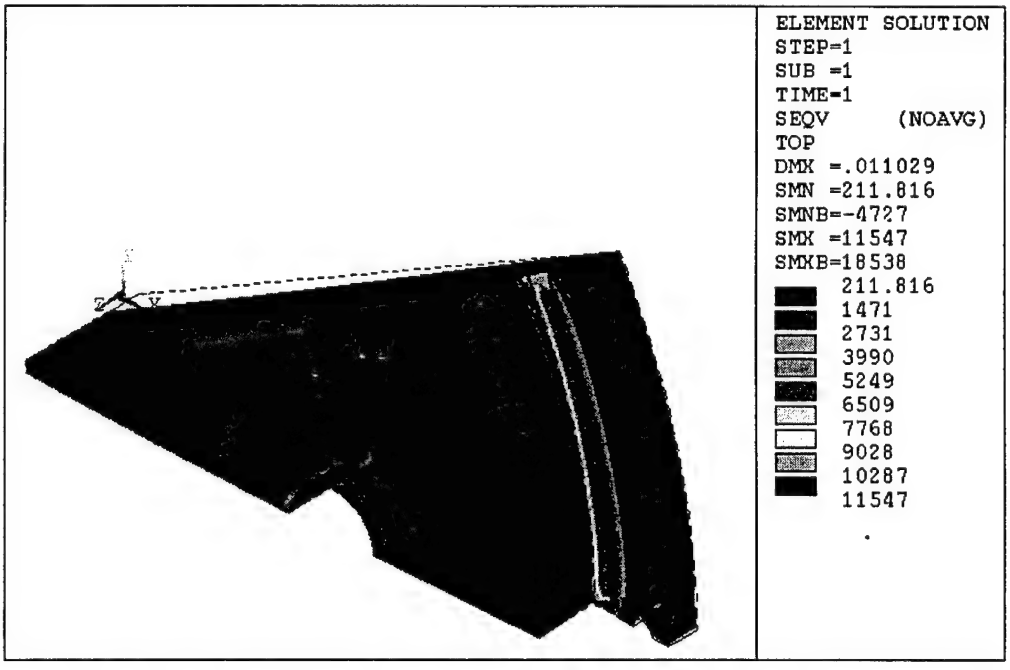

Figure MAF-7: Von Mises Stress Distribution of End-caps for Shallow Water Pressure Vessel

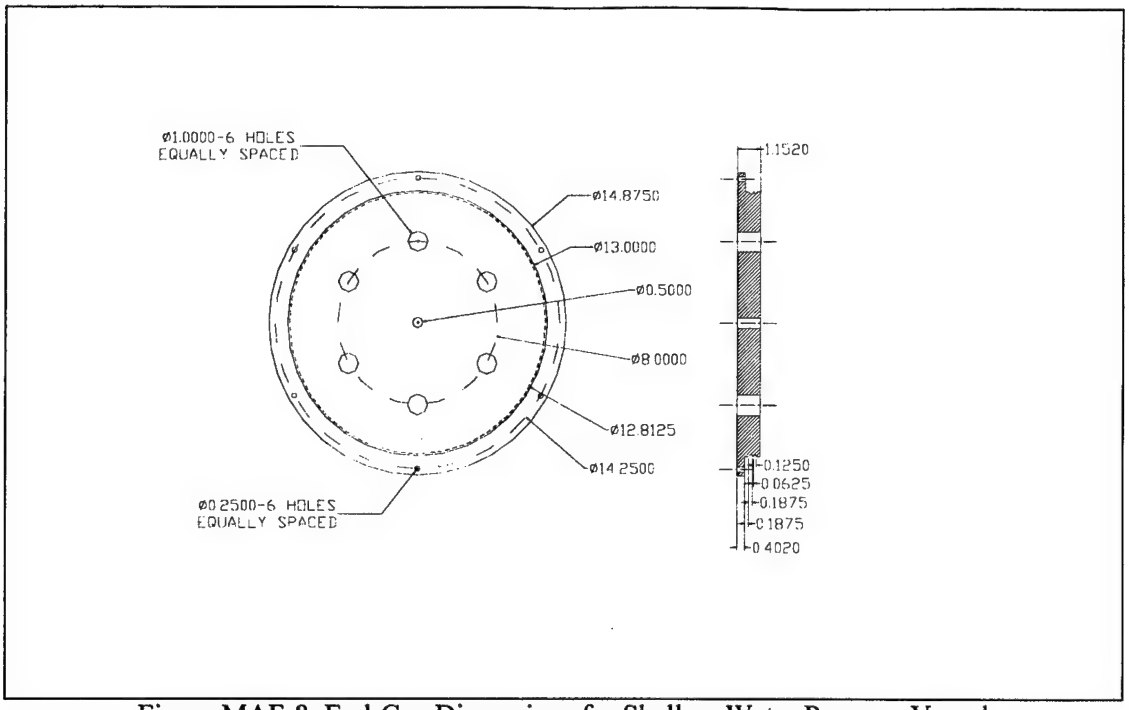

Figure MAF-8: End-Cap Dimensions for Shallow Water Pressure Vessel

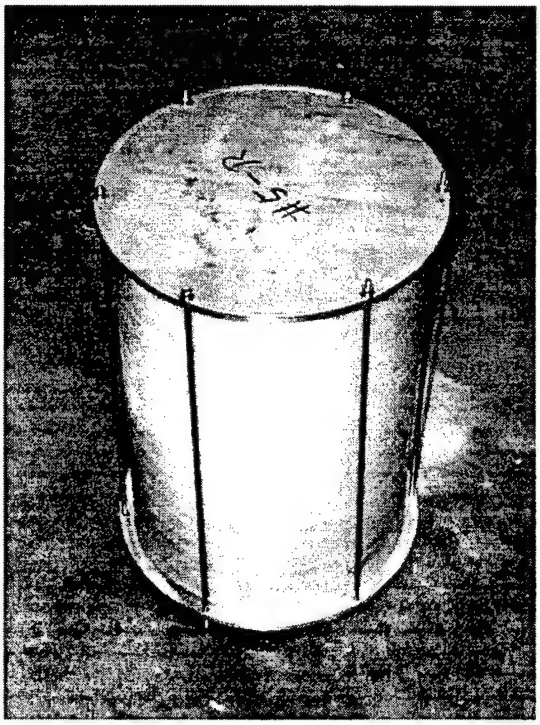

Figure MAF-9: Photograph of the E-glass/Epoxy Shallow Water Pressure Vessel with its Aluminum End-Caps and Tie-Rods

Mechanical-Electrical Design (MED)

Project Leaders: Mr. Curtis Ikehara & Mr. Oliver Easterday
Personnel: Mr. Szu-Min Chang, Ms. Colleen Kaku & Mr. Keith Sunderlin

Objectives

Integration of the mechanical and electrical components of the SAUVIM Integration

Current Status (Tasks Completed During 8/1/98 - 7/31/99):

Work in the MED group is starting to entail major fabrication work in addition to the ongoing tasks of designing and fabricating of sub-assemblies.

Major progress highlights include:

- Design of foam and mounting systems is complete; and the fabrication of mounting restraints is in progress.
- Major vehicle sub-assemblies are in varies stages of progress: ballast tray, fin units, foam, thruster, and pressure vessel saddles.
- Wiring design for power and thruster systems complete. Cable specification for sensor and inter-vessel communication determined.
- Battery tray mounting and power distribution system is nearing completion. The power supply system of SAUVIM is reaching the advanced stages of construction with the fastening and cradle systems almost complete along with the distribution wiring and DC power supply setup for intra-vessel mission loads.
- The robotic arm tray for the passive and active arms is nearing completion; and the tray and its rails have been mounted into the frame.

The battery trays have been completed, and a full compliment of lead acid batteries for the vehicle has arrived. Mounting of the trays onto the frame is complete; sizing of the strapping to secure the batteries is underway as well as adding minor hardware to complete the restraint system. (Figure MED-1 & 2).

The pressure vessel saddles are almost complete. The main rails have been installed on the frame, and the completion of the individual polyethylene saddle supports and the strapping to firmly secure the vessels remains to be completed. Calculation of anticipated stresses on the walls of the pressure vessels from adding a pre-load strapping (to prevent shifting and resistance to vibration and shock loading) must be completed in order to size and locate the saddle mounts, which will be cut from HDPE sheet stock on a band saw.

The robotic arm tray along with the rail and slider shoe hardware is complete. Mounting of the tray into the SAUVIM frame is in progress and should be completed soon. (Figure MED-3)

Design of the SAUVIM vehicle recovery and launch frame (Figure MED-4) is complete and is currently being fabricated. This steel frame is used for a crane-based launch/recovery of the fully loaded vehicle as well as shore side transfer. The first sample of cargo strap that is intended for the

final vehicle has been ordered to verify fit, routing through the vehicle frame, and component clearance.

Design of the main ballast tray is complete (Figure MED-5). Construction of ballast tray is now underway. Ordering of minor hardware for the ballast tray (fasteners, shafting, castors, etc.) is nearly complete. The next step will be to mount the tray onto the frame and complete detailed design of the translation mechanism.

The arm camera housing for the AORD homing sensor was fabricated in-house along with the prototype general optical instrument housing (Figure MED-6). Shallow water leakage testing was performed on the optical housings. A full compliment of general optical housings has been out-sourced to UH's SNUG Harbor facility. Mounting and location of the optical housings onto the SAUVIM frame is the next task to address for these assemblies. The cameras systems include one rear-mount monochrome camera, a pair of forward facing color cameras, one homing sensor arm-mounted camera, and 3-4 additional monochrome cameras for alternative angles and close in forward views that will be mounted in the nosecone section of the vehicle.

The power system schematic, power distribution, thruster control wiring and the battery wiring diagrams (Figures MED-7, 8, 9 & 10, respectively) have been completed down to the lead levels, and the procurement of underwater cabling has begun. The inter-vessel and sensor/accessories connector assignments and specifications are complete. Assignment of the individual conductor paths to I/O ports, and the associated accessories and sensors is underway.

The geometry of the floatation foam for the vehicle was redesigned to allow for two standard interchangeable shapes. This will vastly expedite balancing and trimming of the vehicle once SAUVIM is ready for static balance adjustment in water. A complete set of shaped foam for the operational vehicle has been ordered, and upon arrival, will be mounted on to the frame. The clamping system has been under construction using a set of lightweight insulation foam prototypes. (Figure MED-11 & 12)

The MED proof pressure test facility is in the process of redesign/construction to allow for easier access into the tank unit as the old retaining collar was wearing out. The design of a new lid and tie rod system to retain pressure has been completed; most of the items have been fabricated.

Other activities that have been completed, include:

1. Wiring design for power and thruster systems complete, and cable specification for sensor and inter-vessel communication determined.
2. The designs of the main power switches and the electrical junction boxes for the vehicle have been completed. Fabrication is underway. These items have been added since the last SAUVIM progress report to add functionality to the SAUVIM vehicle as well as add some flexibility to the manner and routing in which accessories and sensors can be wired up. (Figures MED-13 & 14)
3. A commodity source of self-sealing bolts has been located, and a lot of 100 procured. Modification of some of the bolts into bleeder bolts along with proof testing is the next step. These were chosen over the custom designed bolt for reasons of economy and standardization.
4. Completion of testing of the wire-in leads for the low-power lighting and diode laser acrylic housings is complete. Fabrication is in progress. This AORD task will have crossover value for the general low intensity illumination system for the vehicle.

5. Component testing for fitness and survival in corrosive and high-pressure environments continues. Planned are tests to evaluate various coating materials and sealing greases to forestall galvanic crevice corrosion.
6. Robotic Arm tray has been completed; mounting of it is in progress
7. Designs of the foam and the mounting systems are completed. The fabrication of mounting rails is in progress.
8. Fin unit detailed designs are complete except the geometry of the fin itself (Figure MED-15).
9. The battery charging system for operational deployment has been designed, all components have been ordered, and system is ready for assembly.
10. The thruster tubes have been fabricated. (Figure MED-16)

Recent procurements include:

1. 6 24-volt batteries to completely fill the SAUVIM power banks.
2. 3 altimeter sonars to complete acoustic ranging system.
3. The complete set of shaped foam floatation for SAUVIM vehicle. These were cut to a set of template patterns provided to the vendor.
4. First sets of inter-vessel connectors, these include the active arm interface connectors and all the battery/power supply system cabling.
5. A commodity built thruster that will undergo evaluation and be a candidate for the SAUVIM in operational deployment.
6. The DC-DC power supply and conditioning equipment for mission loads.

Future Tasks

- Pool-based testing of commodity thruster unit for verification of specifications, ordering complete set of eight upon successful testing.
- Complete competitive bidding and acquisition of all underwater cabling and connectors on the vehicle.
- Perform/Arrange fabrication of the following assemblies: fin-unit, cable management conduct, PV saddle restraints, and wet ballast tanks.
- Re-initiate proof testing of various electrical/electronic components upon completion of our in-house pressure test facility.
- Complete installation of major components onto the frame including: floatation, wet ballast tanks, hard ballast, ballast tray, composite pressure vessels, thruster tubes and thrusters, and batteries.
- Initiate intra-vessel wire up of components including DC-DC power converters, VME computers, INS instrumentation, and vehicle systems status sensors.

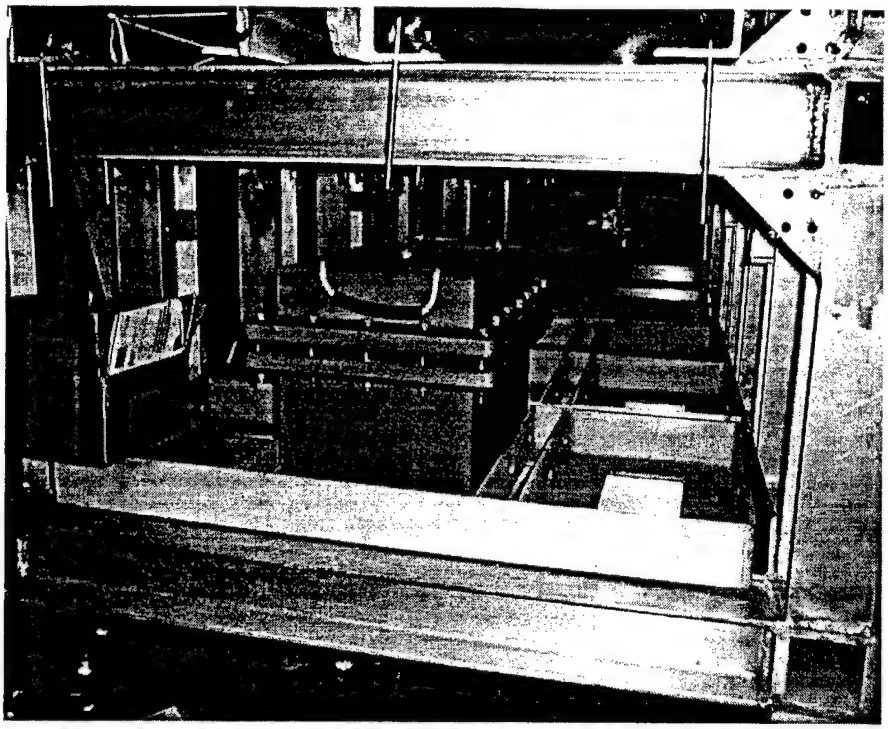

Figure MED-1: Rear View of the SAUVIM Frame with Four Battery Trays in Place

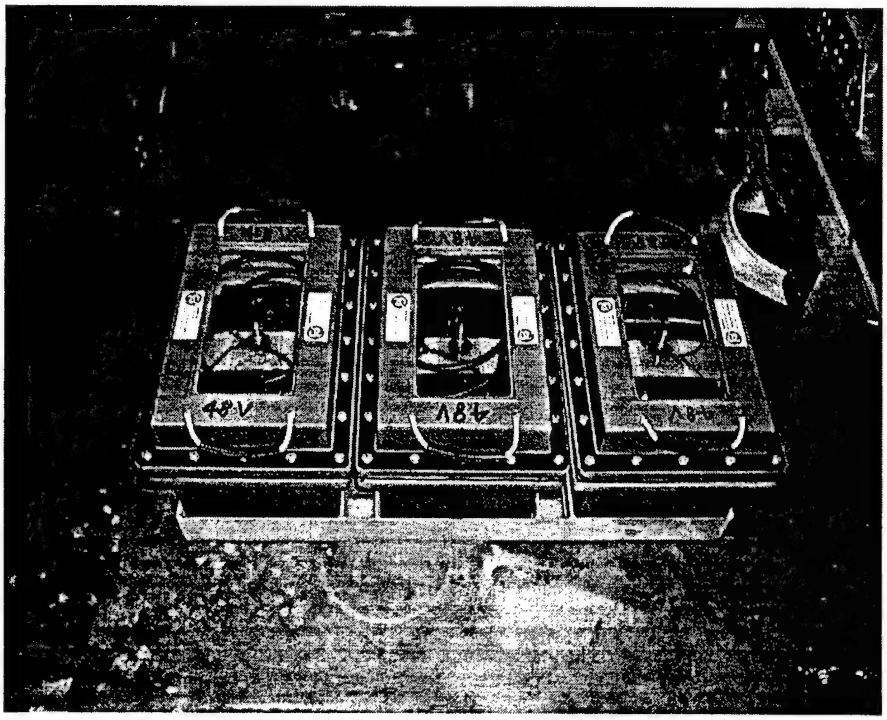

Figure MED-2: Battery Tray with One-Bank of Oil-Compensated Cells

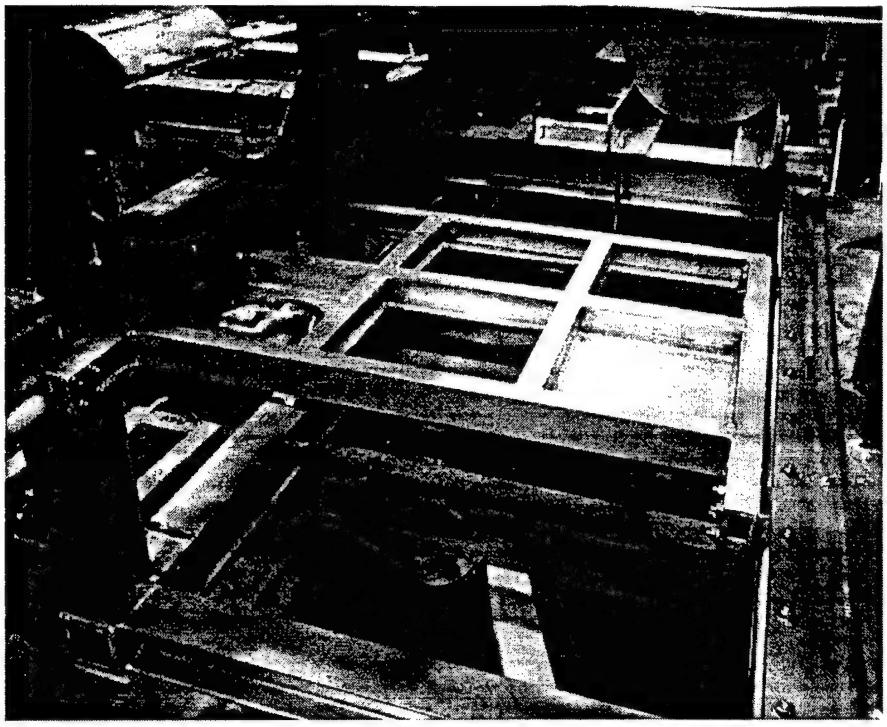

Figure MED-3: Robotic Manipulator and Passive Arm Tray Mounted on Frame

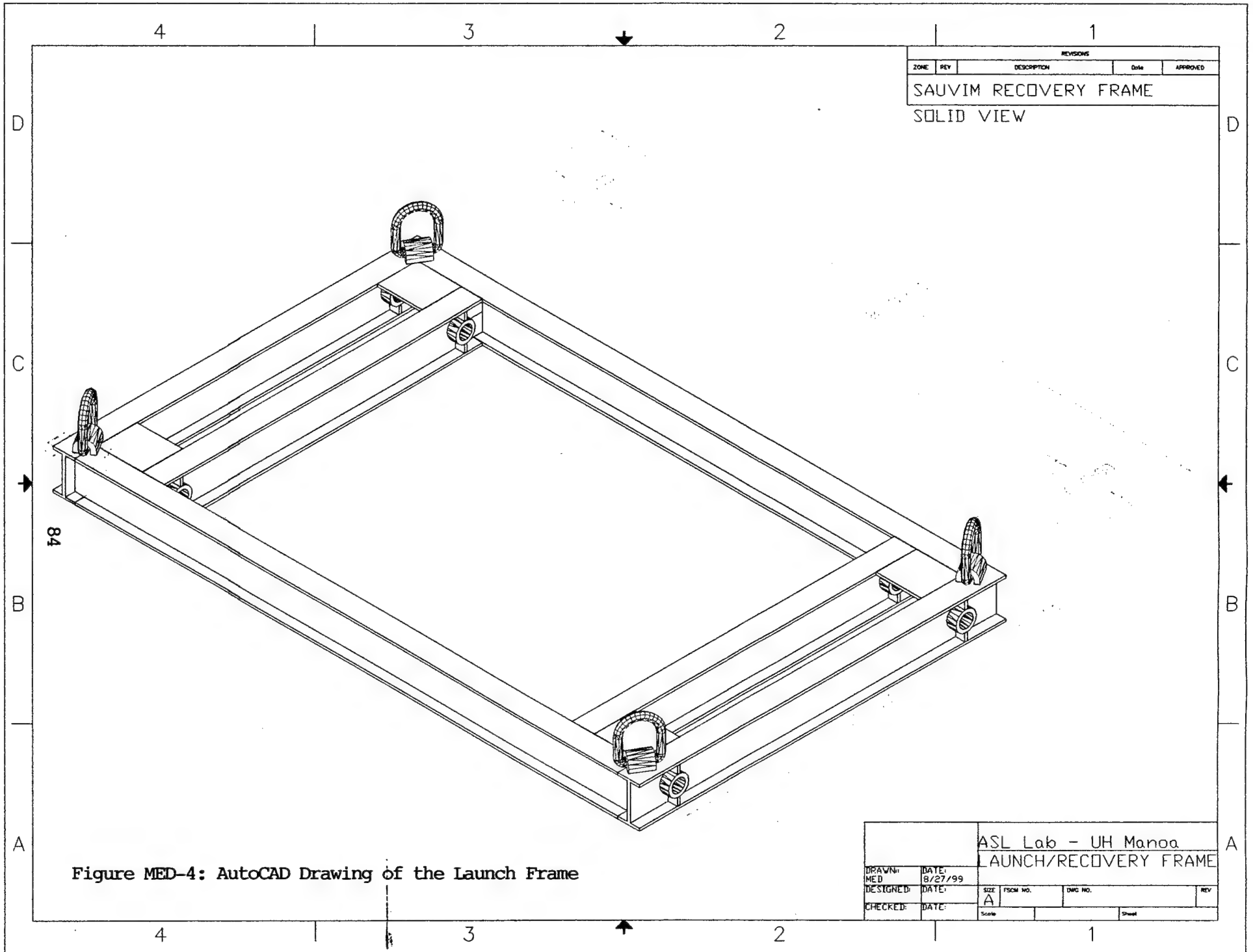

Figure MED-4: AutoCAD Drawing of the Launch Frame

Figure MED-5: AutoCAD Drawing of the Main Ballast Tray

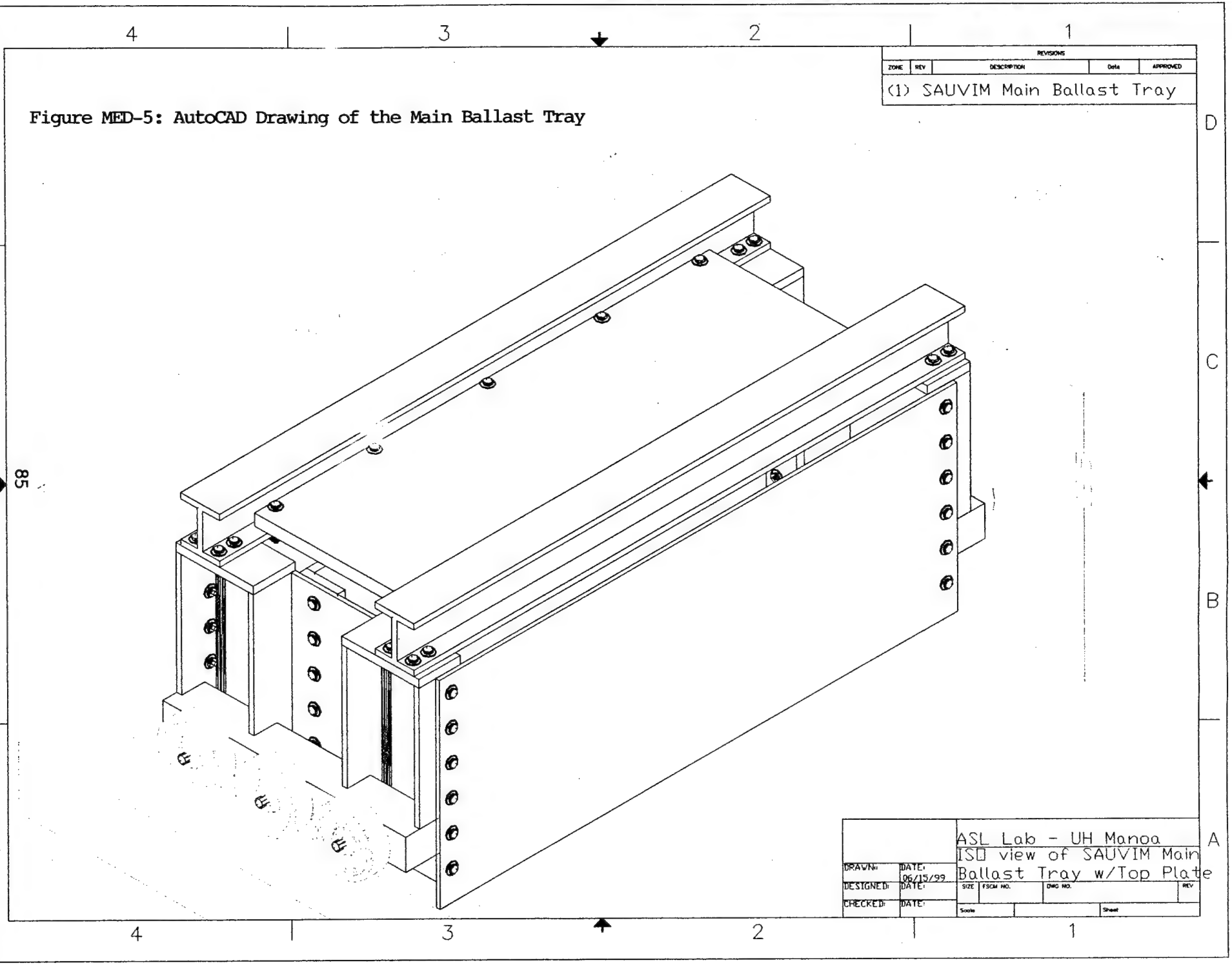

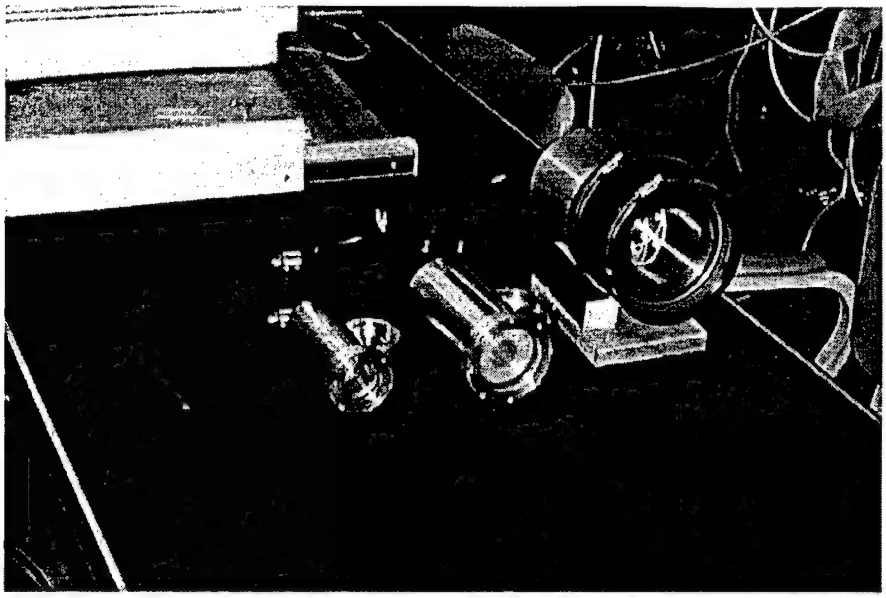

Figure MED-6: Various Camera Housings

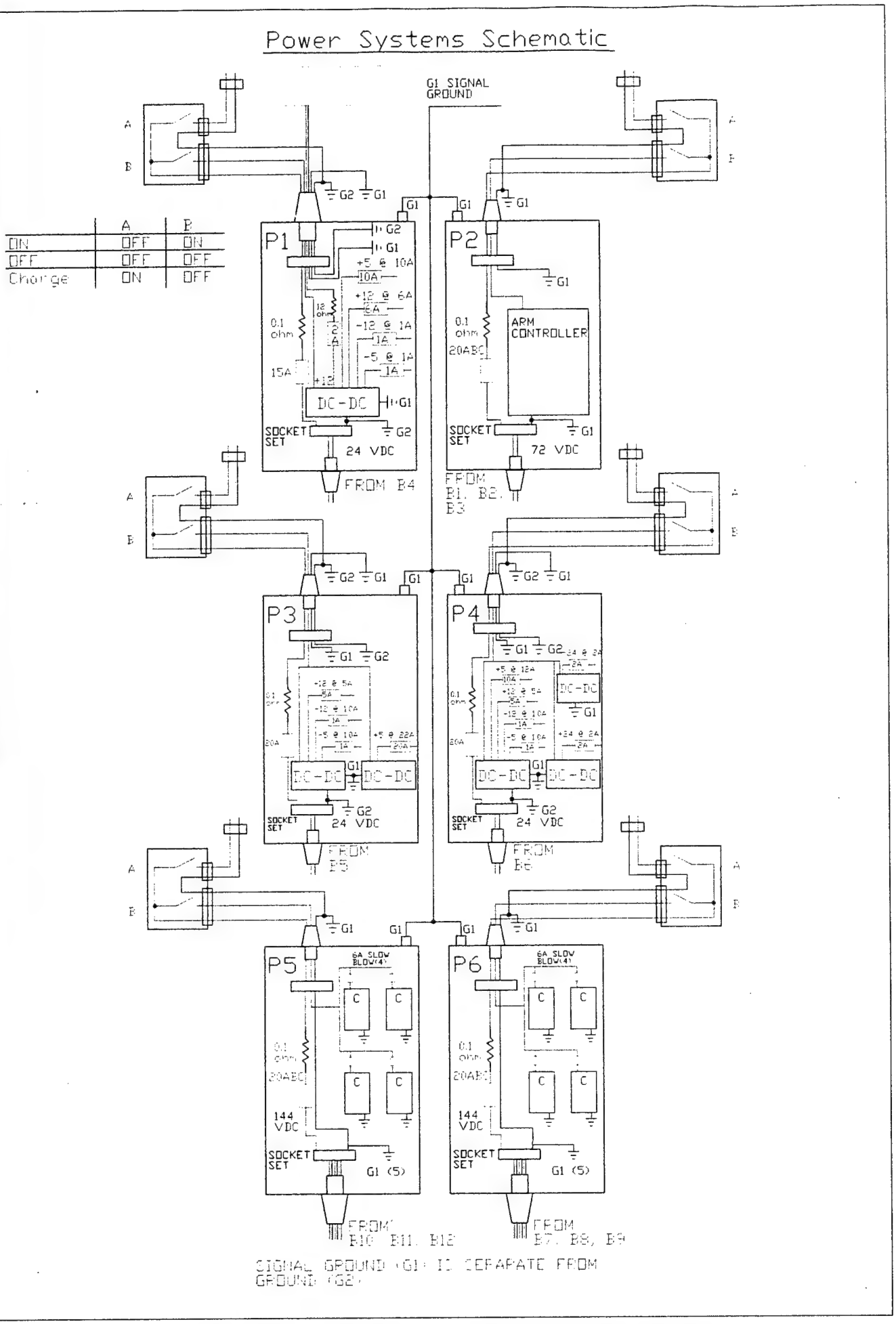

Figure MED-7: Schematic of the Power System Layout

Figure MED-8: Diagram of the Power Distribution

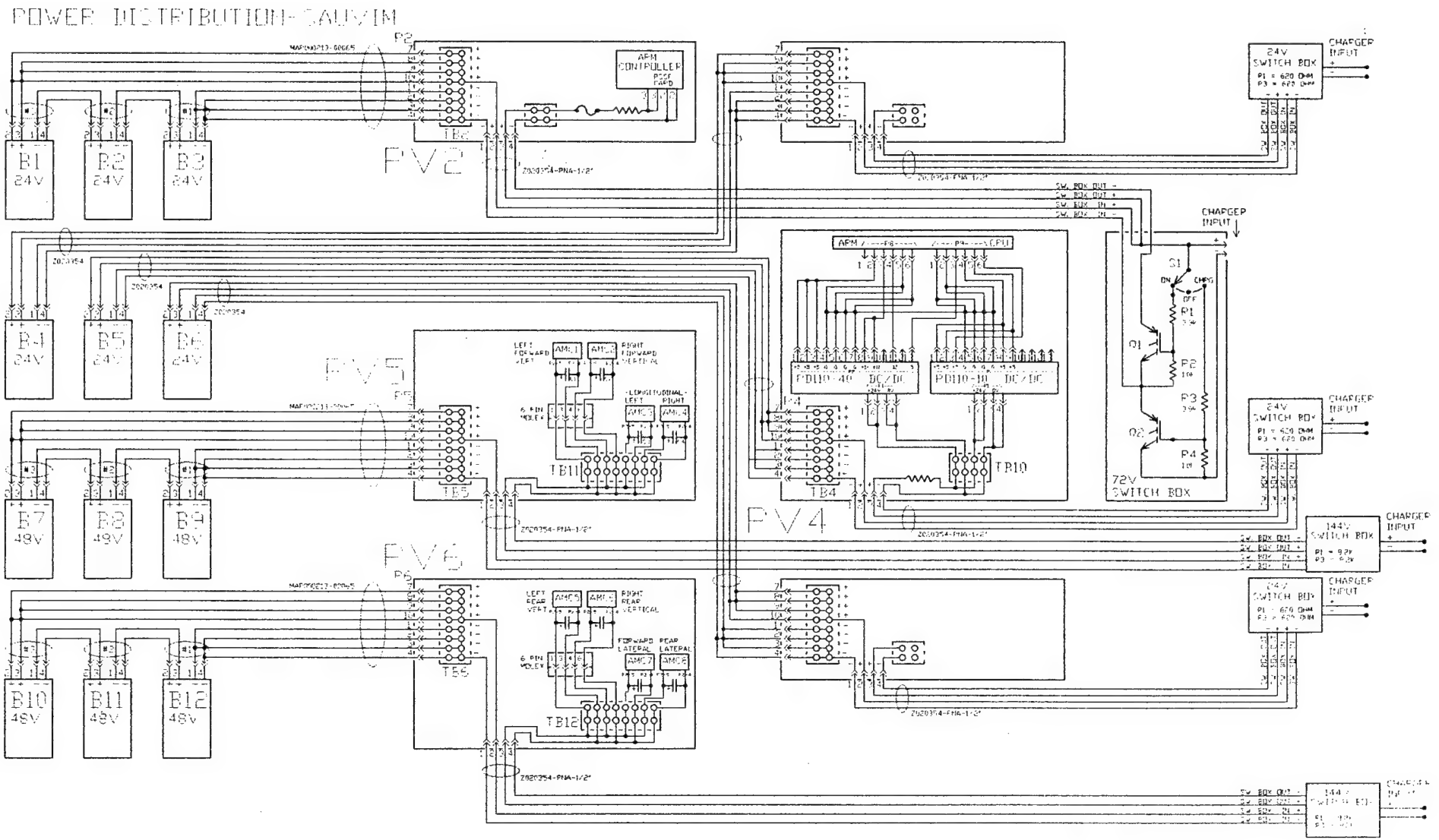

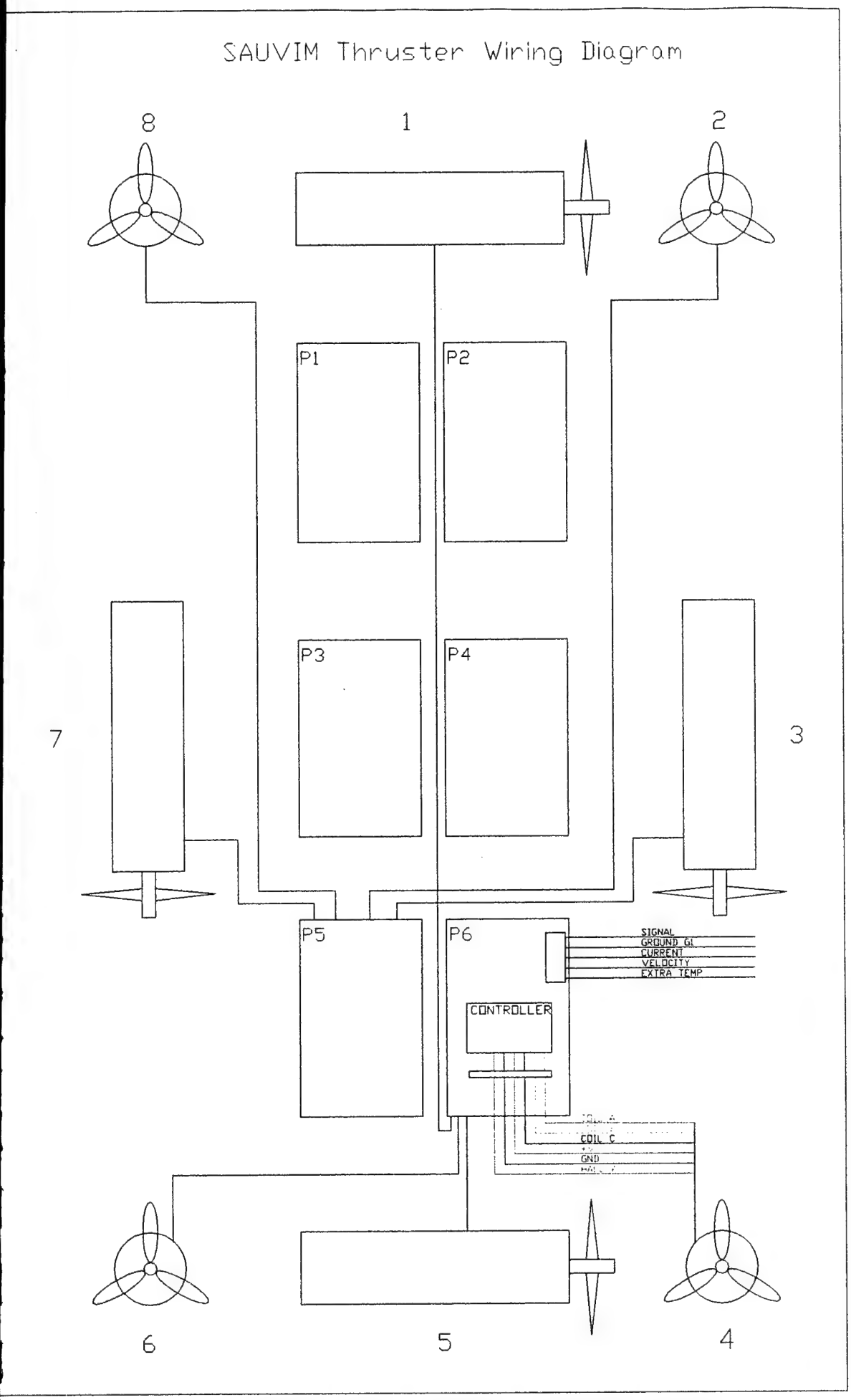

Figure MED-9: Diagram of Thruster Wiring

Battery Wiring Diagram

Arm Bank:
72 VDC @ 38 Amp-Hour
2.74 kW-hr (9.85 MJ)

Bottle P1:
24 VDC @ 38 Amp-Hour
0.91 kW-hr (3.28 MJ)

Bottle P3 - Navigation CPU:
24 VDC @ 38 Amp-Hour
0.91 kW-hr (3.28 MJ)

Bottle P4 - Arm CPU:
24 VDC @ 38 Amp-Hour
0.91 kW-hr (3.28 MJ)

Thruster Bank #1
144 VDC @ 18 Amp-Hour
Bottle P5: Longitudinal and Rearward Vertical oriented pair.
2.52 kW-hr (9.33 MJ)

Thruster Bank #2
144 VDC @ 18 Amp-Hour
Bottle P6: Lateral and Forward Vertical oriented pair.
2.52 kW-hr (9.33 MJ).

Figure MED-10: Diagram of Battery Wiring

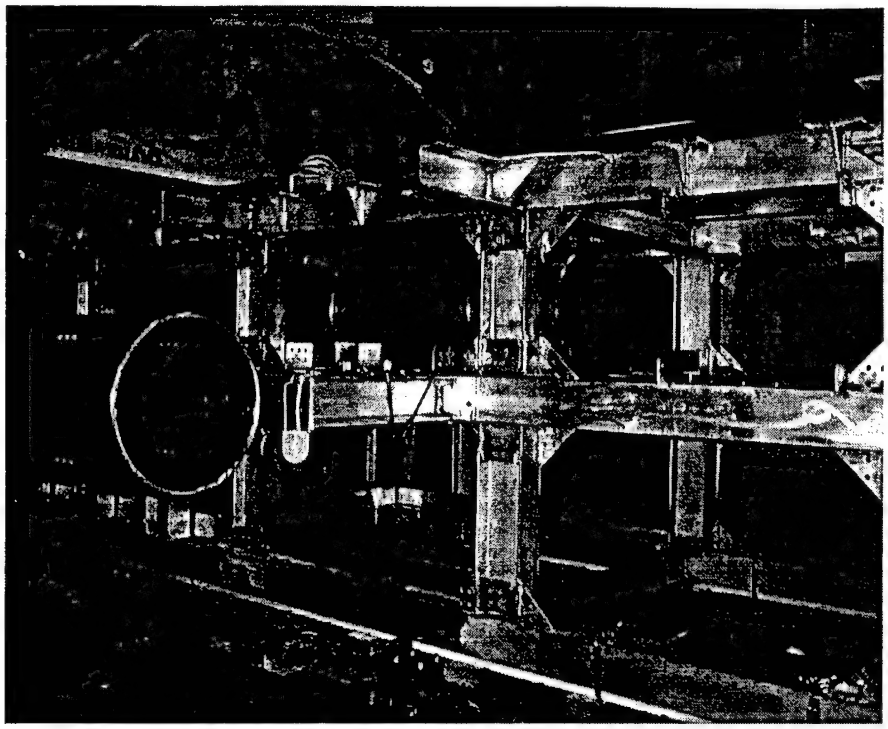

Figure MED-11: Side View of the SAUVIM Frame with Pressure Vessels, Mock Floatation Foam, and Thruster Tubes

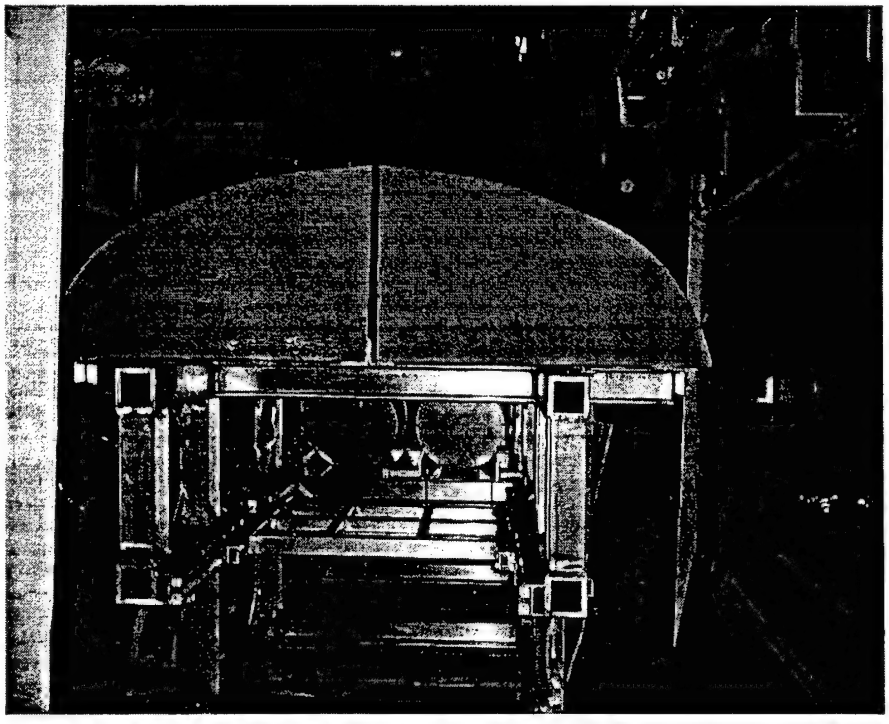

Figure MED-12: Frontal View of the SAUVIM Frame with Floatation Foam, Pressure Vessels, and Robotic Arm Tray

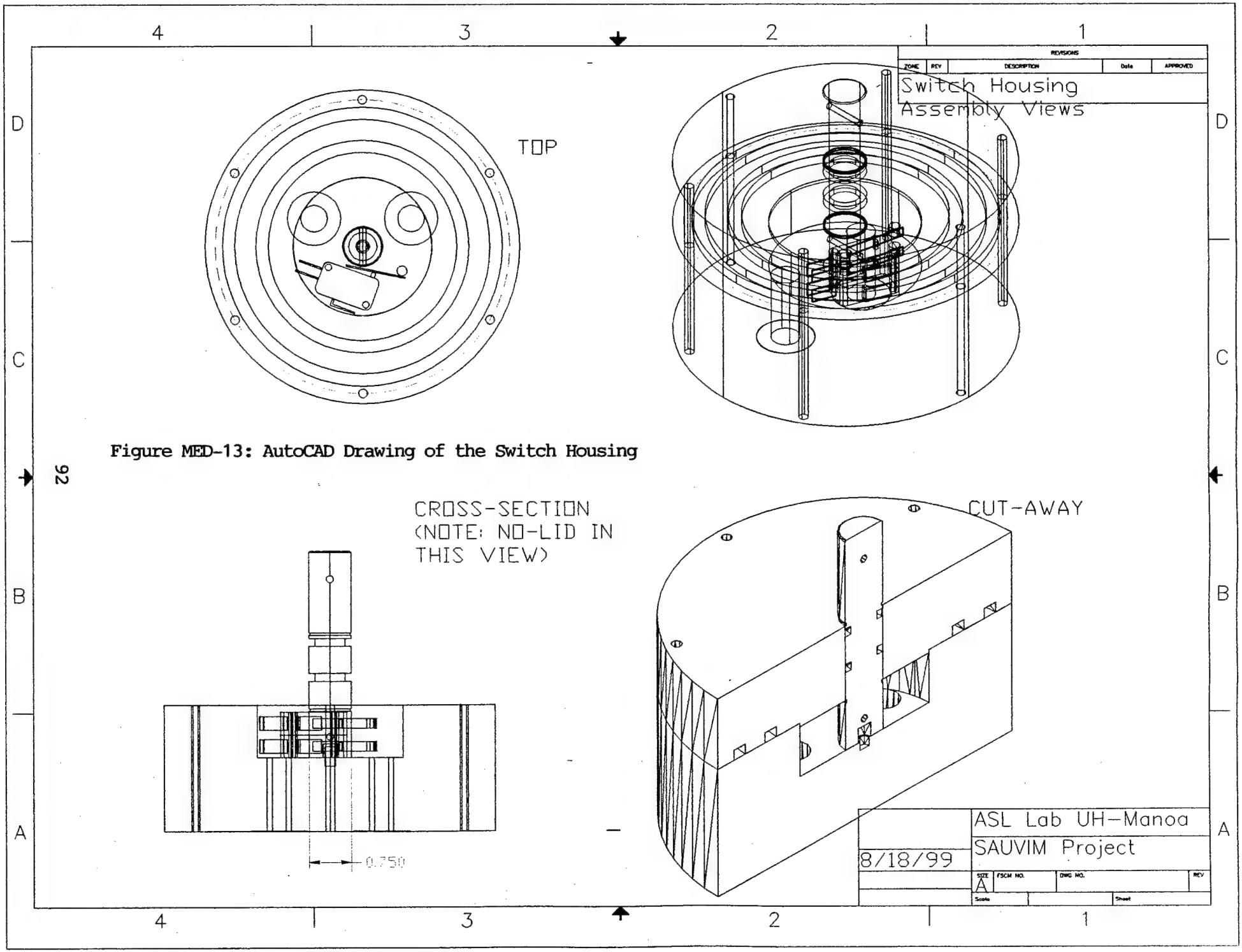

Figure MED-13: AutoCAD Drawing of the Switch Housing

Figure MED-14: Fabricated Junction Boxes

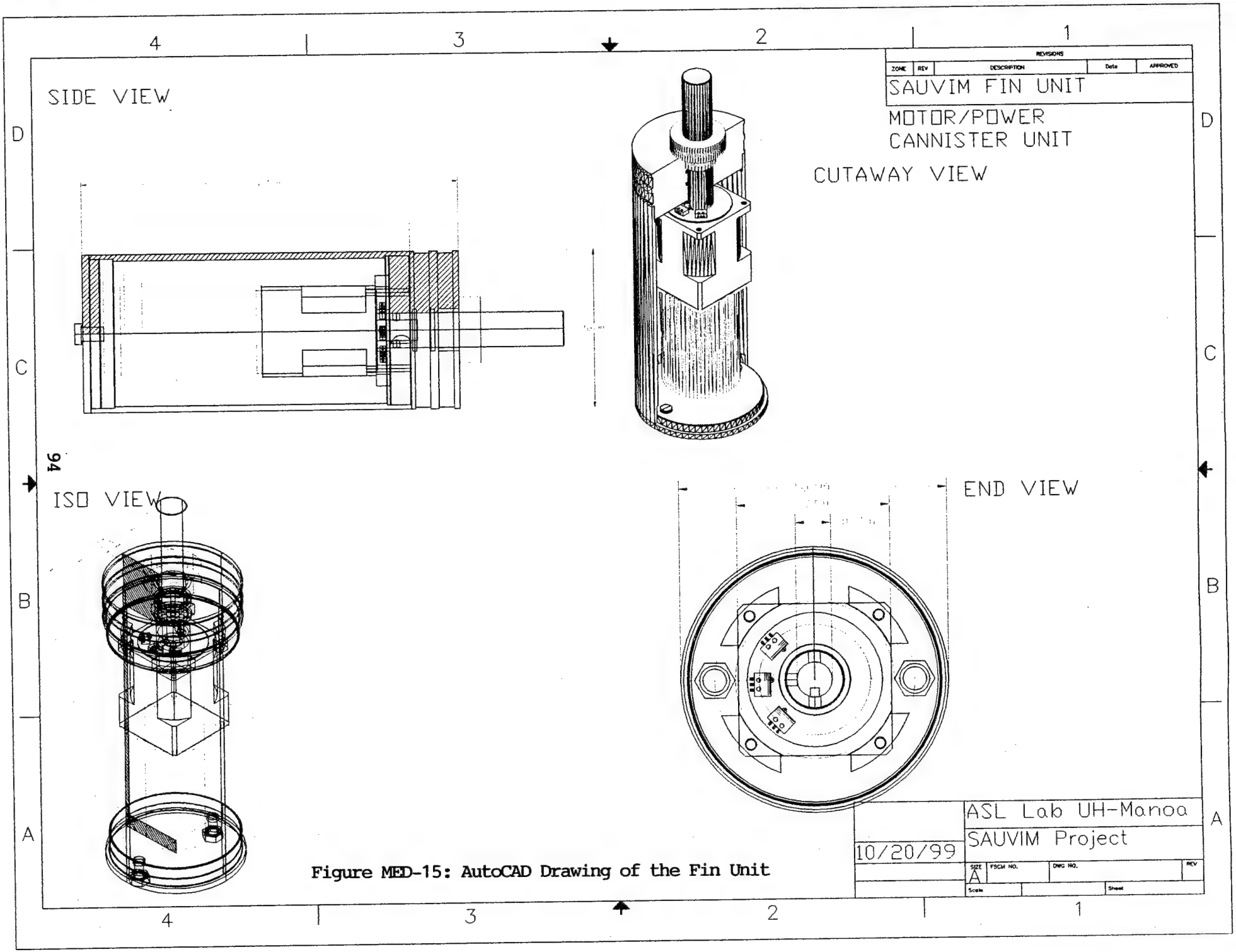

Figure MED-15: AutoCAD Drawing of the Fin Unit

Figure MED-15: AutoCAD Drawing of the Fin Unit

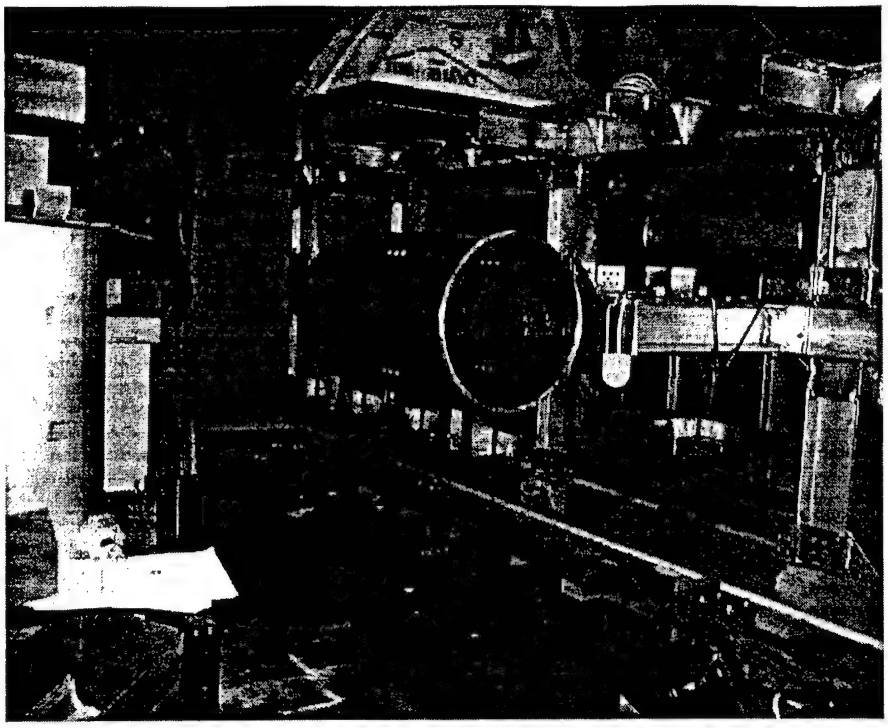

Figure MED-16: Horizontal Thruster Tube.

References

Aloimonos, Y., *Visual Navigation: From Biological Systems to Unmanned Ground Vehicles*, Mahwah, NJ, Lawrence Erlbaum Associates, 1997.

ANSYS User's Manual (Version 5.2), Ansys, Inc., Houston, TX, USA, 1994.

Antonelli, G., and S. Chiaverini, "Task-Priority Redundancy Resolution for Underwater Vehicle-Manipulator Systems", in Proceedings of the 1998 IEEE International Conference on Robotics & Automation, pp.756-761, Leuven, Belgium, 1998.

Antonelli, G., S. Chiaverini, and N. Sarkar, "Explicit Force Control for Underwater Vehicle-Manipulator Systems with Adaptive Motion Control Law," IEEE Hong Kong Symposium on Robotics and Control, Hong Kong, July 1999a.

Antonelli, G., S. Chiaverini, and N. Sarkar, "External Force Control for Underwater Vehicle-Manipulator Systems," Conference on Decision and Control, Phoenix AZ, Dec. 1999b.

Antonelli, G., N. Sarkar, and S. Chiaverini, "Explicit Force Control Scheme for Underwater Vehicle-Manipulator Systems," IEEE/RSJ Internation Conterence on Intelligent Robots and Systems, Kyongju, Korea, Oct. 1999c.

Auran, P.G. and O. Silven, "Ideas for Underwater 3D Sonar Range Sensing and Environmental Modeling", Proceeding of CAMS'95, pp. 284-290, 1995.

Bollinger, J.G. and N.A. Duffie, *Computer Control of Machines and Processes*, Reading, MA, Addison-Wesley Publishing Company, 1989.

Brush, D.O. and B.O. Almroth, *Buckling of Bars, Plates, and Shells*, New York: McGraw-Hill, Inc., 1975.

Candus de Wit, C., B. Siciliano, and G. Bastin (Editors), *Theory of Robot Control*, Springer-Verlag, Berlin, Germany, 1996.

Chan, T.F. and R.V. Dubey, "A Weighted Least-Norm Solution Based Scheme for Avoiding Joint Limits for Redundant Joint Manipulators", *IEEE Transaction on Robotics and Automation*, vol.11, no.2, pp.286-292, 1995.

Chiaverini, S., "Singularity-Robust Task-Priority Redundancy Resolution for Real-Time Kinematic Control of Robot Manipulators," *IEEE Transaction on Robotic and Automation*, vol. 13, 398-410, 1997.

Chiaverini, S. and L. Sciavicco, "The Parallel Approach to Force/Position Control of Robotic Manipulators," IEEE Transaction on Robotics and Automation, vol. 9, pp. 361-373, 1993.

Choi, S.K., J. Yuh, and G.Y. Takashige, "Design of an Omni-Directional Intelligent Navigator, *Underwater Robotic Vehicles: Design and Control*, TSI Press, pp. 277-297, 1995a.

Choi, S.K. and J. Yuh, "Development of an Omni-Directional Intelligent Navigator", *IEEE Robotics and Automation Magazine*, 1995b.

Choi, S.K., and J. Yuh, "Experimental Study on a Learning Control System with Bound Estimation for Underwater Robots", *International Journal of Autonomous Robots*, 3 (2 & 3), pp. 187-194, 1996.

Clayton, B.R., *Mechanics of Marine Vehicles*, London, England, London Press, pp. 597, 1982.

Craig, J.J., *Introduction to Robotics: Mechanics and Control*, Reading, MA, Addison-Wesley, 1986.

Cristi, R., M. Caccia, G. Veruggio and A.J. Healey, "A Sonar Based Approach to AUV Localization", Proceeding of CAMS'95, pp. 291-298, 1996.

Cui, Y., T.K. Podder, and N. Sarkar, "Impedance Control of Underwater Vehicle-Manipulator Systems," IEEE/RSJ Internation Conterence on Intelligent Robots and Systems, Kyongju, Korea, Oct. 1999.

Cunha, J.P., R.R. Costa, and L. Hsu, "Design of a High Performance Variable Structure Position Control of ROV's," *IEEE Journal of Oceanic Engineering*, vol. 20, no. 1, pp.42-55, 1995.

DeBitetto, P.A., "Fuzzy Logic for Depth Control of Unmanned Undersea Vehicles," Proceedings of the Symposium of Autonomous Underwater Vehicle Technology, pp. 233-241, 1994.

D'egoulange, E. and P. Dauchez, P., "External Force Control of an Industrial PUMA 560 Robot," journal of Robotic Systems, vol. 11, pp. 523-540, 1994.

Doebelin, E.O., *Measurement Systems: Application and Design*, New York, McGraw-Hill Book Company, 1975.

Dote, Y., *Servo Motor and Motion Control Using Digital Signal Processors*, Englewood Cliffs, NJ, Prentice-Hall Publishing, 1990.

Dougherty, F. and G. Woolweaver, "At-Sea Testing of an Unmanned Underwater Vehicle Flight Control System," Proceedings of the Symposium of Autonomous Underwater Vehicle Technology, pp. 65-73, 1990.

Dunningan, M.W., D.M. Lane, A.C. Clegg, and I. Edwards, "Hybrid Position/Force Control of a Hydraulic Underwater Manipulator," IEEE Proceedings Control Theory and Application, vol. 143, no. 2, pp. 145-151, March 1996.

Ferrerri, G., G. magnani, and P. Rocco, "Toward the Implementation of Hybrid Position/Force Control in Industrial Robots," *IEEE Transaction on Robotics and Automation*, vol. 16, pp. 838-845, 1997.

Geyer, R. A., *Submersibles and Their Use in Oceanography and Ocean Engineering*, Amsterdam, Elsevier Scientific Pub. Co., 1977.

Ghasemi Nejhad, M.N., R.D. Cope, and S.I. Guceri, "Thermal Analysis of in-situ Thermoplastic Composite Tape Laying", *Journal of Thermoplastic Composite Materials*, vol. 4, pp. 20-45, 1991a.

Ghasemi Nejhad, M.N., R.D. Cope, and S.I. Guceri, "Thermal Analysis of In-Situ Thermoplastic-Matrix Composite Filament Winding", *Journal of Heat Transfer*, vol. 113, no. 2, pp. 304-313, 1991b.

Ghasemi Nejhad, M.N., "Thermal Analysis for Thermoplastic Composite Tow/Tape Preheating and Pultrusion", *Journal of Thermoplastic Composite Materials*, vol. 10, pp. 504-523, 1997.

Goheen, K.R., and R.E. Jeffery, "Multivariable Self-Tuning Autopilots for Autonomous and Remotely Operated underwater Vehicles", *IEEE Journal of Oceanic Engineering*, vol. 15, pp.144-151, 1990.

Goldberg, D. E., *Genetic Algorithms in Search, Optimization, and Machine Learning*, Addison-Wesley, 1989.

Harding, K.G. and D.J. Svetkoff (chairs/editors), Three-dimensional Imaging and Laser-based Systems for Metrology and Inspection III (Pittsburgh, PA), International Society for Optical Engineering, Bellingham, Washington, 1997.

Healy, A.J. and D.B. Macro, "Slow Speed Flight Control of Autonomous Underwater Vehicles: Experimental Results with NPS AUV II", Proc. of ISOPE, pp. 523-532, 1992.

Healy, A.J. and D. Lienard, "Multi-variable Sliding Mode Control for Autonomous Diving and Steering of Unmanned Underwater Vehicles," *IEEE Journal of Oceanic Engineering*, vol. 18, no. 3, pp. 327-339, 1993.

Hollerbach, J.M. and K.C. Suh, "Redundancy Resolution of Manipulator Through Torque Optimization", *IEEE Journal of Robotics and Automation*, vol RA-3, No.4, pp. 308-316, 1987.

Holman, J.P. and W.J. Gajda, Jr., *Experimental Methods for Engineers*, New York, McGraw-Hill Book Company, 1989.

Hsu, L., R. Costa, and F. Lizarralde, "Underwater Vehicle Dynamic Positioning Based on a Passive Arm Measurement System", *International Advanced Robotics Programme*, pp. 23-32, 1994.

Ishii, K., T. Fujii, and T. Ura, "A Quick Adaptation Method in Neural Network Based Control System for AUVs," Proceedings of the Symposium of Autonomous Underwater Vehicle Technology, pp.269-274, 1994.

Intervention/ROV'91 Conference & Exposition, Hollywood, Florida, Sponsored by the ROV Committee and the South Florida Section of the Marine Technology Society, 1991.

Kajita, H. and K. Kosuge, "Force Control of Robot Floating on the Water Utilizing Vehicle Restoring Force," Proceedings of the 1997 IEEE/RSJ International Conference on Intelligent Robot and Systems, vol.1, pp. 162-167, 1997.

Kato, N., Y. Ito, K. Asakawa, and Y. Shirasaki, "Guidance and Control of Autonomous Underwater Vehicle AQUA Explorer 1000 for Inspection of Underwater Cables", Proc. 8th Int. Symposium on Unmanned, Untethered Submersible Technology, Sept. 1993.

Kawaguchi, K., C. Ikehara, S.K. Choi, M. Fujita, and J. Yuh, "Design of an Autonomous Underwater Robot: ODIN II," World Automation Congress, Montpellier, France, May 1996.

Kernighan, B.W. and D.M. Ritchie, *The C Programming Language*, Englewood Cliffs, NJ, Prentice-Hall, Inc., 1978.

Klafter, R. D., *Robotic Engineering: an Integrated Approach*, Prentice Hall, 1989.

Klein, C.A. and C.S. Huang, "Review of Pseudoinverse Control for Use with Kinematically Redundant Manipulators," *IEEE Trans. on System, Man, and Cybernetics*, vol. SMC-13, pp. 245-250, 1983.

Kochin, N.E., I.A. Kibel, and N.V. Rose, *Theoretical Hydrodynamics*, John Wiley & Sons, 1965.

Lamb, H., *Hydrodynamics*, Dover, 1945.

Lewis, D.J., J.M. Lipscomb, and P.G. Thompson, "The simulation of Remotely Operated Underwater Vehicle", Proceeding of ROV 1984, pp. 245-252, 1984.

Lewis, E.V., *Principles of Naval Architecture*, Jersey City, NJ, Society of Naval Architects and Marine Engineers, 1988-1989.

Liegeois, A., "Automatic Supervisory Control of the Configuration and Behavior of Multibody Mechanisms," *IEEE Trans. on Systems, Man, and Cybernetics*, vol. SMC-7, No.2, pp.868-871, 1977.

Mahesh, H., J. Yuh, and R. Lakshmi, "A Coordinated Control of an Underwater Vehicle and Robot Manipulator", *Journal of Robotic Systems*, Vol.8, No.3, pp.339-370, 1991.

Mallick, P.K., *Fiber-Reinforced Composites: Materials, Manufacturing, and Design*, New York: Marcel Dekker, Inc., 1993

Marco, D.B., *Autonomous Control of Underwater Vehicles and Local Area Maneuvering*, Ph.D. Dissertation, Naval Postgraduate School, 1996.

McLain, T.W., S.M. Rock, and M.J. Lee, "Experiments in the Coordinated Control of an Underwater Arm/Vehicle System", *Autonomous Robots 3*, pp. 213-232, Kluwer Academic Publisher, Netherlands, 1996.

McMillan, D.O., and R. McGhee, "Efficient Dynamic Simulation of an Underwater Vehicle with a Robotic Manipulator," *IEEE Trans. on Systems, Man, and Cybernetics*, Vol.25, No.8, pp.1194-1206, August, 1995.

Milne-Thomson, L., *Theoretical Hydrodynamics*, Macmillan, 1968.

Nakamura, Y., and H. Hanafusa, "Task Priority based Redundancy Control of Robot Manipulators", Robotics Research: The Second International Symposium, Cambridge, MA: MIT Press, pp.155-162, 1985.

Nie, J., J. Yuh, E. Kardash, and T.I. Fossen, "On-Board Sensor-Based Adaptive Control of Small UUVs in Very Shallow Water", IFAC Symposium on Control Applications for Marine Systems, 1998.

Nie, J., J. Yuh, E. Kardash, and T.I. Fossen, "On-Board Sensor-Based Adaptive Control of Small UUVs in Very Shallow Water", International Journal of Adaptive Control and Signal Processing, vol. 13, 1999.

Ogata, K., *Discrete-time Control Systems*, Prentice-Hall, New Jersey, 1987.

Pascoal, A., M. J. Rendas, V. Barroso, C. Silvestre, P. Oliveria and I. Lourtie, "Simulation Study of an Integrated Guidance System for an Autonomous Underwater Vehicle", Acoustic Signal Processing for Ocean Exploration (Eds. J.M.F. Moura and I.M.G. Lourtie), pp. 587-592, 1993.

Podder, T.K., "Dynamics and Control of Kinematically Redundant Underwater Vehicle-Manipulator Systems," Technical Report, Autonomous Systems Laboratory, University of Hawaii, no. ASL-98-01, July 1998.

Proceedings of the 1996 Symposium on Autonomous Underwater Vehicle Technology, Monterey, California, 1996.

Raibert, M.H. and J.J. Craig, "Hybrid Position/Force Control of Manipulators," *Transactions of the ASME Journal of Dynamic Systems, Measurement, and Control*, vol. 12, pp. 126-133, 1981.

Sagatun, S.I. *Modeling and Control of Underwater Vehicles: Lagrangian Approach,* Dr. Ing Thesis, Norwegian Institute of Technology, 1992.

Sarkar, N. and T.K. Podder, "Adaptive Control of Underwater Vehicle-Manipulator System Subjected to Drag Optimization, Proceedings of the IEEE International Conference on Robotics and Automation, pp. 387-392, Detroit, MI, May 1999a.

Sarkar, N., J. Yuh, and T.K. Podder, "Adaptive Control of Underwater Vehicle-Manipulator System Subjected to Drag Optimization, Proceedings of the IEEE International Conference on Intelligent Robots & Systems, Seoul, South Korea, October 1999b.

Shahinpoor, M., *A Robot Engineering Textbook*, New York, Harper & Row Publishers, 1987.

Shames, I.H, *Introduction to Solid Mechanics*, Prentice-Hall, Inc., 1989.

Smith, J. and K. Sugihara, "GA toolkit on the Web", Proc. of the First Online Workshop on Soft Computing (WSC1), pp.93-98, 1996.

Sonmez, F.O. and H.T. Hahn, "Analysis of the On-line Consolidation Process in the Thermoplastic Composite Tape Placement", *Journal of Thermoplastic Composite Materials*, v. 10, pp. 543-572, 1997.

Sprong, M.W. and M. Vidyasagar, *Robot Dynamics and Control*, New York, John Wiley & Sons, 1989.

Submersible Technology: Proceedings of an International Conference (Subtech '85), Aberdeen, UK, pp. 29-31, 1985.

Sugihara, K., "GA-based On-line Path Planning for SAUVIM", Proc. 11th Int'l Conf. on Industrial and Engineering Applications of Artificial Intelligence and Expert Systems (IEA-98-AIE), pp.329-338, 1998a.

Sugihara, K. and J. Smith, *Genetic Algorithms for Adaptive Planning of Path and Trajectory of a Mobile Robot in 2D Terrain, IEICE Trans. on Information and Systems*, to appear 1998b.

Sugihara, K. and J. Yuh, "GA-based Motion Planning for Underwater Robotic Vehicles", Proc. 10th Int'l Symp. On Unmanned Untethered Submersible Technology (UUST-10), pp.406-415, 1998c.

Tarn, T.J., G.A., Shoultsand, and S.P. Yang, "A Dynamic Model of an Underwater Vehicle with a Robotic Manipulator using Kane's Method", *Autonomous Robots 3*, pp. 269-283, Kluwer Academic Publisher, Netherlands, 1996.

Tupper, E.C., *Introduction to Naval Architecture*, Oxford, Butterworth-Heinemann Publishing, 1996.

Unimate PUMA Robot: Volume 1 – Technical Manual 398H1, Unimation Inc., Condec Company, Danbury CT, 1981.

Unimate PUMA Mark II Robot: 500 Series, Volume 1 – Equipment Manual, Unimation, Westinghouse Corporation, Danbury CT, 1984.

Unimate Industrial Robot: Programming Manual, User's Guide to VAL II Version 2.0 (398AG1), Unimation, Westinghouse Corporation, Danbury CT, 1986.

Unimate – Supplement to the User's Guide to VAL II: VAL II-IVM PC Supervisor Interface (397W1), Unimation, Westinghouse Corporation, Danbury CT, 1987.

Vinson, J.R., and R.L. Sierakowski, *The Behavior of Structures Composed of Composite Materials*, Netherlands, Kluwer Academic Publishers, 1987.

Werdermann, C., K. Friedrich, M. Cirino, and R.B. Pipes, "Design and Fabrication an On-line Consolidation Facility for Thermoplastic Composites", *Journal of Thermoplastic Composite Materials*, vol. 2, pp. 293-306, 1989.

Wit, C.C.D., E.O. Diaz, and M. Perrier, "Robust Nonlinear Control of an Underwater Vehicle/ Manipulator System with Composite Dynamics", Proc. IEEE Conf. on Robotics and Automation, pp.452-457, 1998.

Whitney, D.E., "Historical Perspective and State of the Art in Robot Force Control," *International Journal of Robotic Research*, vol. 6, no.1, pp. 3-14, 1987.

Yang, K.C., J. Yuh, and S.K. Choi, "Experimental Study of Fault-tolerant System Design for Underwater Robots", Proc. IEEE Conf. on Robotics and Automation, pp. 1051-1056, 1998a.

Yang, K.C., J. Yuh, and S.K. Choi, "Experimental Study of Fault-tolerant System Design for Underwater Robots", *Journal of System Sciences*, 1998b.

Yuh, J., "Learning Control for Underwater Robotic Vehicles", *IEEE Control System Magazine*, vol.15, No.2, pp.39-46, 1994a.

Yuh, J., *Underwater Robotic Vehicles: Design and Control*, Workshop on Future Research Directions in Underwater Robotics, TSI Press, p. 361, 1994b.

Yuh, J., "An Adaptive and Learning Control System for Underwater Robots", 13th World Congress International Federation of Automatic Control, A, pp. 145-150, 1996.

Yuh, J., S.K. Choi, C. Ikehara, G.H. Kim, G. McMurtry, M. Ghasemi Nejhad, N. Sarkar, and K. Sugihara, "Design of a Semi-Autonomous Underwater Vehicle for Intervention Missions (SAUVIM)," Proceeding of the Underwater Technology '98, 1998a.

Yuh, J. and J. Nie, "Experimental Study on Adaptive Control of Underwater Robots," Proceedings of the IEEE International Conference of Robotics and Automation, Detroit, MI, May 1999.

Yuh, J., J. Nie, and W.C. Lee, "Adaptive Control of Robot Manipulators Using Bound Estimation", IEEE International Conference on Intelligent Robots and Systems, 1998b.

Annual Report Appendix

Appendix 1: SAUVIM Velocity Analysis

Appendix 2: SAUVIM Test Plan (Phase I – Shallow Water)

Appendix 3: Additional SAUVIM Diagrams

Figure ARA-3A: SAUVIM General Wiring Diagram

Figure ARA-3B: SAUVIM General Wiring Diagram – Pressure Vessel P1

Figure ARA-3C: SAUVIM General Wiring Diagram – Pressure Vessel P2

Figure ARA-4D: SAUVIM General Wiring Diagram – Pressure Vessel P3

Figure ARA-5E: SAUVIM General Wiring Diagram – Pressure Vessel P4

Figure ARA-6F: SAUVIM General Wiring Diagram – Pressure Vessel P5

Figure ARA-7G: SAUVIM General Wiring Diagram – Pressure Vessel P6

Appendix 4: Table of SAUVIM Specifications

Appendix 1: SAUVIM Velocity Analysis

Motivation:

To get an initial, estimation analysis of the vehicle's performance, these series of simplified calculations were performed. These are **not** intended to be a full-featured dynamic analysis; they are merely reasonable and precise estimates of the following: 1) the acceleration responsiveness of the SAUVIM to the planned thruster units - a set of eight Technodyne Model 1020 brushless motor thrusters; 2) the ultimate cruising speed of the vehicle under neutrally buoyant thrust conditions as well as weighted descent; and 3) an estimate of the rotational (yaw-) responsiveness of the vehicle.

Introduction:

In all cases, we use SAUVIM's response in terms of lineal and angular distance covered versus time elapsed since application of thrust at 100% of the rating supplied on the manufacturer's data sheet for the given thruster set. The other information is detailed in the velocity (or angular speed) versus the time elapsed since the application of the full rated thrust. The initial state of the vehicle in all cases is a full stop position. The SAUVIM vehicle faired is of the following shape:

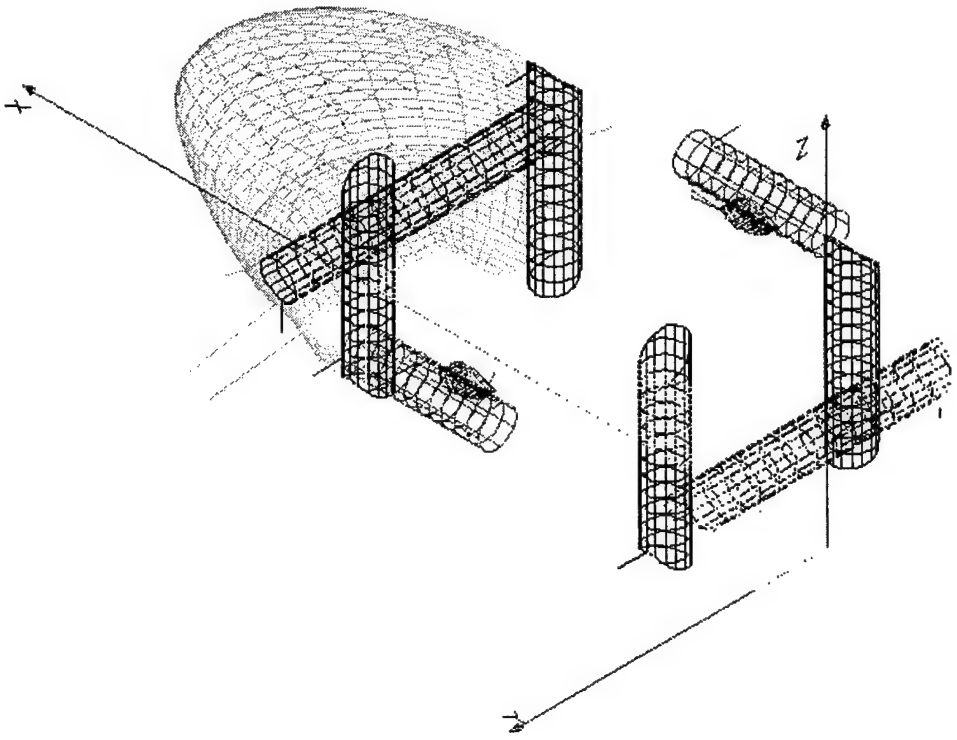

Figure 1: Isometric View of the SAUVIM Fairing with Thruster Tubes

For purposes of this analysis, the longitudinal direction is along the x-axis, the lateral direction is along the y-, and vertical direction in the z-. Four thrusters (the black tubes parallel to the z-axis) point vertical with the more powerful thrust vector pointed down, two point fore and aft (the pink tubes on pylons), the aft direction is the more powerful thrust vector. The two lateral thrusters (black

tubes parallel to the y-axis) face with the more powerful vector pointing along +y, this choice is arbitrary and is made to ensure a balanced pair of thrust in either lateral direction.

Method:

For velocity, a force balance equation was employed: $Force_{thrusters} = Drag_{vehicle} + (Mass_{vehicle})$

$$T_{thrusters-set} = \frac{1}{2}\rho C_R A \dot{\theta}^2 + I\ddot{\theta}$$

where the terms, are F is the maximum thruster output force in newtons (kg_f which is equivalent to 10N), each Technodyne model 1020 outputs 21.4 kg_f (214N or 47 lb_f) in the forward direction and 14.5 kg_f each (145N or 32 lb_f) in the reverse direction. These values were obtained right off of the Technodyne data sheets. Value should be within ±10% of actual value.

ρ, is density of seawater in kg/m^3 (=1024 kg/m^3). This was obtained from an introductory Oceanography text. Value should be within ±2-3% of actual value.

C_D, is Drag coefficient for SAUVIM in dimensionless form. For the drag in the forward longitudinal direction, 0.35 was used for the faired vehicle and 0.85 was used for the unfaired vehicle. The former number is a composite of the CFD results from CHAM (0.40), HSI (0.25), and the figure cited for a Ford Taurus (0.32). Value may be within ±30% of actual value, these estimates are very preliminary until a combination of thorough CFD study and/or model testing is carried out.

A, is Cross-sectional area from frontal/rearward vantage point in m^2 (= 3.74 m^2 frontal, = 10.19 m^2 lateral, =13.15 m^2 vertical) These values are derived directly from the ACADr13 model of the SAUVIM fairing. Value should be within ±2% of actual value.

m, is mass of the SAUVIM vehicle includes dry mass as well as entrained water mass within the fairing and the vehicle components, in kg (= 17,800 kg/39,000 lbs for faired SAUVIM, 8,160 kg/18,000 lbs for unfaired SAUVIM). The faired vehicle mass estimate is taken directly from the

v, is velocity of vehicle in m/sec (reported as knots though, initially set to 0 m/sec).

$\ddot{x}$, is acceleration at a given time in m/sec^2 (initially set to 0 m/sec^2).

Solution for of the differential equation (x-dot (v) and x-dot-dot) proceeds by integration along the time steps using Euler's method: the initial acceleration and velocity were '0', subsequent steps reference the previous time steps which are spaced at one second intervals. The rest of the terms were treated as constants.

For yaw response the form of the equation is $Couple_{thruster} = Drag_{vehicle\text{-}rot.} + (I_{vehicle})$

$$F_{thrusters} = \frac{1}{2}\rho C_D A v^2 + m\ddot{x}$$

The variables in here are the rotational equivalents of the variables in equation (1), detailed notes on their values will be discussed on the case analysis.

Cases: The following cases have been explored:

Case I - Forward/Rearward (longitudinal translation) with fairing
Case II - Forward/Rearward (longitudinal translation) without fairing
Case III - Lateral Starboard/Port (lateral translation) with fairing.
Case IV - Lateral Starboard/Port (lateral translation) without fairing.
Case V - Vertical up/Vertical down (vertical translation) with fairing
Case VI - Vertical up/Vertical down (lateral translation) without fairing
Case VII - Yaw response with fairing
Case VIII - Yaw response without fairing

Assumptions and results pertinent to each will be detailed case-by-case bases. Many items that are in a complete rigorous analysis have been discounted among these are: duct water-mass inertia, vehicle damping coefficient, duct drag losses, C_D variations with velocity change, off-centric application of forces from the center of inertial and drag resistances and resultant thrust reductions off of the maximum to accommodate balancing, reduction in thrust from the Model 1020 as SAUVIM vehicle gains speed and propulsive effective thrust drops off (propeller advance ratio effects).

The following table 1 summarizes the variables used for each case.

Table 1: Different Case Studies for Thruster Tests

Case	Thruster Force	C_D (or C_R)	A	m (or I_{zz})
Units	N		m^2	kg (kg m^2)
I - Forward with fairing	419.8	0.35	3.74	17800
I - Astern with fairing	284.5	0.35	3.74	17800
II - Forward without fairing	419.8	0.85	3.74	8160
II - Astern without fairing	284.5	0.85	3.74	8160
III - Lateral Starboard with fairing	419.8	0.75	10.19	17800
III - Lateral Port with fairing	284.5	0.75	10.19	17800
IV - Lateral Starboard without fairing	419.8	0.80	10.19	8160
IV - Lateral Port without fairing	284.5	0.80	10.19	8160
V - Vertical up with fairing	839.6	1.2	13.15	17800
V - Vertical down with fairing	569.0	1.2	13.15	17800
V - Vertical up without fairing	839.6	1.4	10.00	8160
V - Vertical down without fairing	569.0	1.4	10.00	8160
VII - Yaw with fairing	?	?	10.19	17800
VIII - Yaw without fairing	?	?	10.19	8160
IX - Unpowered 30° descent cruise	N/A	N/A	N/A	N/A

Assumptions/Results: Case-by-case breakdown will proceed.

Case I & II - This is the baseline SAUVIM case where the neutrally buoyant vehicle is accelerated straight forward. It is assumed here, as for all the subsequent cases in this analysis, that the line of action of the thruster vectors is lined up sufficiently close to the center of inertial mass as well as the singular center of drag force action to preclude having to reduce thrust in any of the set to counter the resulting rotational drifts that would occur (e.g. all forces are centric in nature). The two longitudinal thrusters are rated at 47 lb_f/each (214 N) in the forward direction and 32 lb_f/each (145 N) in the reverse direction.

The area, 3.74m^2, was obtained from the ACADR13 solid model. This is the profile cross-sectional area seen from along the vehicle's X-axis as is standard practice in drag calculations using dimensionless drag data.

For estimating the vehicle mass two methods were used; for the unfaired vehicle the mass was estimated from the itemized tally spreadsheet (Sensit4.wb3) of all the major components with some adjustment made for water that would be entrained within the major cavities of the vehicle (the wiring space above the batteries, around the pressure vessels within the main component box - for details see Figure MED-10). The table below summarizes the approximate void space within each of the major cavity spaces of the vehicle. The foam space cavity is not included as it is assumed to completely occupy SAUVIM's dry mass. The venting value is an estimated guess at the amount of water in a given cavity. It also estimates the water spillage throughout the vehicle components, and therefore, will not contribute to the inertial mass of the vehicle. The approximately 1640 kg figure of entrained water is added to the unfaired SAUVIM mass for the startup run calculations in table 2.

Table 2: Unfaired SAUVIM Entrained Water Mass Estimates

Volume Name	Cavity Height (in)	Cavity Length (in)	Cavity Breadth (in)	Volume (ft^3)	% Volume Occupied	Adjusted Volume	Water in Voids (lbs)	Venting Estimate	Adjusted Mass (lbs)
Battery	21.5	75.0	45.0	42.0	34%	27.52	1717.25	0.50	858.62
Ballast	21.5	32.0	45.0	17.9	11%	15.87	989.99	0.50	494.99
Arm	21.5	32.0	45.0	17.9	8%	16.50	1029.82	0.70	720.87
PV	23.0	165.0	45.0	98.8	17%	82.07	5121.35	0.30	1536.41
Approximate Mass of Water entrained inside Vehicle (lbs)									3610.89
Approximate Mass of Water entrained inside Vehicle (kg)									1639.34

The resulting unfaired SAUVIM effective inertial mass is around 6,900 kg. To give and idea of the relative volume ration between free space that floods and solid SAUVIM components the approximate volumes of some of the major components is given in table 3.

Table 3: Approximate Volumes of Components

Approximate Volumes of:	ft^3	m^3
12 Batteries	14.47	0.41
6 Pressure Vessels	16.76	0.47
Arms and Tray	1.41	0.042
Ballast Tray and Ballast	2.05	0.058

For the faired vehicle the wet mass figure of 17,800 kg was arrived at simply be assuming that the SAUVIM is neutrally buoyant and determining the enclosed volume of water within the fairing shell (done in the ACADR13 model). This assumes a completely stagnant pocket of water within the fairing, which clearly not the case with the actual vehicle as the will be ports, ducts and open areas in the fairing for water to spill through. Since the worst case is to assume a completely sealed fairing, this assumption was made.

Meanwhile, a fairly conservative coefficient of drag was adopted (in the dimensionless form) as well. For forward motion a C_D of 0.35 was used. This was arrived at based on preliminary results from the Phoenics CFD code ($C_D = 0.40$), work done at Pacific Marine with CFD code ($C_D = 0.25$), and some book sources. Chosen from these book sources was the C_D of some concept cars having a very similar form to the SAUVIM fairing (C_D = 0..35, 0.23, pg.12-3, $C_D = 0.25$, pg. 12-9 Fluid-Dynamic Drag, Practical Information on Aerodynamic Drag and Hydrodynamic Resistance, Hoerner, S.F., AIAA press - 1965). These values were cited for shapes that are operating in ground effect and therefore only approximate the SAUVIM fairing in a free stream environment, hence the selection of a more conservative value for C_D. The same C_D was used for both forward and rearward motion.

The results of the analysis are summarized in these graphs, the first of which shows the SAUVIM velocity as a function of time elapsed since thruster startup, SAUVIM displacement since thruster startup and the same in a shortened time span. It can be seen with the fairing on that the ultimate forward velocity possible with the twin Technodyne 1020's will be 1.5 knots (0.79 m/sec) forward and a little over 1.2 knots at full reverse (0.65 m/sec). Full speed will be reached after 90 seconds of runup. Without the fairing, acceleration will be much better and the full speed will be reached within 20 seconds, however, high speed will drop to 1.0 knots (0.50 m/sec) and 0.8 knots (0.41 m/sec) for forward and reverse directions, respectively.

It can be seen from the third graph that pulsing the thrusters in the forward direction for the faired vehicle for 3 seconds will result in 15cm of translation, the unfaired SAUVIM will have moved 35cm.

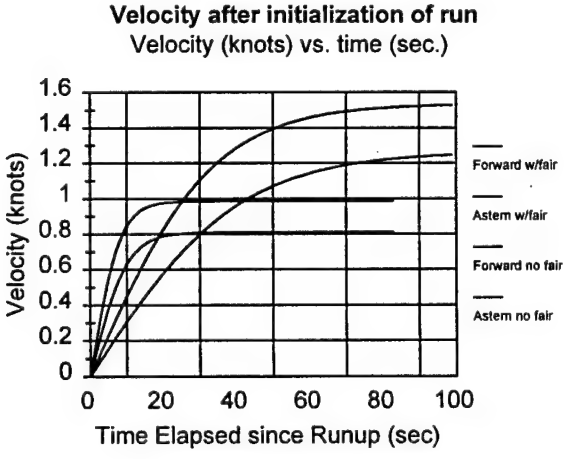

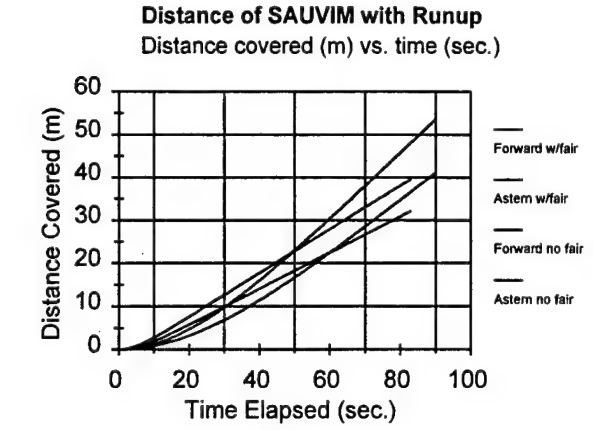

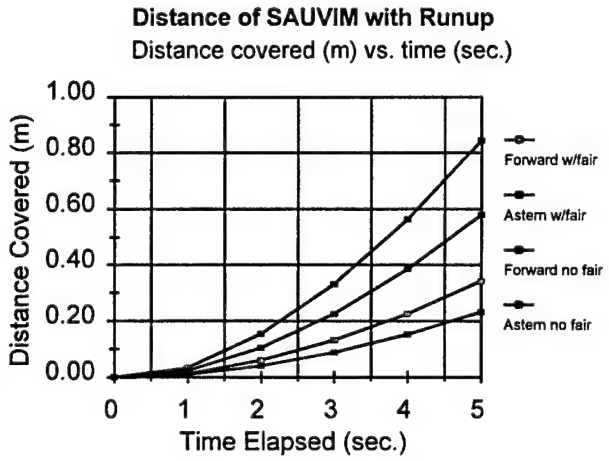

Case III & IV - The mass assumptions are the same as in cases I & II, here lateral motion is concerned. The major changes here concern, profile area, the direction of the Technodyne 1020's favored thrust direction, and C_D changes. For the C_D of both the faired and unfaired vehicle there are no variances with direction to either side as the SAUVIM is symmetric across the XZ-plane. The C_D for the faired vehicle a value of 0.75 was estimated (the data of a circular cylinder of similar aspect ratio in cross-flow with $C_D = 0.70$ was used a basis for this value, from Hoerner, S.F., AIAA press - 1965, pg. 3-16). This value was degraded to 0.80 for the unfaired vehicle to account for sharper edges on the ends of the unfaired vehicle, though the bulk cross-section remains largely unchanged. Though not accounted for in this analysis, due to the relatively complete coverage of floatation foam over the vehicles flooded spaces from this direction the entrained water mass value for the unfaired SAUVIM should probably be adjusted upward.

The more powerful thruster direction of the 1020's was chosen to be applicable for starboard motion, this was chosen arbitrarily; avoidance of any yawing during paired lateral thrusting will probably necessitate orienting the thrusters in this fashion until the symmetrical propellers are retrofitted. The profile area as seen from along the y-axis is 10.19 m^2. This was obtained from the ACAD R13 fairing model. The results are shown here, it can be seen that the maximum lateral speeds are around 0.63 knots (0.32 m/s) and 0.52 knots (0.26 m/s) for starboard and port directions with the fairing. Without the fairing these values become 0.61 knots (0.31 m/s) and 0.50 knots (0.26 m/s). Note from

the first graph that the maximum speeds are reached within 10 and 30 seconds for the unfaired and faired conditions, respectively.

A three second pulse of full thrust will move the vehicle from about 9-28 cm depending on the fairing and favored direction of thrust.

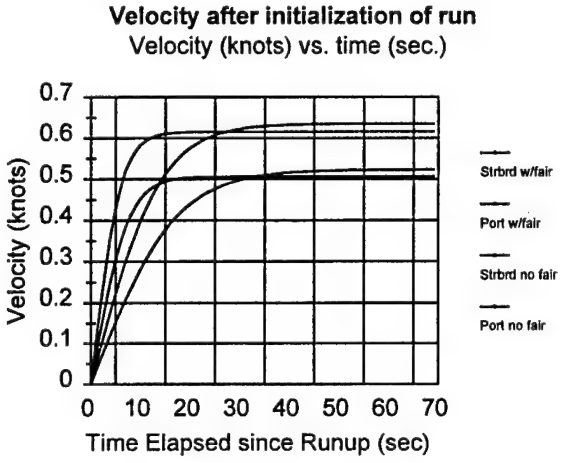

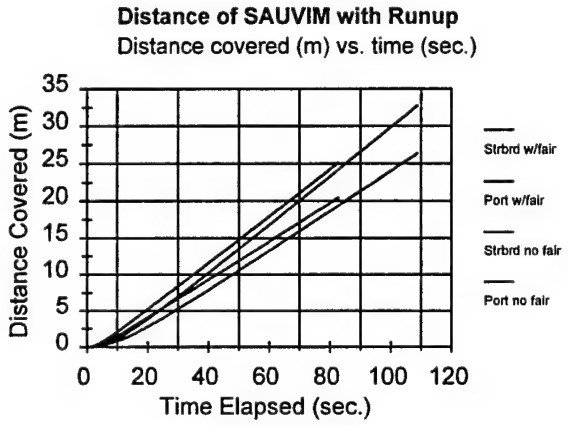

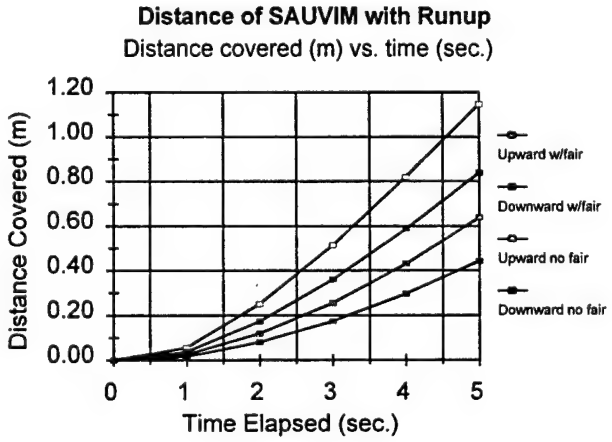

Case V & VI - These cases account for vertical motion. The greater power of the thrusters is due to a set of four Technodyne 1020's being selected for this direction. The favored direction of thrust in this analysis was chosen for the downward direction. This is a design issues but was chosen to fight the gravitational field should the SAUVIM be slightly heavy which due to foam compressibility is a more likely state to be in upon cruise to the bottom. So around 840 N can be applied to move vertically up and about 570 N can be applied in the downward direction. The C_D for this direction was chosen to be 1.2; this was cited for cylinders at moderate Reynolds number flows. At Reynolds flow values typical for our vehicle the C_D for cylinders actually drops to around 0.7, but this is due the migration of regions of separation back on the smooth surface of a cylinder. Since the roughly circular SAUVIM fairing form has edges that trip off flow separation in fixed locations, unlike a smooth cylinder in moderate Reynolds number flow, the higher value for C_D is chosen.

The cross-sectional area is now 13.15 m^2 , this is the profile area of the fairing as seen from the top. It is somewhat less for the unfaired vehicle as the nosecone and tail cone do add about 30% more area to the silhouetted area as opposed to the unfaired vehicle.

The results here indicate the faired vehicle can expect vertical maximum speeds on the order of 0.65 knots and 0.54 knots downward when faired and 0.62 knots and 0.51 knots when unfaired. It can be seen that a three second pulse of the thrusters at full rated load will move the vehicle from about 18-55 cm depending on the thrust direction and the presence of the fairing.

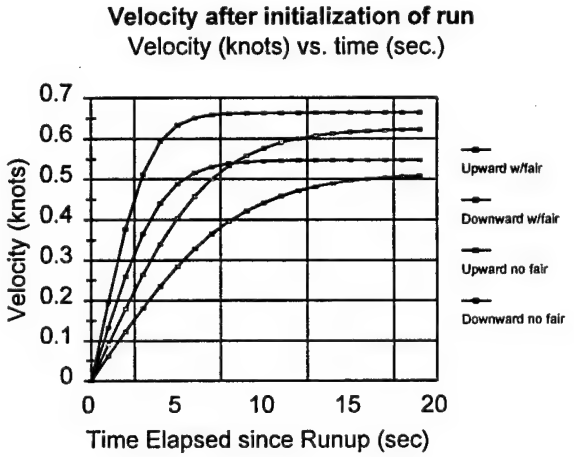

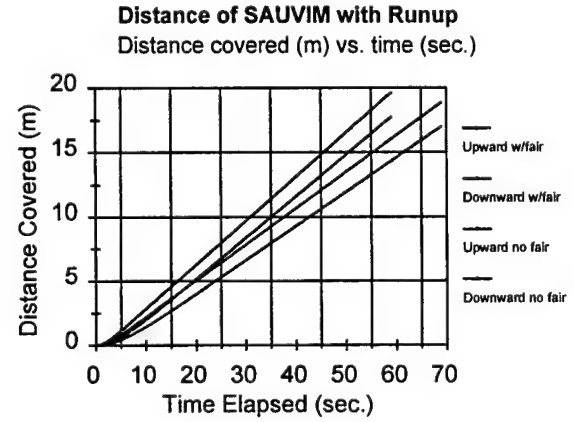

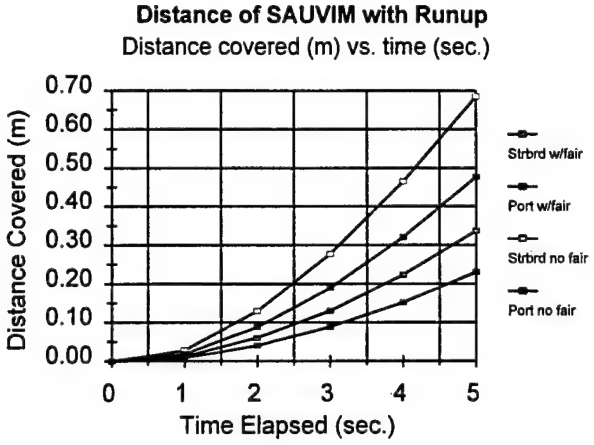

Case VII & VIII - These cases concern yaw rotation. In this case the SAUVIM vehicle pivots about an axis parallel to the z-axis with application of thrust in opposite directions of both the longitudinal and lateral pairs of the thrusters. This has been calculated for both the faired and unfaired vehicle variants. The following assumptions run throughout the models:

- The principle rotational moment for the faired vehicle will assume the fairing volume is a uniform mass with the density of seawater. Treating the volume within the fairing model as a uniform mass and using a solid function to recover the inertial moment derived the moment value.

- $C_{D\text{-}rot}$ for the SAUVIM will be that of a rectangular parallelepiped of similar aspect ratio. The value was degraded somewhat for the unfaired vehicle owing to separation around the edges on the aft and forward ends.

- Two sets of thrusters will contribute to the couple moment, the lateral and longitudinal pairs, furthermore no wake coupling effects will be accounted for.

- The principle moment for the unfaired vehicle was found by applying the mass moment formula to the major components that are tracked on the datasheet.

- The couples coming off of the thrusters we using the minimum thrust rating at the shortest moment arm from the inertial axis. For the lateral pair of thrusters this was 14.5 kg of thrust at 60 inches from the inertial axis, for the longitudinal pair it was again 14.5 kg at 60 inches from the inertial axis.

- The inertial axis (I_{ZZ}) was calculated to be at vehicle coordinates for the X=85in and Y=0 in for the unfaired vehicle, the location of I_{ZZ} on the faired vehicle was at X=85in and Y=0in again.

- The magnitude of I_{ZZ} is 41,850 kg-m^2 for the faired vehicle and reduces to 6,615 kg-m^2 when the fairing is removed.

The graphs below summarize the results. As expected the faired vehicle has a slower initial response than the unfaired variant; however, the ultimate high rotational speed is not critical as the likely

maneuvers will be completed before obtaining the maximum speed. All of the angular distances are given in degrees.

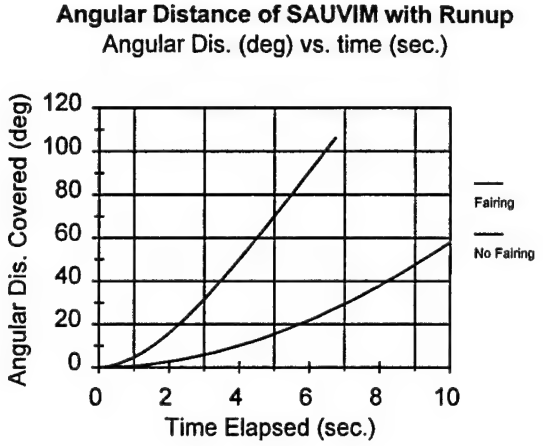

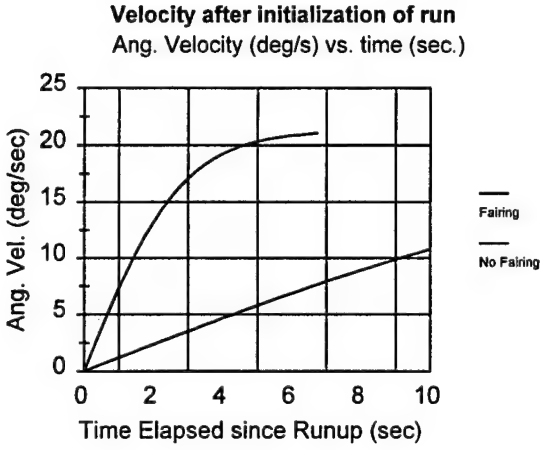

Unpowered Cruise - This case is still under investigation.

General Observations:

A free-flooded fairing incurs both advantages and disadvantages to a vehicle equipped with it, though it may be very useful for open ocean operations, it does result in a real hit on inertial response of the vehicle upon thruster startup and short term pulsing for active station-keeping. The vehicle will not be nearly as responsive to thruster inputs with it installed although cruising range and inertial damping to disturbances will be increased. For a vehicle cruising at near constant speeds or involved in station keeping for extended periods in a steady current using passive inertial damping, the fairing may yield a distinct advantage even though it effectively doubles the vehicle inertial mass from 8,200 kg to 17,800 kg.

Cruising range under full power is affected by the fairing. Consider the longitudinal thrusters only. These thrusters are powered by three lead-acid DeepSea SB-48/18 batteries, arranged in a serial bank to provide 144VDC at 18 Amp-Hours of continuous draw (2.60 kW·hr). This gives the vehicle with

two Technodyne thrusters drawing 1550 Watts continuously the following ranges: 2.70 nautical miles (5.0 km) with the fairing and 1.73 nautical miles (3.2 km) without the fairing.

Recommendations:

The Theoretical Modeling (TM) dynamics group may want to explore the following parametric changes to the SAUVIM vehicle:

Fairing size changes - Fairing size changes in the lineal distances will have a square-law change influence on the profile areas and therefore the magnitude of the drag forces. A 10% reduction in fairing size may reduce hydrodynamic drag to about 81% of the baseline case; meanwhile the inertial mass will drop to about 75% of the baseline case. Maximum cruise speed will climb about 10-12% and initial responsiveness will climb modestly, however, loss of the vehicle expansion/design flexibility that the prototype has will be suffered. The most feasible fairing size change is to redistribute some of the foam up on the top of the vehicle to down within the battery tray area and into some of the larger pockets formed between the pressure vessels. A side effect of doing this relocation would be a shorter separating distance between the centroid of the volume of all the SAUVIM components and the center of mass; this would result in a more tightly responsive vehicle to ballast trim, thruster and fin trim inputs, conversely also to arm inputs and being buffeted by currents, external influences.

Thruster Power Changes: Migrating from the Technodyne 1020 to the 2010 model would nearly quadruple the thrust from each unit (Technodyne 2010 data sheets rating 143 lb_f (650 N) forward and 80 lb_f (364 N) reverse). The Technodyne manufacturing representative has stated that these values are only about 75% of the thrust that the 2010 can actually sustain under continuous load. Raising thruster power by a factor of four will double the maximum speed as drag is a square law dependency on velocity. Note though that the cruising range under maximum cruise speed possible with 2010 units is only about 50% of that with the smaller thruster units running at their maximum rated thrust. Of course economic concerns enter here as the Model 2010 units cost around $9,500 apiece as opposed to the $5,800 that the 1020 units run.

Decent Cruise: This is not critical for shallow water variant of the SAUVIM but will become a critical portion of the mission phases as the SAUVIM proceeds into deep-water missions. The ability to glide in a controlled fashion and make course corrections to ensure arrival close to the task site with minimal, if any, thruster application will be critical from the standpoint of the small cruising range imposed by the battery bank energy limits and the minimization of time during which fixed electrical loads (e.g. computers, long-baseline sensors, etc) draw power. Hence further exploration of this mode of vehicle motion warrants conceptual consideration, if not detailed analysis, even prior to commencement of shallow water operations.

Recommended Tasks: These steps will be needed for a more accurate dynamic model the TM-dynamics group should consider the following tasks: 1) locate the center of drag action for the three principle directions, 2) locate the inertial center for both the faired and unfaired vehicles using the AutoCAD fairing model and the Quattro spreadsheet tally of the major SAUVIM component masses, 3) from the former two steps and knowing where the thrusters are located determine the thrust tuning adjustments needed to cancel non-centric effects and 4) determine and map the combined drag/inertial resistance centroid location with velocity location.

Also it will be worth determining the effects of the three planned fins on the vehicle dynamics for both powered and decent cruise. This will be of great value in sizing of the foils for the fin units to ensure the right balance between vehicle-response and vehicle-handling concerns.

Appendix 2: SAUVIM Test Plan (Phase I – Shallow Water)

Objective

- To test essential hardware and software functions and to check the integrity of the system.

In this write-up, it is assumed that the vehicle is completed for experiments. The joystick-based controller will be used in most cases. After the completion of these basic tests, a simple "dead-reckoning" control algorithm and a simple object-following control algorithm will be tested for initial closed-loop control and navigation purposes. The basic tests plans are:

Test Plan 1

Goal - Test the basic emergency handling functions.

The weight dropping functions will be tested. This test is made of two parts. In the first part, weight will be dropped as the vehicle reaches desired depth by monitoring depth sensor. (The desired depth is not determined yet, but it should be limited within 60 ft so that divers can reach to the vehicle for recovery.) The second part will simulate leakage in the pressure vessels. Timer switch can be connected to one of the leakage sensors to simulate the leakage. During the test, battery level will be monitored and logged.

Sensors: depth sensor, leakage sensor, battery gauges
Actuator: weight drop

Test Plan 2

Goal - Test if all the sensors and other hardware devices are working properly and to log acquired data for future analysis.

The sensors, which provide information of vehicle movement, will be checked to see if they provide correct values. These values will be stored in a local storage device and transmitted to the other computer for backup. Thrusters will be turned on in short intervals (for example, 30 seconds for each thruster). As the vehicle moves, the INS and electric compass data will be monitored. Thruster will be operated with open loop controller for the simplicity in early phase of development. The fins will be tested while the vehicle stops and moves.

Sensors: INS, electric Compass
Actuator: thrusters, fins

Test Plan 3

Goal - Test the sonar-based sensors.

The sonar-based sensors such as altimeters and scan sonar will be tested. The vehicle will be fixed at an arbitrary point to minimize disturbance to sensor signals. Operator can place objects in front of each altimeter and check the readings from the sensors. The distance of the objects from the vehicle and the size of the objects are not determined. The readings will be stored in a local storage and transmitted to the remote operator. Because scan sonar will not be used by the first phase, all the data

will be stored in a local storage for future analysis. The data can be analyzed with experimental algorithm or program, but the specific plan is not yet determined.

Sensors: altimeters, scan sonar
Actuator: none

Test Plan 4

Goal - Test the basic vehicle maneuvering function and miscellaneous functions.

The basic maneuvering function will be tested. The vehicle will move using thruster and fins based on the data from sensors. Sonar data will be monitored but will not be used in navigation until next phase starts. Only open loop control will be used. Lights will be turned on and off during navigation. The other sensors, which are not mentioned here, will be monitored and logged for future reference.

Sensors: INS, compass, depth sonar, altimeter, scan sonar, battery level.
Actuator: thrusters, fins, light switch

Figure ARA-3A: SAUVIM General Wiring Diagram

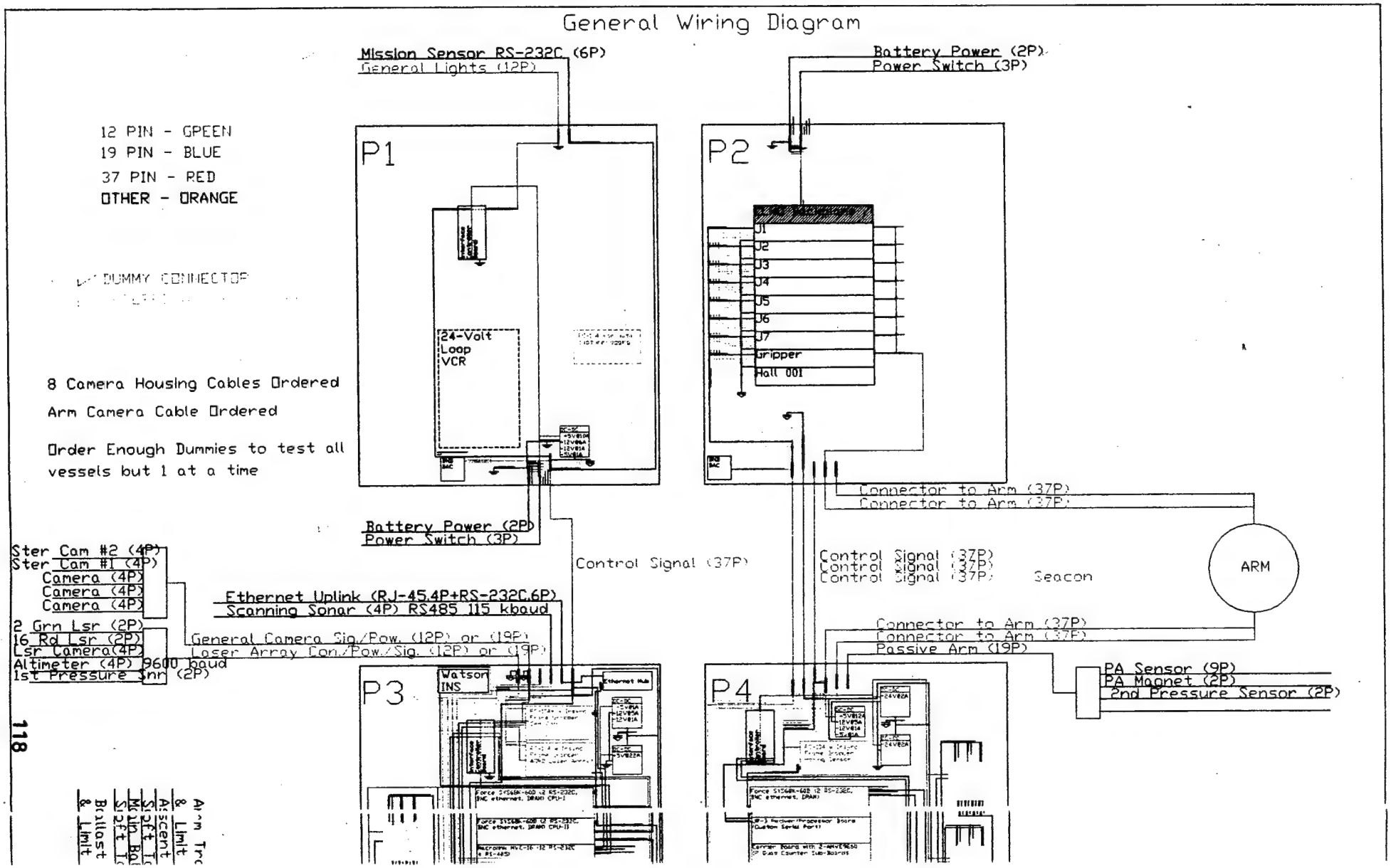

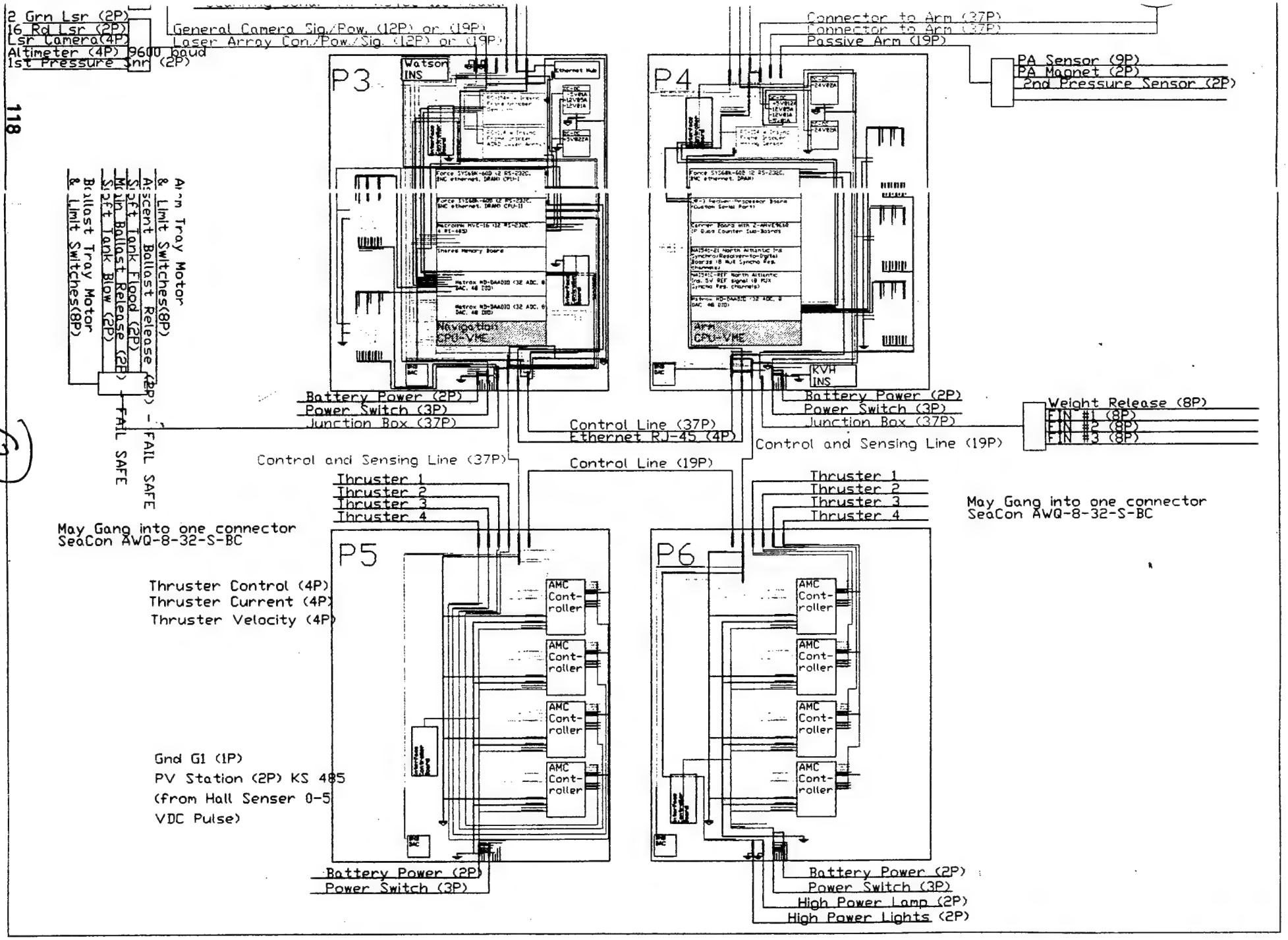
2 Grn Lsr (2P)
16 Rd Lsr (2P)
Lsr Camera(4P)
Altimeter (4P) 9600 baud
1st Pressure Snr (2P)
General Camera Sig./Pow. (12P) or (19P)
Laser Array Con./Pow./Sig. (12P) or (19P)
Connector to Arm (37P)
Connector to Arm (37P)
Passive Arm (19P)
PA Sensor (9P)
PA Magnet (2P)
2nd Pressure Sensor (2P)
P3
Watson INS
Navigation CPU-VME
P4
Arm CPU-VME
KVH INS
Arm Tray Motor
& Limit Switches(8P)
Ascent Ballast Release (2P)
Shift Tank Flood (2P)
Main Ballast Release (2P)
Shift Tank Blow (2P)
Ballast Tray Motor
& Limit Switches(8P)
FAIL SAFE
FAIL SAFE
Battery Power (2P)
Power Switch (3P)
Junction Box (37P)
Control Line (37P)
Ethernet RJ-45 (4P)
Battery Power (2P)
Power Switch (3P)
Junction Box (37P)
Control Line (19P)
Weight Release (8P)
FIN #1 (8P)
FIN #2 (8P)
FIN #3 (8P)
Control and Sensing Line (37P)
Control and Sensing Line (19P)
Thruster 1
Thruster 2
Thruster 3
Thruster 4
May Gang into one connector
SeaCon AWG-8-32-S-BC
Thruster 1
Thruster 2
Thruster 3
Thruster 4
May Gang into one connector
SeaCon AWG-8-32-S-BC
P5
P6
AMC Cont-roller
Thruster Control (4P)
Thruster Current (4P)
Thruster Velocity (4P)
Gnd G1 (1P)
PV Station (2P) KS 485
(from Hall Senser 0-5
VDC Pulse)
Battery Power (2P)
Power Switch (3P)
Battery Power (2P)
Power Switch (3P)
High Power Lamp (2P)
High Power Lights (2P)

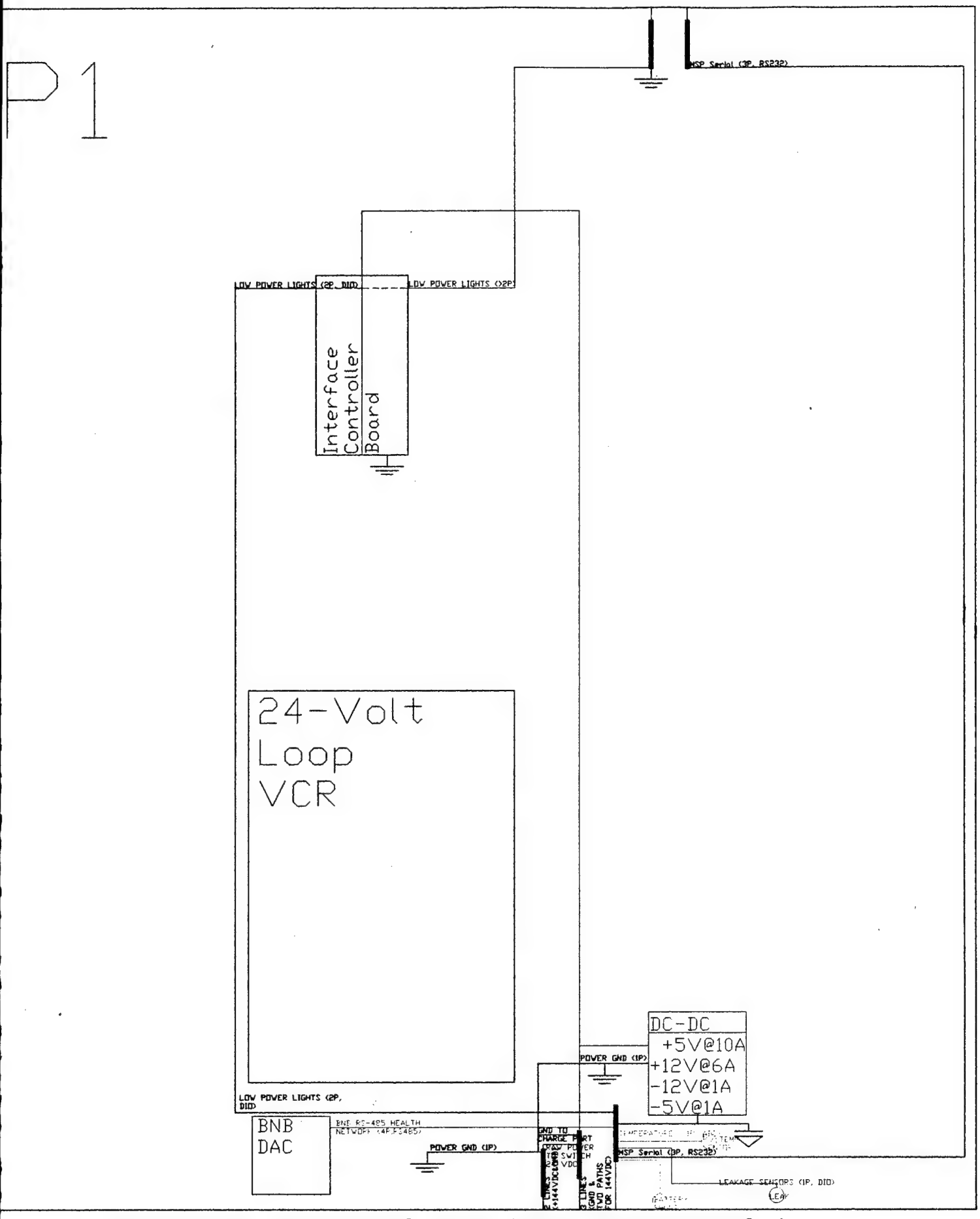

Figure ARA-3B: SAUVIM General Wiring Diagram - Pressure Vessel P1

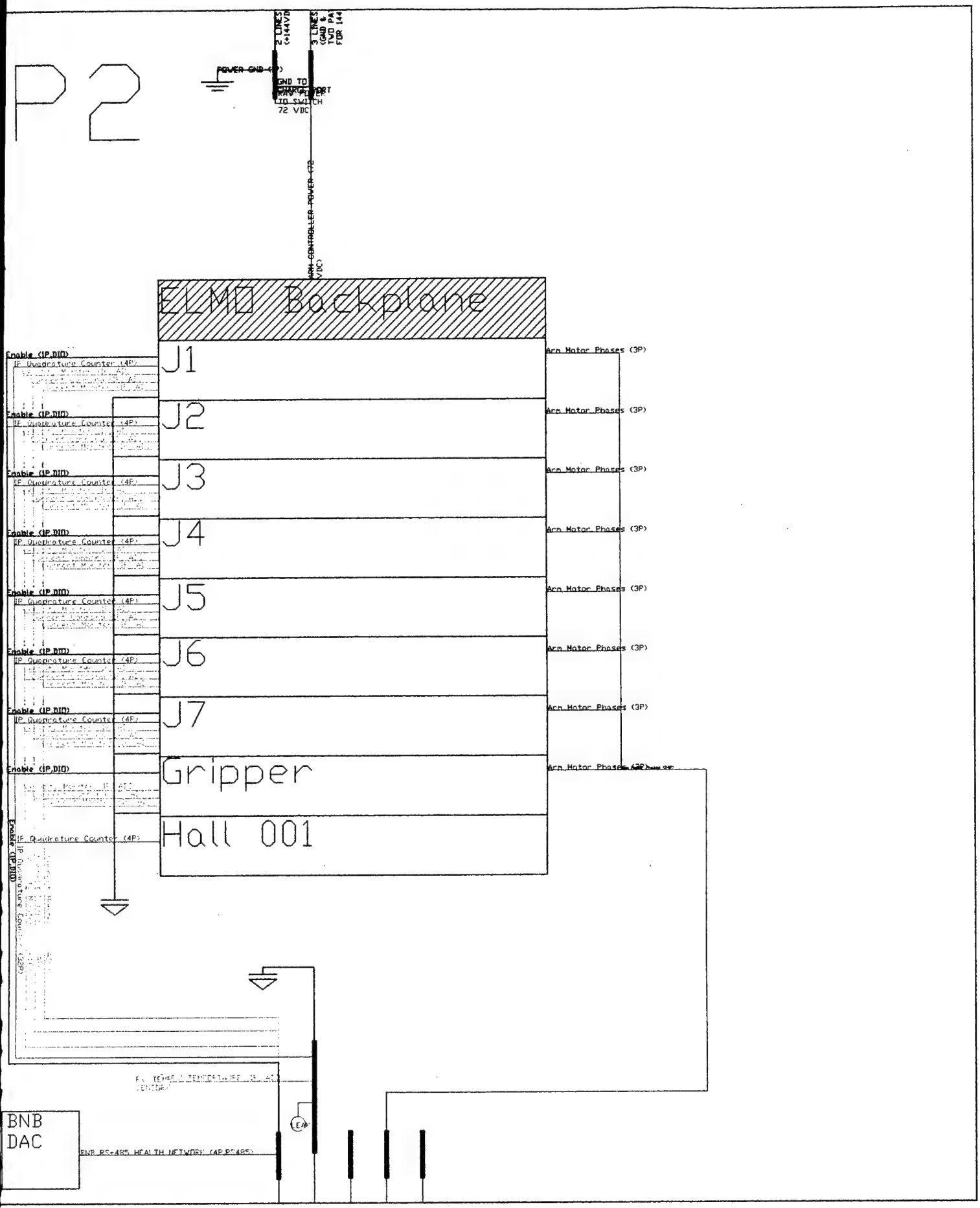

Figure ARA-3C: SAUVIM General Wiring Diagram - Pressure Vessel P2

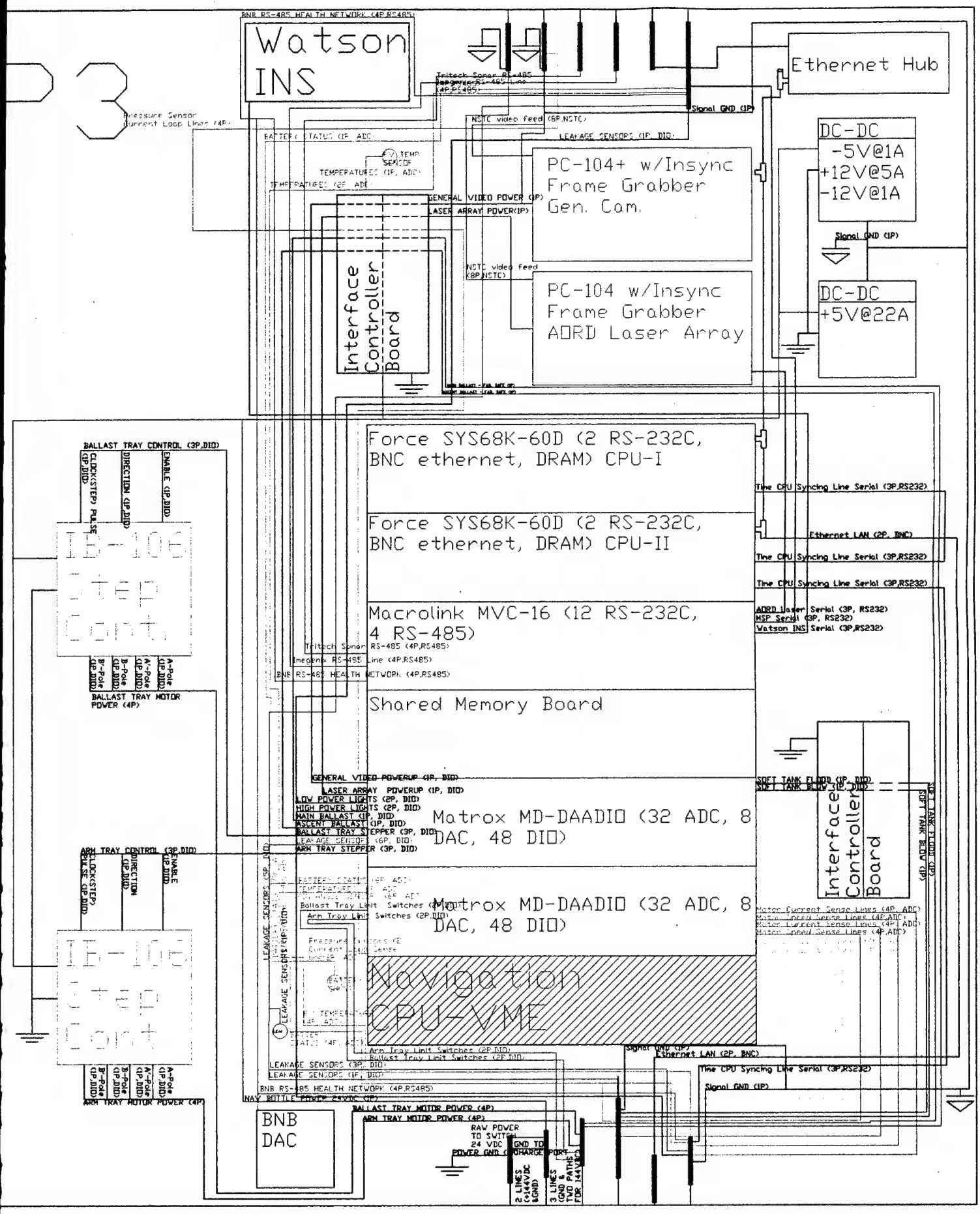

Figure ARA-4D: SAUVIM General Wiring Diagram - Pressure Vessel P3

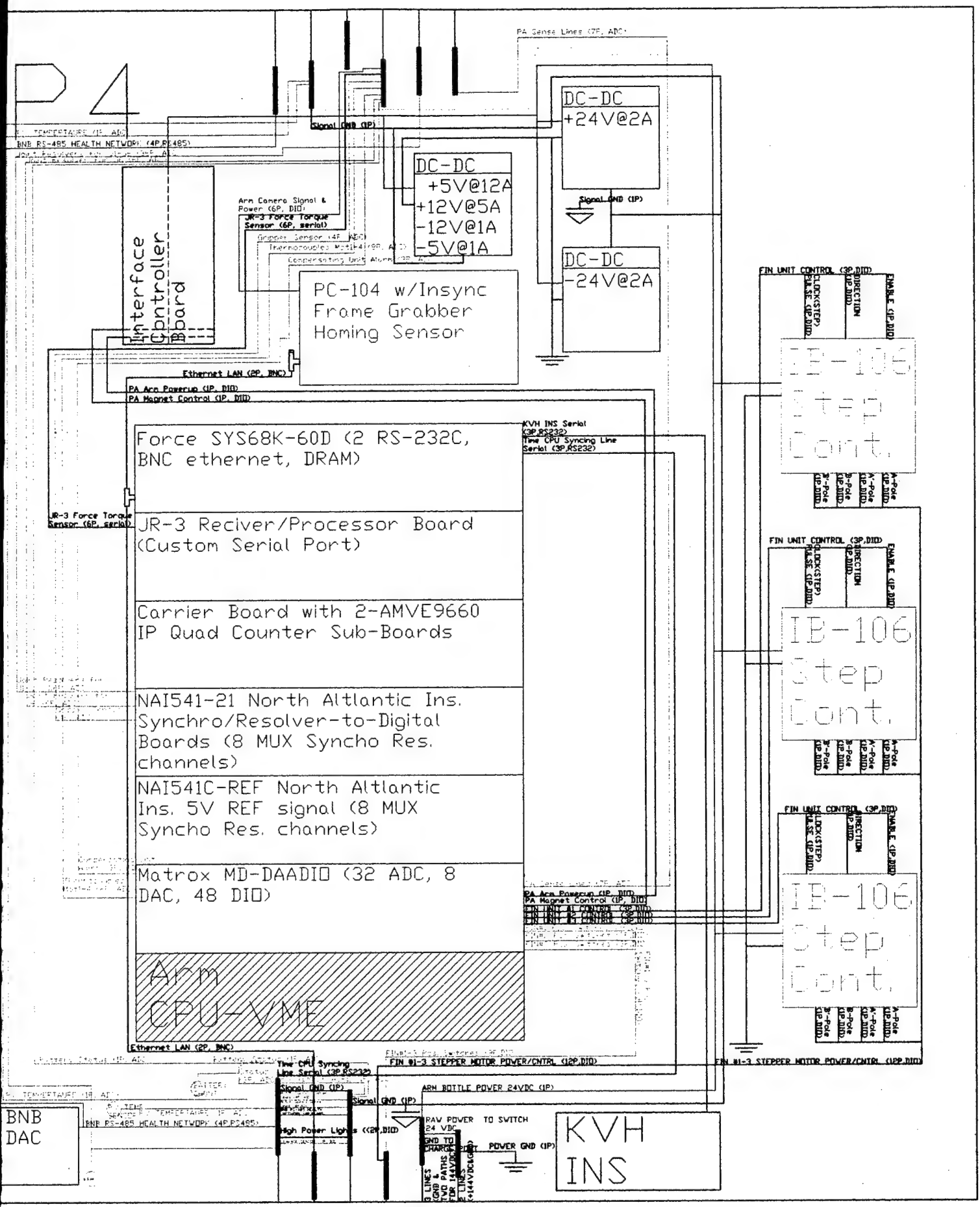

Figure ARA-5E: SAUVIM General Wiring Diagram - Pressure Vessel P4

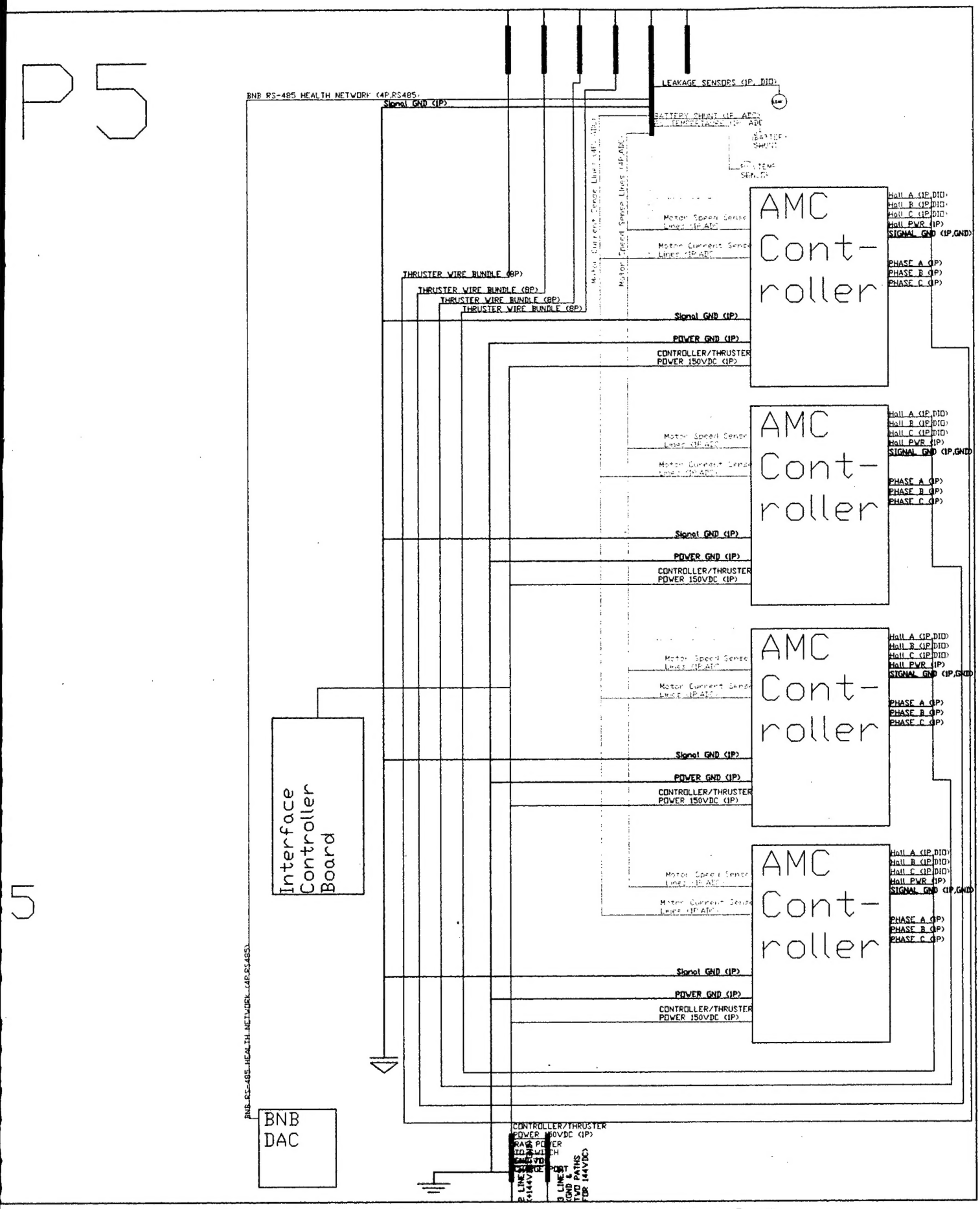

Figure ARA-6F: SAUVIM General Wiring Diagram - Pressure Vessel P5

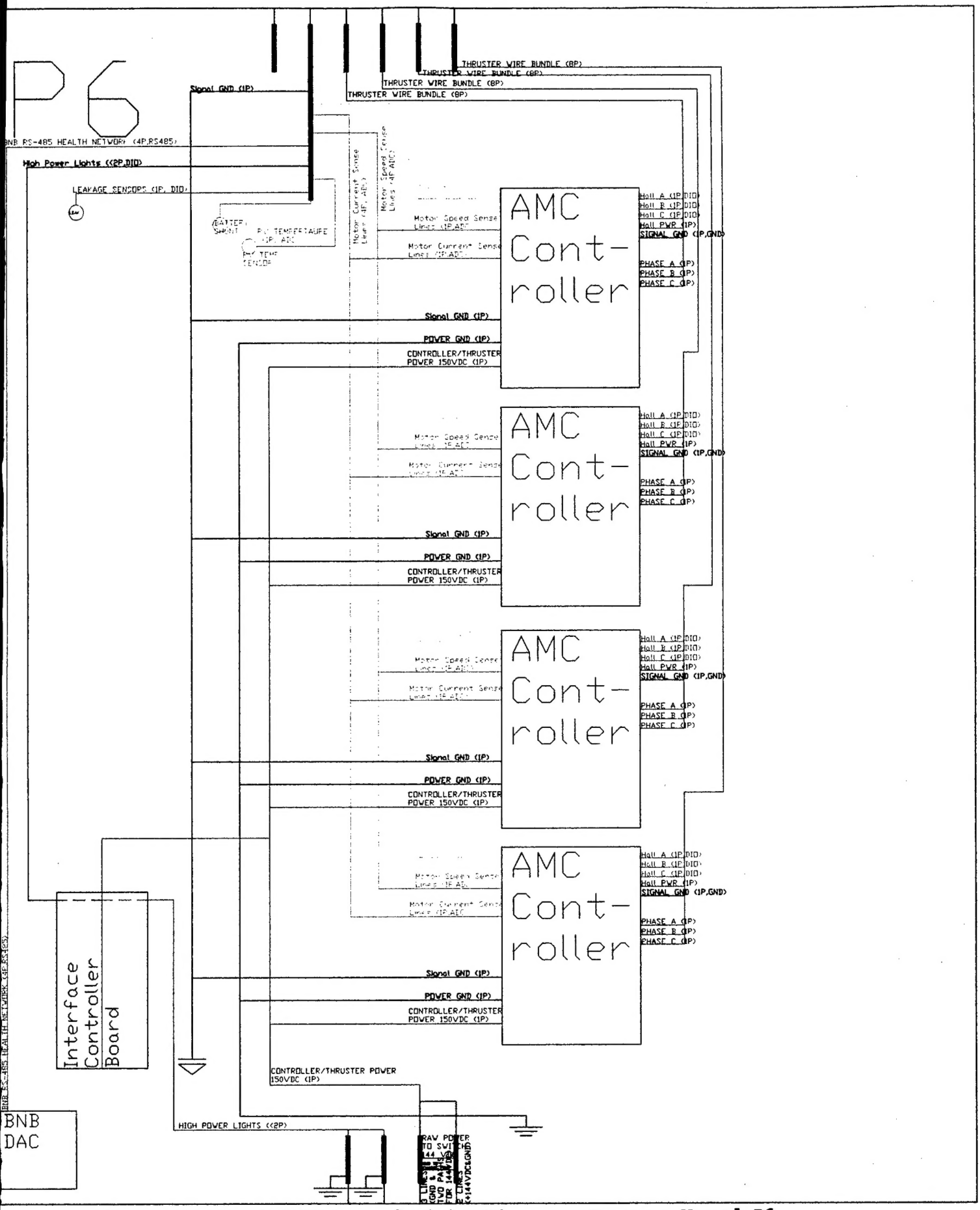

Figure ARA-7G: SAUVIM General Wiring Diagram - Pressure Vessel P6

Appendix 4: Table of SAUVIM Specifications

Feature	SAUVIM Specifications
Hull and Frame	Length ≅ 6.1 m, Height ≅ 1.5 m, & Width ≅ 2.1 m; & High-density composite fairing with a acrylic nose cone mounted on an open 6061 Aluminum frame.
Weight	Dry (estimate) ≅ 6000 kg; & Wet (estimate) ≅ -2kg at 6000m.
Control and propulsion	Cruising by Dorsal and bow mounted control rudders; & Station-Keeping by (8) 23 kg thrusters.
Drive	Direct drive brushless motor (8 thrusters for instantaneous movement). Inherently built-in redundancy.
Speed	Cruising speed 3 knots (maximum)
Lift	46 kg for 1 hour
Power Supply	Thruster - Deepsea batteries at 5000 w-hr CPU - Deepsea batteries at 2500 w-hr Robotic Arm - Deepsea batteries at 2500 w-hr
Range	20 km (maximum)
Pressure Vessel	Six composite cylinders (0.33m ID x 0.46m length); sized for standard 6U VMEbus; & one pressure vessel port (MSP), which can be replaced with a specialized mission package to be designed and fabricated by end-user.
Depth Rating	6,000 meters
Manipulator 1	7 degree of freedom, 1.4 m reach, 8.0-kg lift grip capacity at a full extension.
Manipulator 2	(not determined at this time)
Main Computer	(3+) MC68060 computers mounted in two separate 6U VMEbus with communication; crossed wired to handle half of the sensors and thrusters; 8MB RAM; 4MB Flash EPROM; & a 1GB hard disk.
Micro-controllers	(2+) PC-104 and (1+) PC-104+ micro-controllers for various sensor and thruster control.
Attitude and Angular Rate	3 rotations (roll, pitch, yaw) accelerometer INS system for CPU1; & a lower cost system for CPU2
Collision and Altitude Sonar	4 uni-directional sonar sensors and 1 scanned sonar units; range 2 to 100m.
Short Distance Positioning and Ranging	Laser with controllable beam system; passive arm; & passive optical homing system.
Depth	(2) Absolute pressure sensors 0 - 10,000 psia; & redundancy via LBL or USBL.
Video Imagery	(2) Vehicle mounted, independently controllable pan/tilt low light color cameras with zoom, auto iris, auto focus; (1) Arm mounted color, wide angle camera with auto iris; (1) rear mounted b/w, wide angle camera; & (6+) flood lights.
Monitoring System	A graphic, visualization system via a combination of SGI workstations and/or PCs. Capable of monitoring and limited supervisory control.

REPORT DOCUMENTATION PAGE

Form Approved
OMB No. 0704-0188

1. REPORT DATE *(DD-MM-YYYY)*	2. REPORT DATE	3. DATES COVERED *(From - To)*
07-31-99	Technical	Aug. 1998 - July 1999

4. TITLE AND SUBTITLE

Development of a Semi-Autonomous Underwater Vehicle for Intervention Missions

5a. CONTRACT NUMBER

5b. GRANT NUMBER

N00014-97-1-0961

5c. PROGRAM ELEMENT NUMBER

6. AUTHOR(S)

J. Yuh, S. Choi, C. Ikehara, G. McMurtry, M. Ghasemi-Nejhad, N. Sarkar, K. Sugihara, and S. Itoga

5d. PROJECT NUMBER

5e. TASK NUMBER

5f. WORK UNIT NUMBER

7. PERFORMING ORGANIZATION NAME(S) AND ADDRESS(ES)

University of Hawaii at Manoa
Dept. of Mechanical Engineering
2540 Dole Street, Holmes Hall 302
Honolulu, HI 96822

8. PERFORMING ORGANIZATION REPORT NUMBER

9. SPONSORING/MONITORING AGENCY NAME(S) AND ADDRESS(ES)

Program Officer Chris F. Hillenbrand
Office of Naval Research, Code 82 Program Office
1176 Howell Street B990/4
Newport, RI 02841-2650

10. SPONSOR/MONITOR'S ACRONYM(S)

11. SPONSORING/MONITORING AGENCY REPORT NUMBER

12. DISTRIBUTION AVAILABILITY STATEMENT

Available for public release.

13. SUPPLEMENTARY NOTES

14. ABSTRACT

The primary research objective of the SAUVIM project is to develop an autonomous underwater vehicle capable of intervention missions. Unlike fly-by or survey type AUVs, SAUVIM possesses a manipulator work package, and an advanced control and sensory systems for navigation, stationkeeping, and manipulation. The vehicle also possesses state-of-the-art technology for composite pressure vessel development and genetic algorithm based adaptive and intelligent path-planning methodology. The vehicle will be flexible to a diverse field of applications due to the modularity of the hardware architecture. An independent mission sensor package can be modified to specific, scientific, data-gathering or intervention tasks. The pioneering research and development in the intervention-based underwater vehicle technology will address new potentials in the hazardous, unstructured, underwater environment.

15. SUBJECT TERMS

AUV, Intelligent COntrol & Navigation, Dynamics, and Underwater Robotics

16. SECURITY CLASSIFICATION OF:			17. LIMITATION OF ABSTRACT	18. NUMBER OF PAGES	19a. NAME OF RESPONSIBLE PERSON
a. REPORT	b. ABSTRACT	c. THIS PAGE			Prof. Junku Yuh
U	U	U	SAR	133	19b. TELEPONE NUMBER *(Include area code)* 808-956-6579